



## **University of Bradford eThesis**

This thesis is hosted in [Bradford Scholars](#) – The University of Bradford Open Access repository. Visit the repository for full metadata or to contact the repository team



© University of Bradford. This work is licenced for reuse under a [Creative Commons Licence](#).

# **Automated System Design for the Efficient Processing of Solar Satellite Images**

J S Zraqou

BSc, MSc

PhD

2011



# **Automated System Design for the Efficient Processing of Solar Satellite Images**

Developing Novel Techniques and Software Platform for the  
Robust Feature Detection and the Creation of 3D Anaglyphs and  
Super-resolution Images for Solar Satellite Images

By

Jamal Sami Zraqou

BSc, MSc

A thesis submitted for the degree of Doctor of Philosophy



2011

School of Computing, Informatics & Media

University of Bradford

## **Dedication**

To my father and mother,  
my lovely daughter Aseel,  
my lovely son Basel.

## **Abstract**

The Sun is of fundamental importance to life on earth and is studied by scientists from many disciplines. It exhibits phenomena on a wide range of observable scales, timescales and wavelengths and due to technological developments there is a continuing increase in the rate at which solar data is becoming available for study which presents both opportunities and challenges. Two satellites recently launched to observe the sun are STEREO (Solar TERrestrial RELations Observatory), providing simultaneous views of the SUN from two different viewpoints and SDO (Solar Dynamics Observatory) which aims to study the solar atmosphere on small scales and times and in many wavelengths. The STEREO and SDO missions are providing huge volumes of data at rates of about 15 GB per day (initially it was 30 GB per day) and 1.5 terabytes per day respectively. Accessing these huge data volumes efficiently at both high spatial and high time resolutions is important to support scientific discovery but requires increasingly efficient tools to browse, locate and process specific data sets.

This thesis investigates the development of new technologies for processing information contained in multiple and overlapping images of the same scene to produce images of improved quality. This area in general is titled Super Resolution (SR), and offers a technique for reducing artefacts and increasing the spatial resolution. Another challenge is to generate 3D images such as Anaglyphs from uncalibrated pairs of SR images. An automated method to generate SR images is presented here. The SR technique consists of three stages: image registration, interpolation and filtration. Then a method to produce enhanced, near real-time, 3D solar images from uncalibrated pairs of images is introduced.

Image registration is an essential enabling step in SR and Anaglyph processing. An accurate point-to-point mapping between views is estimated, with multiple images registered using only information contained within the images themselves. The performances of the proposed methods are evaluated using benchmark evaluation techniques. A software application called the SOLARSTUDIO has been developed to integrate and run all the methods introduced in this thesis. SOLARSTUDIO offers a number of useful image processing tools associated with activities highly focused on solar images including: Active Region (AR) segmentation, anaglyph creation, solar limb extraction, solar events tracking and video creation.

## **Acknowledgment**

This thesis would not have been possible unless the assistance of my supervisor Dr. Rami Qahwaji. Without his supervision, advice, and guidance from the very early stage of my research, this thesis would not have progressed nor have seen the light. Above all, he provided me with continuous encouragement and support in various ways. His encouragement to provide high-quality work made me ambitious and work harder.

I am also grateful to my second supervisor Dr. Stan Ipson who encouraged and supported me to achieve several parts of my work and gave me many constructive ideas. His in-depth knowledge and practical experiences in the field of image processing helped me not only in pursuing imaging challenges which I came across during my research period but also helped me to initiate ideas and accomplish them successfully in my life.

I am also grateful to Dr. William Thompson (NASA Goddard Space Flight Centre – STEREO mission), Mr Kevin Addison (Web Developer, NASA Goddard Space Flight Centre, STEREO and SDO missions), and Dr. Markus J. Aschwanden (Solar & Astrophysics Laboratory) for their guidance and support in this work. The necessary information regarding to the STEREO and SDO missions was provided by them.

I would like to kindly thank my parents and my children Aseel and Basel. They have been a constant source of inspiration to me. They have lost a lot due to my research abroad. Their love and encouragement have encouraged me to be patient during the PhD period.

Lastly, I offer my regards and blessings to all of those who supported me in any respect during the three years of studies.

## Publications

- **J. Zraqou, R. Qahwaji, T. Colak and S. Ipson.** *SOLARSTUDIO: A Tool For Visualizing and Processing Large Sets of Solar Images*”, A journal paper Submitted to *Solar Physics*, Under review, 2010.
- **Zraqou J., Alkhadour W., Qahwaji R., Ipson S. and Ugail H.** “*Enhanced 3D Perception using Super-Resolution and Saturation Control Techniques for Solar Images*”, September 2009. *UbiCC Journal*, 4 (4): 1-23.
- **T. Colak, R. Qahwaji, J. Zraqou, and S. Ipson** , "*3D Modeling and Solar Image Processing Algorithms Developed by Space Weather Research Team in University of Bradford* " Presentation in Solar Image Processing Workshop V, Sep 2010.
- **R. Qahwaji, T. Colak, M. Al-Omari, O. Ahmed, J. Zraqou, and S. Ipson,** "*Present and Future Directions in the Automated Prediction of Solar Flares,*" in *Space Weather Workshop: The meeting of Science, Research, Applications, Operations, and Users*. Boulder, Colorado: [http://www.fin.ucar.edu/UCARVSP/spaceweather/abstract\\_view.php?recid=1010](http://www.fin.ucar.edu/UCARVSP/spaceweather/abstract_view.php?recid=1010), 2009.
- **Alkhadour W., Ipson S., Qahwaji R. Hugh J., and Zraqou J.** “*Creating Colour Anaglyph With Less Ghosting From Stereo Pair Images*”, January 2009. International Conference in Information Technology, Amman, Jordan.

# Table of Contents

<b>ABSTRACT</b> .....	<b>I</b>
<b>ACKNOWLEDGMENT</b> .....	<b>II</b>
<b>PUBLICATIONS</b> .....	<b>III</b>
<b>TABLE OF CONTENTS</b> .....	<b>IV</b>
<b>LIST OF FIGURES</b> .....	<b>VI</b>
<b>LIST OF TABLES</b> .....	<b>X</b>
<b>LIST OF ABBREVIATIONS</b> .....	<b>XI</b>
<b>CHAPTER ONE</b> .....	<b>1</b>
<b>1 INTRODUCTION</b> .....	<b>1</b>
1.1 BACKGROUND .....	5
1.1.1 <i>Super-resolution</i> .....	5
1.1.2 <i>Anaglyphs</i> .....	8
1.2 FACTORS DEGRADING STEREO IMAGES .....	9
1.3 APPLICATIONS .....	12
1.4 RESEARCH AIMS AND OBJECTIVES .....	14
1.5 OUTLINE OF THE THESIS.....	17
<b>CHAPTER TWO</b> .....	<b>19</b>
<b>2 LITERATURE REVIEW</b> .....	<b>19</b>
2.1 SOLAR DATA .....	19
2.2 GEOMETRIC REGISTRATION.....	28
2.3 ACTIVE REGION SEGMENTATION .....	36
2.4 SUPER RESOLUTION .....	37
2.5 ANAGLYPHS.....	43
2.6 VISUALIZING AND MANIPULATING SOLAR IMAGES .....	46
2.7 DISCUSSIONS AND SUMMARY .....	48
<b>CHAPTER THREE</b> .....	<b>52</b>
<b>3 GENERATING SETS OF CORRESPONDING POINTS FROM UNCALIBRATED PAIRS OF IMAGES</b> .....	<b>52</b>
3.1 INTRODUCTION .....	52
3.2 COMPARISONS BETWEEN SIFT, SURF AND KLT ALGORITHMS.....	53
3.3 THE OBSERVED PROBLEMS .....	58
3.4 AN AUTOMATED METHOD FOR MISMATCHES REDUCTION.....	59
3.4.1 <i>Removing redundant and conflicting CPs</i> .....	61
3.4.2 <i>Mismatch elimination</i> .....	61
3.5 EXPERIMENTAL RESULTS.....	69
3.6 CONCLUSIONS .....	73
<b>CHAPTER FOUR</b> .....	<b>75</b>
<b>4 SUPER RESOLUTION FOR SOLAR IMAGES</b> .....	<b>75</b>
4.1 INTRODUCTION .....	75
4.2 REGISTRATION .....	77
4.2.1 <i>Active Regions Detection</i> .....	80
4.2.2 <i>Translation and Error Estimation</i> .....	83
4.3 PROJECTION AND INTERPOLATION.....	86
4.4 SMOOTHING .....	88
4.5 QUALITY MEASUREMENTS.....	90



4.5.1	<i>Mean-Squared Error (MSE)</i> .....	90
4.5.2	<i>Peak Signal to Noise Ratio (PSNR)</i> .....	91
4.5.3	<i>Structural Similarity (SSIM)</i> .....	92
4.6	EXPERIMENTAL RESULTS .....	93
4.6.1	<i>Enlarged super resolution images</i> .....	93
4.6.2	<i>SR image with respect to the reference image without enlargement</i> .....	99
4.7	SUMMARY .....	101
<b>CHAPTER FIVE .....</b>		<b>102</b>
<b>5 GENERATING ANAGLYPHS USING PAIRS OF IMAGES FROM THE STEREO SATELLITES .....</b>		<b>102</b>
5.1	INTRODUCTION .....	102
5.2	ANAGLYPHS FROM CALIBRATED PAIRS OF STEREO IMAGES WITH A SIGNIFICANT ANGLE OF SEPARATION .....	105
5.3	ANAGLYPHS FROM UNCALIBRATED PAIRS OF STEREO IMAGES WITH A SIGNIFICANT ANGLE OF SEPARATION .....	107
5.3.1	<i>Boresighted stereo anaglyphs</i> .....	108
5.3.2	<i>Verging stereo anaglyphs</i> .....	111
5.4	ANAGLYPHS AT LARGE SEPARATION ANGLES .....	113
5.5	ANAGLYPHS FROM PAIRS OF SUPER RESOLUTION IMAGES .....	114
5.6	EVALUATION .....	115
5.7	CONCLUSION .....	119
<b>CHAPTER SIX .....</b>		<b>121</b>
<b>6 SOLARSTUDIO: A TOOL FOR VISUALIZING AND PROCESSING LARGE SETS OF SOLAR IMAGES .....</b>		<b>121</b>
6.1	INTRODUCTION .....	121
6.2	MOTIVATIONS FOR DEVELOPING SOLARSTUDIO .....	121
6.3	THE SOLARSTUDIO IMAGING TOOLS .....	122
6.4	REMOTE IMAGE ACCESS WITH WEB-REQUEST CLASS .....	125
6.5	SOLARSTUDIO COMPONENTS .....	127
6.6	SOLARSTUDIO FEATURES .....	129
6.6.1	<i>Standard Image Processing Tools</i> .....	130
6.6.2	<i>Solar Image Processing Tools</i> .....	132
6.6.3	<i>Near Real-Time Based System</i> .....	135
6.7	COMPARISON WITH PREVIOUS WORKS .....	135
6.8	CONCLUSION .....	136
<b>CHAPTER SEVEN .....</b>		<b>139</b>
<b>7 CONCLUSIONS AND SUGGESTIONS FOR FURTHER WORK .....</b>		<b>139</b>
7.1	OVERVIEW .....	139
7.2	OVERALL CONCLUSIONS .....	140
7.3	DETAILED CONCLUSIONS .....	141
7.4	ORIGINAL CONTRIBUTIONS .....	146
7.5	RESEARCH RESOURCES .....	147
7.6	SUGGESTIONS FOR FURTHER WORK .....	148
7.6.1	<i>Integration with other techniques</i> .....	148
7.6.2	<i>Improvements and research extensions</i> .....	148
<b>REFERENCES .....</b>		<b>150</b>
<b>APPENDIX A. RESULTS OF THE STEREO-CPS METHOD .....</b>		<b>158</b>
<b>APPENDIX B. CONTENTS OF ENCLOSED CD-ROM .....</b>		<b>164</b>

# List of Figures

FIGURE 1.1 STEREO EUVI IMAGES TAKEN FROM STEREO-AHEAD ON 01/02/2007 (A) EUVI 171 Å AT 00:15 UT (B) EUVI 195 Å AT 00:15 UT (C) EUVI 284 Å AT 00:51 UT (D) EUVI 304 Å AT 00:52 UT.....	2
FIGURE 1.2 POSITIONS OF THE STEREO-A AHEAD AND STEREO-B BEHIND SPACECRAFT RELATIVE TO THE SUN (YELLOW). THE ORBITAL RADIUS OF THE EARTH IS BETWEEN THE ORBITAL RADII OF THE TWO SPACECRAFT...	3
FIGURE 1.3 DETERMINATION OF 3-D LOOP GEOMETRY FROM SIMULATED IMAGES OF KNOWN LOOPS FROM TWO VIEWS SEPARATED BY 15°. THE (X, Y, Z) LOCATION OF POINTS (CROSSES) DETERMINED BY TRIANGULATION FROM THE STEREO SATELLITES ARE PLOTTED OVER THE KNOWN TEST LOOPS (SOLID CURVES) [4].....	3
FIGURE 1.4 LOCATIONS OF MATCHING REGIONS IN A PAIR OF STEREO IMAGES WITH SEPARATION ANGLE OF 8.554° USING THE SURF METHOD WITH A THRESHOLD OF 0.7. ....	6
FIGURE 1.5 A SINGLE FRAME FROM A STATIC VIDEO SCENE ON THE LEFT. AFTER HISTOGRAM EQUALIZATION IS ON THE RIGHT. THE LICENSE PLATE IS STILL UNREADABLE. ....	7
FIGURE 1.6 NOISE REDUCTION BASED ON AVERAGING A NUMBER OF FRAMES. THE AVERAGE IMAGE BECOME CLEARER AS THE THE NUMBER OF FRAMES INCREASES. ....	7
FIGURE 1.7: RED/CYAN ANAGLYPH TO PROVIDE A 3D VIEW OF THE SUN GENERATED FROM A PAIR OF IMAGES TAKEN FROM STEREO'S SPACECRAFTS (AHEAD AND BEHIND) AT 2007/05/09 16:40:45 (YYYY/MN/DD HH:MM:SS). ....	9
FIGURE 1.8 CLOSE UP OF A COSMIC RAY TRACK SEEN ON THE STEREO BEHIND COR2 DETECTOR. THIS EXAMPLE WAS OBTAINED FROM [10]. ....	9
FIGURE 1.9 COSMIC RAY EVENTS DISTORTION CAUSED BY USING THE HIGH COMPRESSION FACTORS APPLIED ON BEACON DATA, AS SEEN BY THE STEREO BEHIND EUVI TELESCOPE ON JANUARY 18, 2010. (A) COSMIC RAY FEATURES DISTORTED BY THE HIGH COMPRESSION FACTORS. (B) THE SAME COSMIC RAY FEATURES SEEN IN THE FULL RESOLUTION DATA.....	10
FIGURE 2.1 STEREO SATELLITE SHOWING MOUNTED INSTRUMENT PACKAGES. ....	21
FIGURE 2.2 EXAMPLES OF STEREO IMAGES THAT ARE PROVIDED BY THE SECCHI INSTRUMENT PACKAGE. THE RIGHT IMAGE SHOWS HOW SECCHI CAN IMAGE THE SOLAR CORONA FROM THE SOLAR DISK TO BEYOND 318 R. ....	22
FIGURE 2.3 THE SUN AT 304 Å DISPLAYING ACTIVE REGIONS, CORONAL HOLES, AND PROMINENCES WHICH MAY LAST WEEKS OR EVEN MONTHS. LIGHT AT THIS WAVELENGTH IS EMITTED BY He II (HELIUM IONIZED ONCE) AT A TEMPERATURE BETWEEN 60,000 K - 80,000 K; NASA. ....	22
FIGURE 2.4 SDO IMAGES TAKEN ON 29/07/2010 (A) AIA 171 (B) AIA 193 (C) AIA 304 (D) AIA 211 (E) AIA 131 (F) AIA 335 (G) AIA 094 (H) AIA 4500 (I) AIA 1700 (J) AIA HMI MAGNETOGRAM (K) AIA COMPOSITE OF 211, 193, 171 WAVELENGTHS (L) AIA COMPOSITE OF 304, 211, 171 WAVELENGTHS. ....	23
FIGURE 2.5 THE SEPARATION ANGLE BETWEEN THE TWO SPACECRAFT AND THE SUN, STEREO-B VIEWS THE EVENTS ON THE FAR SIDE OF THE SUN THAT LAUNCH PARTICLES TOWARD THE EARTH AT THE FIRST TIME; NASA.....	24
FIGURE 2.6 FLOW CHART DIAGRAM FOR THE SIFT ALGORITHM. ....	31
FIGURE 2.7 A PROMINENT AR SHOWING SEVERAL LOOPS AND TWISTING LINES THAT TRACE MAGNETIC FIELD LINES ABOVE IT. CAPTURED IN EUVI 171 Å RADIATION ON DECEMBER 13, 2007. ....	36
FIGURE 2.8 ACTIVE REGIONS (ARS) APPEAR BRIGHT IN THE 195 Å WAVELENGTH IMAGE OF EXTREME UV LIGHT. ....	38
FIGURE 2.9 RED/BLUE GLASSES FILTER THE TWO PROJECTED IMAGES ALLOWING EACH EYE TO SEE ONLY ONE IMAGE. ....	43
FIGURE 2.10 SCREEN-SHOT OF THE SWB TOOL. ....	48
FIGURE 3.1 SIFT (THRESHOLD 0.50) IS APPLIED TO THE PAIR OF STEREO IMAGES (AHEAD AND BEHIND) EUVI 171 Å TAKEN AT 20070905_000600 WITH A SEPARATION ANGLE OF 29.169°. ONE MISMATCH INDICATED BY RED LINE IS EVIDENT.....	54
FIGURE 3.2 SURF IS APPLIED TO A PAIR OF IMAGES TAKEN FROM STEREO SPACECRAFTS AT A SEPARATION ANGLE OF 29.169° AND A THRESHOLD OF 0.80, RESULTING IN 37 CPS WITH 6 MISMATCHES INDICATED BY RED LINES. THE CALCULATION TIME WAS 0.925 S WITH THE SYSTEM DESCRIBED IN THE TEXT. ....	54
FIGURE 3.3 THE VARIATION OF NUMBERS OF CORRECT MATCHES WITH SEPARATION ANGLE FOR THE SIFT METHOD APPLIED TO PAIRS OF STEREO IMAGES. ....	58
FIGURE 3.4 CPS GENERATED FROM SIFT APPLIED ON A PAIR OF STEREO AHEAD AND BEHIND IMAGES TAKEN AT 09 MAY 2007 000630 UT. REDUNDANT CPS ARE OBSERVED. (A) TRIPLY REDUNDANT CPS. (B) TWO DIFFERENT CPS CORRESPOND TO THE SAME POINT IN THE RIGHT IMAGE. ....	59
FIGURE 3.5 SIFT ALGORITHM (THRESHOLD = 0.70) IS APPLIED ON STEREO PAIR IMAGES (FROM AHEAD AND BEHIND) EUV 171 Å AT A SEPARATION ANGLE OF 16.78°. SEVERAL MISMATCHES INDICATED BY RED LINES ARE VISIBLE. ....	60
FIGURE 3.6 TWO MISMATCHES (INDICATED BY RED LINES) FROM APPLYING SIFT TO A PAIR STEREO IMAGES ARE	

VISIBLE. THE SIFT THRESHOLD IS 0.7, THE IMAGES WERE TAKEN AT 05-10-2007 00:06:00 AND $\theta$ IS $34.56^\circ$ .....	61
FIGURE 3.7 FLOW CHART DIAGRAM FOR REMOVING REDUNDANT CPs IN THE RESULTS FROM SIFT AND SURF ALGORITHMS.....	62
FIGURE 3.8 THE FLOW CHART DIAGRAM FOR REDUCING MISMATCHES THAT COULD RESULT FROM THE SURF METHOD.....	64
FIGURE 3.9 PLOT OF DIFFERENCES OF MEDIANS VERSUS CP NUMBERS GENERATED AFTER APPLYING THE SIFT ALGORITHM ON THE PAIR IMAGES REPRESENTED IN TABLE 3-5. OUTLIERS ARE IDENTIFIED AS HAVING AX GREATER THAN THRESHOLD-X OR AY GREATER THAN THRESHOLD-Y.....	65
FIGURE 3.10 SEVERAL MISMATCHES RESULTING FROM AFTER APPLYING SIFT ON A PAIR OF STEREO IMAGES. THE STANDARD SIFT THRESHOLD WAS USED. THE SEPARATION ANGLE IS $29.169^\circ$ .....	66
FIGURE 3.11 PLOT OF DIFFERENCES OF MEDIANS VERSUS CP NUMBERS THAT WERE GENERATED AFTER APPLYING THE SIFT ALGORITHM ON THE PAIR OF STEREO IMAGES THAT IS SHOWN IN FIGURE 3.10. THE MISMATCHES ARE IDENTIFIED AS HAVING AX GREATER THAN THE ESTIMATED THRESHOLD-X OF 0.0164 AND AY GREATER THAN THRESHOLD-Y OF 0.0137. SEVEN CPs WERE IDENTIFIED AS MISMATCHES FROM A TOTAL OF 26 CPs.....	66
FIGURE 3.12 RESULT FROM APPLYING THE MEDIAN BASED METHOD AFTER THE SIFT ALGORITHM. THE MATCHES BEFORE REMOVING THE MISMATCHES ARE SHOWN IN FIGURE 3.10. THE REMAINING MISMATCHES WHICH ARE INDICATED BY RED LINES HAVE SIMILAR DISPLACEMENTS TO THE CORRECT MATCHES.....	67
FIGURE 3.13 CPs FROM THE SURF ALGORITHM ARE VERIFIED USING THE SIFT METHOD TO DISCARD MISMATCHES. THE SURF AND SIFT THRESHOLDS ARE 0.7 AND 0.6 RESPECTIVELY. THE SEPARATION ANGLE IS $8.554^\circ$ . THE QF VALUE FOR THE RESULTING CPs IMPROVED FROM 3.85 TO 1.48.....	68
FIGURE 3.14 STRUCTURE OF THE STEREO-CPs ALGORITHM FOR GENERATING AN IMPROVED SET OF CORRECT MATCHES.....	70
FIGURE 3.15: COMPARISON OF BEFORE AND AFTER APPLYING THE STEREO-CPs METHOD TO PAIRS OF STEREO IMAGES WITH A SEPARATION OF $29.169^\circ$ . (A) CPs FROM SURF METHOD INCLUDING 20 MISMATCHES. (B) CPs REMAINING AFTER THE STEREO-CPs METHOD WITH 1 MISMATCH REMAINING AT THE PAIR POINTS NUMBERED 18.....	72
FIGURE 3.16 ANAGLYPHS GENERATED FROM AN UNCALIBRATED PAIR OF STEREO IMAGES, TAKEN IN MARCH 15, 2007 AT 22:15:40 UT, AT A SEPARATION ANGLE OF $1.935^\circ$ . THE DISTORTED IMAGE IN THE FIGURE (A) HAS BEEN GENERATED FROM A SET OF CPs EXTRACTED FROM SURF WITH QF VALUE OF 1.74. THE FIGURE IN (B) IS GENERATED FROM A SET OF CPs EXTRACTED AFTER APPLYING RANSAC WITH QF VALUE OF 0.46. THE FIGURE IN (C) IS GENERATED FROM A SET OF CPs EXTRACTED FROM THE STEREO-CPs WITH QF VALUE OF 0.35.....	73
FIGURE 4.1 IMAGES OF THE SUN, TAKEN BY THE SECCHI EUVI 304 ON STEREO-A ON MAY 09, 2007. (A), (B), (C) AND (D) WERE TAKEN AT 02:36:05, 02:36:43, 02:37:20, AND 02:37:58 UT RESPECTIVELY.....	78
FIGURE 4.2 DETERMINATION OF THE QUIET REGION VERSUS AR OF THE SUN, WHEREAS THE HIGHEST PIXELS COUNT FROM A 3D PLOT SURFACE OF A "FLATTENED" SOLAR IMAGE. (A) FULL-DISK SOLAR IMAGE, (B) QUIET REGION CROPPED IMAGE, (C) AR CROPPED IMAGE, (D) INTERACTIVE 3D SURFACE PLOT FOR THE SUB-IMAGE IN (B), AND (E) INTERACTIVE 3D SURFACE PLOT FOR THE SUB-IMAGE IN (C).....	81
FIGURE 4.3 FLOW CHART OF ARs DETECTION.....	82
FIGURE 4.4 AR DETECTION; FULL SOLAR DISK IMAGE OF STEREO-A OBSERVED ON 2007-MAY-19. A) AT 00:12:00 UT IN EUVI 195 A; B) AT 00:06:30 UT IN 171 A; C) DETECTED ARs FROM IMAGE (A); D) DETECTED ARs FROM IMAGE (B); E) ENLARGED DETECTED ARs FROM IMAGE (C), AND F) ENLARGED DETECTED ARs FROM IMAGE (D).....	84
FIGURE 4.5 BICUBIC INTERPOLATION BASED ON THE CLOSEST $4 \times 4$ NEIGHBOURHOODS OF KNOWN PIXELS AT POSITION (X,Y).....	87
FIGURE 4.6 FOUR LR SUB-IMAGES ARE CROPPED FROM STEREO-A IMAGE OF SIZE $512 \times 512$ ON MAY-19-07 AT 00:12:00, 00:22:00, 00:32:00 AND 00:42:00 (A, B, C AND D RESPECTIVELY), THAT ARE REQUIRED TO GENERATE SR IMAGE. (A) LR1 (THE REFERENCE IMAGE), (B) LR2, (C) LR3 AND (D) LR4.....	94
FIGURE 4.7 SR SUB-IMAGES, (A) ORIGINAL SUB-IMAGE CROPPED FROM STEREO-B IMAGE OF SIZE $1024 \times 1024$ ON MAY-19-07 AT 00:12:00, (B) ROBUST SUPER-RESOLUTION, (C) ITERATED BACK PROJECTION, (D) PROJECTION ONTO CONVEX SETS, (E) QE SUPER-RESOLUTION, (F) BICUBIC INTERPOLATION, AND (G) PROPOSED METHOD.....	95
FIGURE 4.8 SR SUB-IMAGES, CROPPED FROM STEREO-A EUVI 171 Å IMAGES ON MAY-19-07 AT 00:06:30 OF SIZE $2048 \times 2048$ PIXELS, (A) ORIGINAL, (B) ROBUST SUPER-RESOLUTION, (C) ITERATED BACK PROJECTION, (D) PROJECTION ONTO CONVEX SETS, (E) QE SUPER-RESOLUTION, (F) BICUBIC INTERPOLATION, AND IN (G) THE PROPOSED SR METHOD.....	96
FIGURE 4.9 COMPARISON BETWEEN QE SR AND THE PROPOSED SR METHOD TO SHOW THE INTERPOLATION PERFORMANCE. (A, B, C, AND D) REPRESENT THE SET OF LR IMAGES. (E) RESULT FROM QE SR. (F) RESULT FROM THE PROPOSED SR METHOD.....	98
FIGURE 4.10 THE SR IMAGE IN THE TOP RIGHT SHOWS THE FULL DISK OF THE SUN WITH FINER DETAILS THAN THE	

REFERENCE IMAGE SHOWN IN THE TOP LEFT. THE EDGES OF THE LOOPS IN THE ACTIVE REGION AREA ARE MORE DISTINGUISHABLE THAN THEY APPEAR IN THE LR IMAGE. (A) LR (REFERENCE) IMAGE. (B) SR IMAGE. (C) SUB-IMAGE FROM FIGURE A. (D) SUB-IMAGE FROM FIGURE (B). .....	99
FIGURE 4.11 THE SHAPES OF THE ACTIVE REGION THAT MARKED BY A CIRCLE APPEAR SHARPER IN SR SUB-IMAGE THAN THE LR SUB-IMAGE. THE INVOLVED IMAGES BEFORE CROP ARE OF SIZE 2048×2048 TAKEN BY STEREO-AHEAD ON 5TH JULY 2007 AT 11:37:00 WITH 10 SECONDS SEPARATION TIME.....	100
FIGURE 4.12 EUVI 304 Å SUB-IMAGE TAKEN BY STEREO-AHEAD ON 9TH MAY 2007 AT 02:36:05 WITH 36 SECONDS CADENCE, SHOWS THE LOOPS OF AN ACTIVE REGION THAT RESIDES ON THE RIGHT SIDE OF THE SOLAR DISK. THE EDGES IN SR SUB-IMAGE LOOK MORE DETAILED THAN THE LR SUB-IMAGE. (A) LR SUB-IMAGE. (B) SR SUB-IMAGE. ....	100
FIGURE 5.1 ANAGLYPH OF THE SUN CREATED FROM PAIR OF STEREO-AHEAD SPACECRAFT ON DEC. 19, 2008 WITH 12 HOURS APART. THE CORONAL HOLES ARE THE MOST PROMINENT FEATURES. ....	105
FIGURE 5.2 FULL DISK INVERTED COLOUR EUV 171 IMAGES OF STEREO-A (TOP LEFT) AND B (TOP RIGHT). THE CROSSING VERTICAL AND HORIZONTAL LINES SHOW THE SUN'S CENTER POINT. THE COALIGNMENT INVOLVES CENTRING THE SUNS' CENTERS [33] IN THE IMAGES. ....	107
FIGURE 5.3 STEPS TO CREATE AN ANAGLYPH. (A) AND (B) ARE THE ORIGINAL IMAGES, (C) AND (D) ARE THE ALIGNED AND CONVERTED TO GREY SCALE IMAGES AND (E) IS THE RESULTING ANAGLYPH. ....	108
FIGURE 5.4 ANAGLYPH CREATION FROM A RECTIFIED PAIR OF UN-CALIBRATED IMAGES USING CPs FROM THE STEREO-CPs METHOD. (A) FEATURE MATCHING BY APPLYING STEREO-CPs. (B) RECTIFIED IMAGES AFTER RUNNING DRUI ON IMAGES SHOWN IN FIGURE (A). (C) 3D IMAGE OF THE SUN.....	110
FIGURE 5.5 THE RESULTING CPs FROM STEREO-CPs ARE USED TO ESTIMATE THE DIFFERENT SIZES OF THE FULL SOLAR DISK. THE TOP LEFT AND BOTTOM RIGHT CORNERS OF THE OUTBOUND RECTANGLE FOR EACH IMAGE IS DETERMINED BY FINDING THE MINIMUM AND MAXIMUM X, Y COORDINATES OF THE CPs. ....	112
FIGURE 5.6 3D IMAGES FOR THE FULL DISK OF THE SUN GENERATED FROM UNCALIBRATED PAIRS OF IMAGES. 3D IMAGES USING EUVI OF (A) 195 Å. (B) 304 Å. (C) 171 Å. (D) 284 Å. ....	113
FIGURE 5.7 ANAGLYPH OF THE SUN CREATED BY COMBINING TWO IMAGES TAKEN 12 HOURS APART BY STEREO AHEAD ON AUGUST 7, 2009. THIS FIGURE WAS INCLUDED IN [112].....	114
FIGURE 5.8 ANAGLYPH OF THE SUN COMBINING TWO EUV IMAGES THAT WERE TAKEN ABOUT 8 HOURS APART (JUNE 25, 2010) INTO ONE 3D IMAGE. THIS IMAGE WAS GENERATED BY THE SOLARSTUDIO APPLICATION WRITTEN BY THE AUTHOR. ....	114
FIGURE 5.9 STEPS TO CREATE THE HRA IMAGE.....	115
FIGURE 5.10 THE PERFORMANCE OF THE ALGORITHM PRESENTED IN SECTION 5.3 IS EVALUATED COMPARED WITH THE METHOD OF RESCALING THE FULL SOLAR DISK STEREO PAIRS USING THE CALIBRATION INFORMATION INCLUDED IN HEADER FITS FILES.....	117
FIGURE 5.11 VISUAL COMPARISON TO CLARIFY THE RESCALING PROCESS BY FITTING THE FULL DISK OF THE SUN PAIR OF IMAGES TAKEN ON JUNE, 06 2007 AT 17:36:00. (A) FITTING THE PAIR WITHOUT RESCALING. (B) FITTING AND RESCALING FOR CALIBRATED PAIR. (C) FITTING AND RESCALING FOR UN-CALIBRATED PAIR USING CPs. ....	118
FIGURE 5.12 COMPARISON BETWEEN ANAGLYPH AND HRA. ....	119
FIGURE 5.13 EXAMPLES OF 3D IMAGES OF THE EUVI 171 Å FULL SUN. ON THE LEFT IS THE 3-D IMAGE GENERATED BY COMBINING PAIRS OF LR IMAGES, AND ON THE RIGHT IS THE 3-D IMAGE GENERATED USING HR IMAGES. THE IMAGES WERE TAKEN ON MAY 13, 2007. ....	119
FIGURE 6.1 USE CASE DIAGRAM OF SOLARSTUDIO INDICATING THE MAIN TWO PROCESSES: IMAGE BROWSING AND APPLYING AN IMAGING TOOL. ....	123
FIGURE 6.2 SEQUENCE DIAGRAM TO REPRESENT THE PROCESS OF BROWSING THE REMOTE AND LOCAL IMAGE(S). ....	124
FIGURE 6.3 SEQUENCE DIAGRAM TO REPRESENT THE PROCESS OF APPLYING AN IMAGE TOOL. ....	124
FIGURE 6.4 CLASS DIAGRAM TO REPRESENT ALL CLASSES IN THE SOLARSTUDIO ASSOCIATED WITH THEIR RELATIONS BETWEEN THEM. ....	125
FIGURE 6.5 THE PROCESS OF ACCESSING REMOTE IMAGES IN SOLARSTUDIO PLATFORM. ....	126
FIGURE 6.6 SCREENSHOT OF THE SOLARSTUDIO APPLICATION. THE ABOVE PART OF THE APPLICATION WINDOW IS THE DATABASE SEARCH INTERFACE. IN THIS EXAMPLE A PAIR OF IMAGES OF EUVI 304 IS USED FOR FEATURE DETECTION AND MATCHING, AND TO CREATE ANAGLYPH AND VIDEO FILES. ....	129
FIGURE 6.7 THE SOLARSTUDIO COMPONENTS: DATABASE INTERFACE, STEREO AND SDO REPOSITORIES, THE STANDARD IMAGE PROCESSING OPERATIONS AND SPECIALISED IMAGE PROCESSING OPERATIONS FOR SOLAR IMAGES. ....	130
FIGURE 6.8 A SAMPLE OF SOLARSTUDIO'S GUI OFFERING A PREVIEW OF THE EFFECT OF A GAUSSIAN FILTER BEFORE APPLYING IT TO THE IMAGE. ....	131
FIGURE 6.9 RESIZING SOLAR DISK USING CPs OBTAINED USING THE STEREO_CPs METHOD. THE IMAGES OF SIZE 512×512 PIXELS ARE TAKEN FROM STEREO SPACECRAFTS ON 13/05/2007. THE VERTICAL AND HORIZONTAL LINES INDICATE THE HEIGHTS AND WIDTHS OF THE SOLAR DISKS. (A) AHEAD EUVI 304 Å, SOLAR DISK OF SIZE 317×317 PIXELS (B) BEHIND EUVI, SOLAR DISK OF SIZE 290×290 PIXELS (C) FEATURE	

DETECTION AND MATCHING GENERATED FROM STEREO-CPS (D) AHEAD EUVI 304 Å, SOLAR DISK RESIZED TO 290×290 PIXELS. ....	132
FIGURE 6.10 AN EXAMPLE APPLYING THE SR METHOD, WHICH IS INTEGRATED IN SOLARSTUDIO. THE SDO IMAGES SHOWN IN (A), (B), (C) AND (D), WERE CAPTURED WITH A CADENCE RATE OF 8.25 MINUTES PER IMAGE ON 20 JULY, 2010 (THE REFERENCE IMAGE TAKEN AT 00:26:48) TO PRODUCE THE SR IMAGE (E) SHOWN AT THE SAME SIZE. IMAGE (F) IS THAT OF (A) MAGNIFIED 3 TIMES USING BICUBIC INTERPOLATION AND IMAGE (G) IS THE SR IMAGE (E) DISPLAYED FULL SIZE. ....	133
FIGURE 6.11 SOLARSTUDIO GENERATED 3D VIDEO (FROM WHOLE IMAGES OR FROM USER DEFINED SUB-IMAGES) FROM STEREO PAIRS OF IMAGES TAKEN ON 13/05/2007 BETWEEN 12:41:15 UT AND 13:06:15 UT. ....	134
FIGURE 6.12 MERGING COLOUR CHANNELS FROM A SEQUENCE OF AIA IMAGES. THIS IS USEFUL TO ACCENTUATE FEATURES AND SIMULTANEOUSLY COMPARE BETWEEN MULTIPLE WAVELENGTHS. THE IMAGES WERE TAKEN BY THE SDO SPACECRAFT ON 27/05/2010. (A) AIA 171 Å (B) AIA 193 Å (C) AIA 304 Å (D) COMBINED IMAGE. ....	134
FIGURE 6.13 CA II K3 SUB-IMAGES FOR 20/07/2007, TAKEN FROM BASS200. (A) ORIGINAL SUB-IMAGE. (B) SOBEL EDGE DETECTION APPLIED ON (A). (C) BRIGHTNESS ADJUSTMENT APPLIED ON (A). (D) MERGING SUB-IMAGES OF (A), (B), AND (C). (E) ANAGLYPH IMAGE CONSTRUCTED FROM PAIR OF SUB-IMAGES TAKEN WITH ABOUT 3 HOURS SEPARATION TIME. ....	138

## List of Tables

TABLE 2-1 SPACECRAFT SEPARATION ANGLE PER MONTH.....	25
TABLE 2-2 POSITIONS OF A AND B STEREO SATELLITES ON JUN 1,2008 12:00 [30].....	25
TABLE 2-3 SOME PARAMETER VALUES THAT CAN BE OBTAINED FROM FITS HEADER FILES.....	27
TABLE 3-1 SIFT PERFORMANCE FOR A PAIR OF STEREO EUVI-171 Å IMAGES TAKEN AT 19-05-2007 00:06:30 UT WITH SIZES 731×731 FOR AHEAD AND 761×761 FOR BEHIND. THE NUMBERS OF KEY POINTS RESULTING FROM THESE IMAGES BEFORE THE MATCHING PROCESS ARE 702 AND 620 RESPECTIVELY. THE SEPARATION ANGLE IS 8.554°. A NULL VALUE APPEARS WHEN THE NUMBER OF MATCHES IS LESS THAN 8 WHICH ARE REQUIRED BY THE 8-POINTS ALGORITHM TO ESTIMATE THE QF VALUE. QF IS ESTIMATED BASED ON EQUATION 2-3.....	56
TABLE 3-2 SIFT PERFORMANCE FOR A PAIR OF STEREO EUVI-171 Å IMAGE TAKEN FROM AHEAD AND BEHIND SPACECRAFT AT 05-07-2007 00:06:30 WITH SIZES 792×792 PIXELS. THE NUMBERS OF EXTRACTED KEY POINTS FROM EACH IMAGE ARE 623 AND 576 RESPECTIVELY. THE SEPARATION ANGLE IS 16.780°.....	56
TABLE 3-3 THE PERFORMANCE OF SIFT ON SEVERAL PAIRS OF IMAGES TAKEN FROM STEREO AHEAD AND BEHIND AT DIFFERENT SEPARATION ANGLES. THE STANDARD SIFT THRESHOLD OF 0.7 IS USED. IT CAN BE SEEN THAT THE NUMBERS OF MATCHES DECREASES WITH INCREASING SEPARATION ANGLE. ....	57
TABLE 3-4 THE PERFORMANCE OF SURF ON SEVERAL PAIRS OF IMAGES TAKEN FROM STEREO AHEAD AND BEHIND AT DIFFERENT SEPARATION ANGLES. THE STANDARD SURF THRESHOLD OF 0.8 HAS BEEN USED.....	57
TABLE 3-5 MISMATCHES REDUCTION PERFORMED ON THE PAIR OF IMAGES SHOWN IN FIGURE 3.6. THE MISMATCHES ARE MARKED IN RED COLOUR FOR ALL CPs THAT HAVE AY OR AX GREATER THAN THRESHOLD-Y AND THRESHOLD-X RESPECTIVELY.....	65
TABLE 3-6 RESULTS FROM APPLYING SIFT AFTER SURF TO STEREO IMAGE PAIRS FOR FIVE DIFFERENT SEPARATION ANGLES. QF IS USED TO SHOW THE IMPROVEMENTS IN THE QUALITY OF THE CPs BEFORE AND AFTER SIFT VALIDATION. THE QF VALUES WERE IMPROVED IN ALL EXPERIMENTS EXCEPT WHERE INSUFFICIENT NUMBER OF CPs REMAINED FOR THE 8-POINTS ALGORITHM AS SHOWN BY THE NULL INDICATOR. .....	69
TABLE 3-7 PERFORMANCE COMPARISON BETWEEN SURF, RANSAC AND THE STEREO-CPs METHODS FOR EXPERIMENTS CARRIED OUT ON 102 PAIRS OF TEST IMAGES. ....	70
TABLE 4-1 HIGHLIGHT ARs IN EUVIs IMAGES BASED ON COLOUR EXTRACTION.....	83
TABLE 4-2 MEASUREMENTS OF SUPER-RESOLUTION ACCURACY THAT HAVE BEEN USED IN SOME OF THE PREVIOUS WORKS.....	91
TABLE 4-3 COMPARING SR IMAGES WITH THE ORIGINAL IMAGE OF THE SAME SIZE BASED ON SSIM AND PSNR. THE SOLAR LR IMAGES OF STEREO-B EUVI 195 Å OF SIZE 512x512 AND EUVI 171 Å OF SIZE 1024×1024 HAVE BEEN USED, CAPTURED ON MAY-19-2007 AT 00:12:00. ....	97
TABLE 4-4 PERFORMANCE COMPARISONS BASED ON SSIM AND PSNR. 40 LR SUB-IMAGES HAVE BEEN CROPPED FROM STEREO-A IMAGES OF SIZE 1024x1024, IN MAY-19-2007 BETWEEN 00:06:30 AND 01:46:30 (HH:MM:SS) AND COLAPSED IN 10 SETS.....	97
TABLE 5-1 MATLAB COMMANDS TO BRING TWO IMAGES INTO ALIGNMENT USING THE RESULTING CPs FROM STEREO-CPs METHOD.....	112
TABLE 5-2 PERFORMANCE EVALUATION BETWEEN RESCALING FROM CALIBRATED AND UNCALIBRATED PAIRS OF STEREO IMAGES. THE RATIOS ARE THE ESTIMATED SIZES OF STEREO BEHIND IMAGES TO STEREO AHEAD IMAGES. THE CALIBRATION INFORMATION AND THE PROPOSED METHOD ARE GIVEN THE ABBREVIATIONS CAL AND PM RESPECTIVELY. ....	116
TABLE 6-1 RELATIONAL DATA DEFINITION CREATED TO SAVE THE DATA FOR BOTH STEREO AND SDO USING INFORMATION FROM THE FILE NAMES OF IMAGES. ....	126
TABLE 6-2 THE URI STRUCTURE FOR STEREO IMAGES. ....	126
TABLE 6-3 THE URI STRUCTURE FOR SDO IMAGES.....	126
TABLE 6-4 A COMPARISON OF SOLAR IMAGING TOOLS BASED ON MISSIONS COVERED, INFORMATION NEEDED AND THE FUNCTIONS OFFERED.....	137

## List of Abbreviations

Å	Angstrom
AIA	Atmospheric Imaging Assembly
ASAP	Automated Solar Activity Prediction
CCD	Charge-Coupled Device
CME	Coronal Mass Ejection
CPs	Corresponding Points
DoG	Difference-of-Gaussian
EUV	Extreme Ultra-Violet
FM	Fundamental Matrix
FITS	Flexible Image Transport System
F	Fundamental matrix
GSFC	Goddard Space Flight Centre
HR	High Resolution
KLT	Kanade-Lucas-Tomasi
LE	Localization Error
LR	Low Resolution
ME	Matching Error
MSE	Mean Square Error
NASA	National Aeronautics and Space Administration
NOAA	National Space Weather Prediction Centre
OBJ	Object files
PCA	Principal Component Analysis
QF	Quality Factor
RANSAC	RANdom SAmples Consensus
R	Solar Radii

SDO	Solar Dynamics Observatory
SR	Super Resolution
SIFT	Scale Invariant Feature Transform
SOHO	SOLar and Heliospheric Observatory
STEREO	Solar TERrestrial RELations Observatory
SURF	Speeded Up Robust Features
SWPC	Space Weather Prediction Centre
UKSSDC	UK Solar System Data Centre
VRML	Virtual Reality Modelling Language (files)

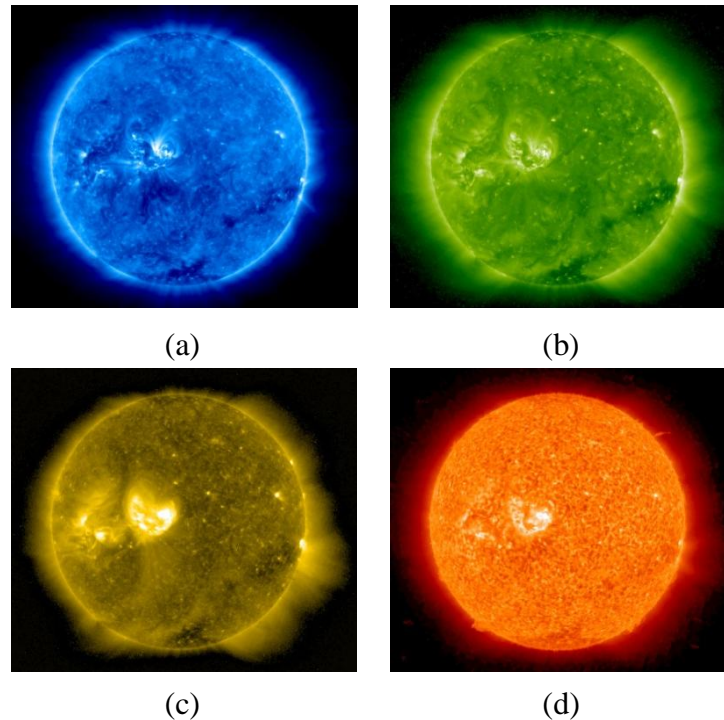


# CHAPTER ONE

## 1 INTRODUCTION

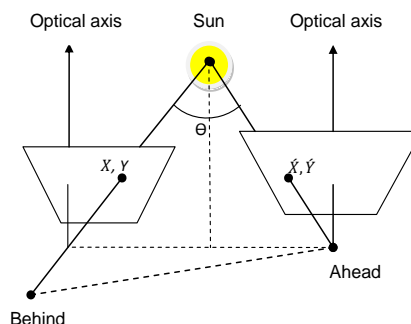
In October 2006 NASA launched the STEREO mission, comprising two spacecrafts placed into orbit around the Sun to provide a continuous stream of images from two separate viewpoints, and in February 2010 NASA launched the SDO (Solar Dynamics Observatory) which aims to study the solar atmosphere on small scales and times and in many wavelengths. The STEREO and SDO missions are providing huge volumes of data at rates of about 15 GB (initially it was 30 GB) and 1.5 TB per day respectively. The STEREO mission provided the first opportunity to obtain 3D views of the Sun's atmosphere [1]. The high level data are provided by the STEREO and SDO science centres (SSC) via event catalogues.

The STEREO science centre browser pages [2] provide JPEG images promptly, with uncompressed FITS images containing calibration information 2 or 3 days later (see page [http://stereo.gsfc.nasa.gov/artifacts/artifacts\\_beacon.shtml](http://stereo.gsfc.nasa.gov/artifacts/artifacts_beacon.shtml)). The initial images, captured at different wavelengths as shown in Figure 1.1, are available in the sizes 128×128, 256×256, 512×512, 1024×1024 and 2048×2048 pixels.

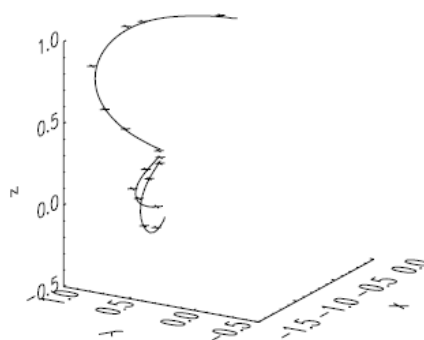


**Figure 1.1 STEREO EUVI images taken from STEREO-Ahead on 01/02/2007 (a) EUVI 171 Å at 00:15 UT (b) EUVI 195 Å at 00:15 UT (c) EUVI 284 Å at 00:51 UT (d) EUVI 304 Å at 00:52 UT.**

As the STEREO mission continues, the separation angle of the two spacecrafts with respect to the Sun, as shown in Figure 1.2, increases by about 44 degrees per year [3]. During the first 400 days of the STEREO mission the separation angle was less than  $50^\circ$  and was suitable for making 3D views for the surface of the Sun. Before the STEREO mission, a test, to determine 3-D loop geometry by triangulation from two simulated views of a known structure separated by  $15^\circ$  was conducted by NASA [4]. The results compared with the known geometry are illustrated in Figure 1.3. For separation angles between about  $50^\circ$  and  $110^\circ$  (between days 400 to 800 into the mission) the data is suitable for determining the trajectory and accurate dimensions of CMEs. The separation angle was  $144^\circ$  in June 2010 and 4 years after launch the separation angle will be about  $320^\circ$ , meaning the two spacecraft will again be close enough to allow 3D viewing, this time of the far side of the Sun as seen from the Earth.



**Figure 1.2 Positions of the STEREO-A Ahead and STEREO-B Behind spacecraft relative to the Sun (yellow). The orbital radius of the earth is between the orbital radii of the two spacecraft.**



**Figure 1.3 Determination of 3-D loop<sup>1</sup> geometry from simulated images of known loops from two views separated by 15°. The (x, y, z) location of points (crosses) determined by triangulation from the STEREO satellites are plotted over the known test loops (solid curves) [4].**

One of the aims here is to apply Super-Resolution (SR) techniques using a set of images, to provide a view of the Sun with a higher image resolution than is available in the individual images, for example, higher resolution anaglyphs to be created than is possible from pairs of original images. In this context, SR is an approach toward resolution enhancement which uses a set of low resolution (LR) observations taken at a high cadence rate so the scene does not change significantly over several images.

<sup>1</sup> A feature in the Sun's corona appears as magnetic flux fixed at both ends, and threading through the solar body, projecting into the solar atmosphere.

Potentially, SR can serve many applications such as web browsing, medical diagnosis, surveillance video, recognition, enlarging consumer photographs and satellite imaging.

The limited spatial resolutions that can be recorded by digital devices and the desire to improve the down sampled images have motivated researchers to research SR. Also even when cameras with sufficiently high resolutions are available, the costs of high precision optics and imaging sensors must be taken into account for many commercial applications. As well as increasing the resolution of the images, SR could achieve this with reduced bit transfer rate, e.g. SR can be used to encode the input video with low resolution at low bit rate and reconstruct a high resolution video efficiently at the decoder side as illustrated in [5].

Although people can use higher resolution cameras, there is a significant demand to generate higher resolution images or video from LR cameras such as mobile phone or web cameras. SR is useful to recognize more details from a set of LR images of a scene such as: enhancing the license plate numbers of moving vehicles in real traffic videos as presented in [6] by fusing the information derived from multiple, sub-pixel shifted, and noisy LR observations, estimating the underlying scene with a resolution as high as possible by combining information from several LR images when viewing the geological structure of planets such as mountains, valleys, rocks, etc, and viewing solar events such as active regions, loops, filaments, etc.

An essential step required to enhance the performance of SR and 3D visualization methods is image registration. Whole image registration can be used to match an image and a map or two images as in SR, while registration of corresponding regions within pairs of images can be used to create two new images in the same horizontal plane reflecting a view like binocular vision. The resulting pseudo-stereo pair of images can be used in the construction of anaglyphs for 3D viewing. The original images will be used as benchmark against which improvements are achieved.

A key factor in the work of this thesis is there is no reliance on camera calibration, which has several advantages over using calibration information. Working without calibration with solar images avoids transferring any calibration errors into, for example, the process of tracking objects. Also changes in calibration do not affect the results. Also working without calibration provides the opportunities to apply the proposed methods on other scenes rather than the Sun. Another key factor is the immediately available JPEG files, rather than the high resolution FITS files available 2 or 3 days later, can be made use of to enable efficient near real-time systems to be created.

The sections to follow provide information relating to SR and anaglyphs with background in Section 1.1. Factors degrading STEREO images that can reduce the 3D perception in anaglyph are discussed in Section 1.2. Some existing applications relating to SR, anaglyphs and solar imaging are presented in Section 1.3. The research aims and objectives of this thesis are introduced in Section 1.4. An outline of the thesis is presented in Section 1.5.

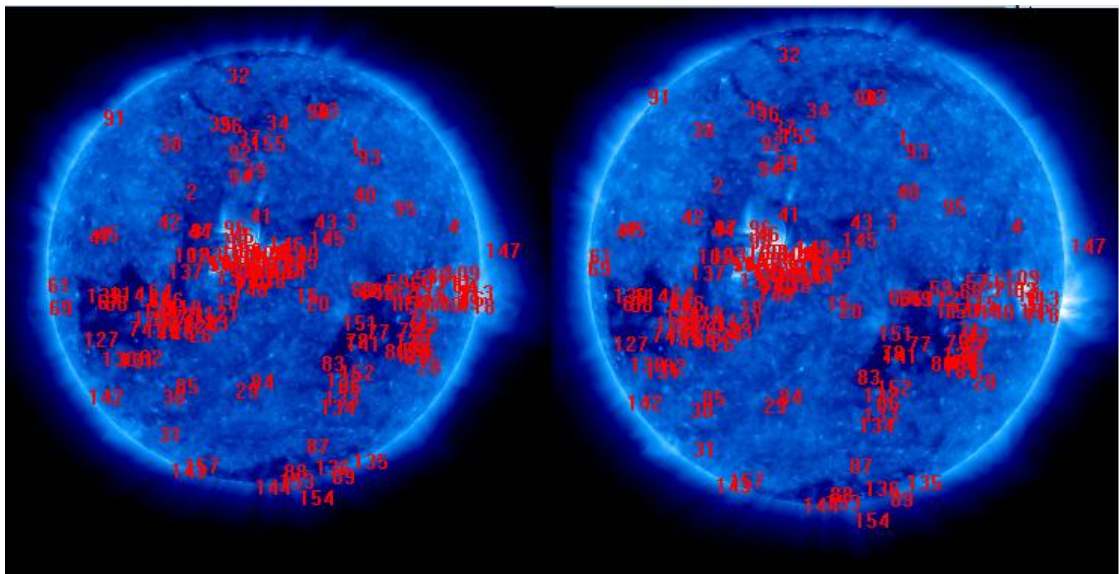
## **1.1 Background**

### ***1.1.1 Super-resolution***

The principal work of a camera is to measure scene intensities, and like any other measuring instrument, has a transfer function which may introduce information loss into the measurement process such as: bandwidth reduction, aliasing and noise which are all common degradations found in imaging systems. Therefore, the resulting images are often unable to completely capture the fine details in a scene.

In principle, several overlapping images of a scene could be used to increase the resolution. This could be achieved if the image registration and restoration are of sufficient accuracy, allowing recovery of image frequencies over any single image.

Image registration aims to spatially align one image to another. The key problem in image registration is to estimate the relative motion between the images of the scene, where each of the LR observations represents a different sampling of the scene. One can use this sub-pixel motion information to produce finer details. In case of moving camera and/or objects, depending on their speed, the shifts among successive LR frames may be more than one pixel. This can be resolved by finding the corresponding points which are the positions of the same scene point in the two images, then adjusting them to form a sub-pixel shift. The pair wise correspondences can be detected and matched using their spatial relations or various descriptors of features. For example, in this research, SURF (Speeded Up Robust Feature) [7] method is used to find the corresponding points (CPs) for STEREO Ahead and Behind pairs of images to extract the shared feature points as shown in Figure 1.4. Having a set of registered images with a common reference frame, enables two principal applications to be developed, Super-resolution and Anaglyphs.



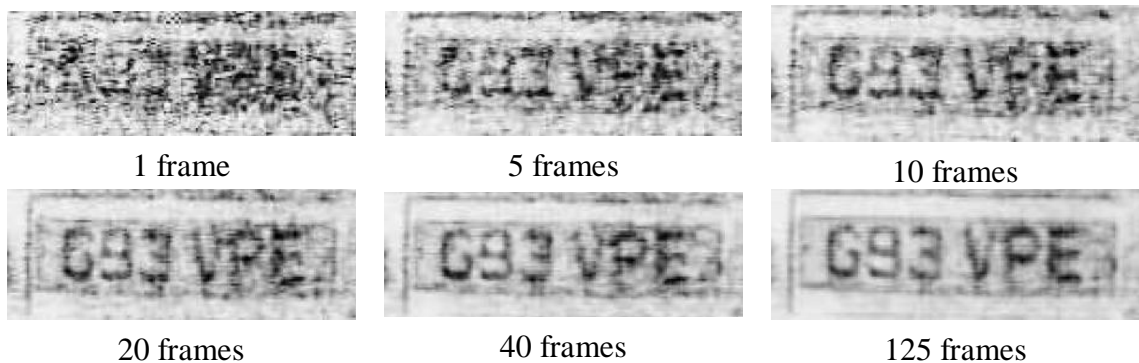
**Figure 1.4 Locations of matching regions in a pair of STEREO images with separation angle of  $8.554^\circ$  using the SURF method with a threshold of 0.7.**

Image restoration techniques attempt to recover the un-degraded scene intensities by combining information from multiple images of the same scene. The

simplest example is temporal averaging, which is an effective way of reducing image noise of static scenes. Figure 1.5 [8] shows a frame taken from a fixed camera for a static scene of a car illuminated by very poor lighting conditions. Histogram equalization of a single frame fails to show the car license plate, but by averaging a number of frames together, the noise is reduced and the plate became clearer as shown in Figure 1.6.



**Figure 1.5** A single frame from a static video scene on the left. After histogram equalization is on the right. The license plate is still unreadable.



**Figure 1.6** Noise reduction based on averaging a number of frames. The average image become clearer as the the number of frames increases.

In the case of multiple cameras (viewpoints), the problems of image restoration are increased. To achieve SR, every image should be mapped accurately into a global reference frame leading the same scene point to be allocated to the same position in every image in which it appears.

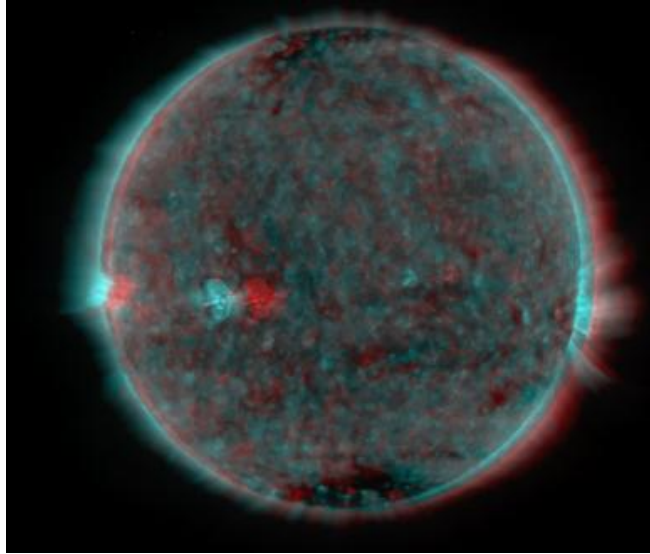
### *1.1.2 Anaglyphs*

Perceiving depth information by presenting the left and right images of a stereo pair to the left and right eyes respectively can be achieved using techniques which can be divided into Time-Multiplexed stereo rendering and Time-Parallel stereo rendering. The first method presents the two images of the stereo pair to the left and right eyes alternately. Additional hardware is used to ensure that each eye views the correct image, such as shuttered glasses with synchronised liquid crystal display (LCD) or cathode-ray tube (CRT) display. In the second method, the stereo images are displayed at the same time and another mechanism ensures each eye sees only the intended image. The most common example of this type is the anaglyph which uses glasses with different colour filters over each eye. There are some others, such as head mounted LCD or CRT based display devices, polarization based systems and glasses free 3D displays.

The anaglyph is a useful way of generating stereoscopic images in a cost-effective and technically simple way. The anaglyph is obtained by combining a pair of stereo intensity images using a pair of complementary colours (often red for left image and blue/green for the right one), in a single image. When viewed through a pair of glasses with matching colour filters, the user's visual cortex fuses the viewed images, providing they were not captured from points too far apart, so the brain interprets them as a 3D impression as shown in Figure 1.7.

In summary, if SR is used to create high resolution images that provide more details than individual LR images, creating anaglyphs from such SR pairs of images should enable 3D views of the scene enhanced over those from pairs of LR images.



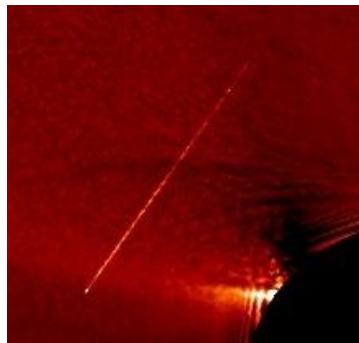


**Figure 1.7: Red/cyan anaglyph to provide a 3D view of the sun generated from a pair of images taken from STEREO's spacecrafts (Ahead and Behind) at 2007/05/09 16:40:45 (yyyy/mn/dd hh:mm:ss).**

## 1.2 Factors degrading STEREO images

Not everything seen in STEREO images is related to the Sun or the solar atmosphere as explained in [9]. Some image features are caused either by the telescope optics, the cameras used to capture the images, or the way the STEREO spacecrafts are operated. These features can be quite confusing and below are some examples:

- Tracks caused by cosmic rays or energetic particles from the Sun passing through the STEREO detectors as shown in Figure 1.8.

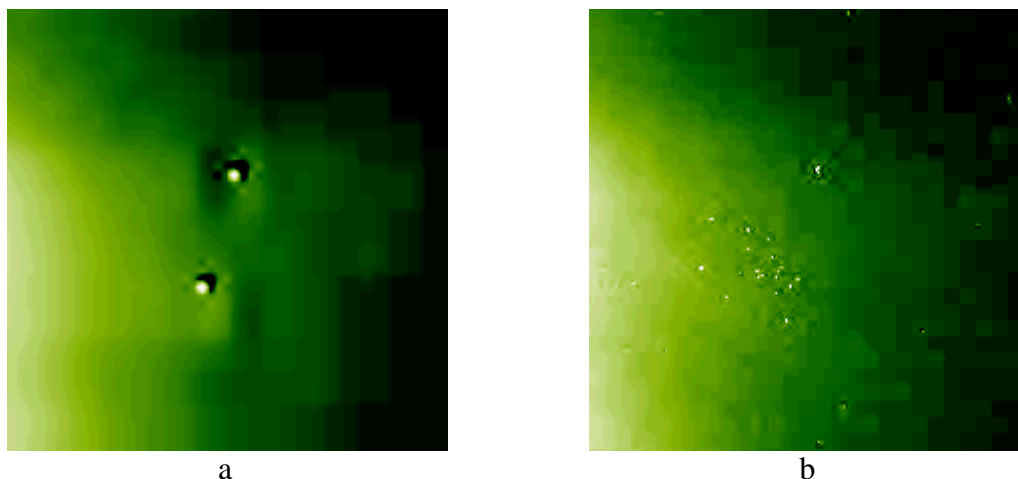


**Figure 1.8 Close up of a cosmic ray track seen on the STEREO Behind COR2 detector.**

**This example was obtained from [10].**

- Visible artefacts in the temporary beacon images caused by the use of high

compression factors are shown in Figure 1.9. Even the full resolution data have some compression applied to them, which results in a small amount of distortion of the brightest cosmic rays as discussed in reference [11]. More cosmic rays can be seen in the full resolution data as than in the highly compressed data as shown in Figure 1.9 (a) and (b).



**Figure 1.9 Cosmic ray events distortion caused by using the high compression factors applied on beacon data, as seen by the STEREO Behind EUVI telescope on January 18, 2010. (a) Cosmic ray features distorted by the high compression factors. (b) The same cosmic ray features seen in the full resolution data.**

Generally, image degradations are mainly due to the loss of information in camera images characterized by their particular transfer functions. Each camera has a limited resolution due to the sampling by its imaging transducer – usually a CCD (Charge-Coupled Device) array. CCD arrays are also subject to several sources of noise including thermal noise, shot noise, and electronic noise in the amplifier circuits. The images are subject to optical blur even when using diffraction limited lenses and lens aberrations or poor focusing can make this much worse. In addition, motion blur occurs if the camera is moving, causing the light entering the camera from a point in the scene to be spread over several CCD cells during the open shutter time of the camera. Lighting conditions may not be the same for all images, due to automatic camera

adjustments or illumination changes, so compensating adjustments need to be made. Finally, pixel transformations applied to image such as rotation, resizing, de-noising, convolution etc. may lead to loss of some of the information contained in the original image.

To perceive a scene in 3D, the left and right eyes must see views of the scene from slightly different positions and these are provided in an anaglyph by combining the two views in different colours and using colour filters to ensure each eye sees only the intended view. Although anaglyphs provide an inexpensive way of achieving 3D visualization, they also have drawbacks, the main one being that it is not easy to represent full-colour images. Each pixel in an anaglyph, fused by the visual cortex of the viewer, gets its colour from both left and right images, which is grey for the red/cyan combinations and yellow for the red/green combination. This makes it a challenging task to accurately display the colours of the original stereo image into a single pixel in the anaglyph image. Other drawbacks include; ghosting or crosstalk, which occurs when the eye not only see the image which is supposed to see but also a part of the other image which should be totally blocked from the sight of this eye. This can be caused by: phosphor afterglow, Liquid Crystal Shutter (LCS) leakage, and LCS timing [12], retinal or binocular rivalry, which happens because not all colours are represented by the display device; or colour merging, which means that colour components of the left and right images are transferred to the same colour [13].

In addition, losses of 3-D perception can result from: artefacts possible resulting from change of resolution of an image (e.g. zooming into or upsizing of an image), errors in fitting (e.g. the corresponding pairs of objects in a registered pair of images must have the same size and be on the same horizontal plane).

As mentioned previously, STEREO and SDO both provide images of the Sun at huge data rates. Hence, it is not easy process to download, browse and analyze

significant areas of interest for these data volumes on a remote server, simply because these processes overload the existing Internet and network infrastructures. Also from a scientist's viewpoint, the process of retrieving large data volumes from even a few repositories, and dealing with immobile data sets poses the problems of searching, browsing and extracting interesting images while avoiding the search for a needle in a haystack problem.

For the purpose of achieving super resolution, this thesis is concerned with solar images taken at high cadence rates, so it is not expected that the Sun will change over the timescale of the images used, and for the purpose of anaglyphs, it is concerned with solar images taken from the two spacecrafts STEREO-A and STEREO-B at small separations angles.

### **1.3 Applications**

In this section, a list of exciting applications involving SR, anaglyphs and solar image visualization tools are discussed. Images with a high pixel density are desirable in many applications, such as high resolution (HR) medical images for medical diagnosis, high quality video conferencing, space and planetary surveillance, etc. The resolution directly available is not always enough and achieving super-resolution from uncalibrated images is an attractive field of study. Algorithms that are robust enough to be applied to real image data are beginning to emerge [8]. A comprehensive forensic video/image processing software [14] called "Cognitech Video Investigator" is used to enhance, denoise, deblur, and super-resolve zoom forensic video evidence (e.g. faces and license plates). Another successful application is the Salient Stills software [15] that tries to create photo quality still image from low quality interlaced video streams.

Anaglyphs are a simple and inexpensive technique for 3D visualization and are used in a wide range of applications. They have been used for entertainment

applications in film and television, and for educational and scientific applications in schools and distance learning and in virtual laboratory applications.

In [16] an anaglyph stereoscopic method was found to improve the quality of the geo-morphological maps from nadir Spot-HRV images, which face problems resulting from vegetation cover which obscures the topographic features. In [17], anaglyphs are used as a visualization technique to support scientific application for NASA's 2003 Mars Exploration Rover Mission. Reference [18] introduced a method for using an anaglyph technique for a medical application, which is the investigation of membrane traffic. They used anaglyphs for exploring budding viral particles Force Microscope images.

ColorCode 3D, described in a patent [19], provides a stereo viewing system that uses amber and blue filters. ColorCode 3D offers the 3D perception nearly full colour viewing with existing television and paint mediums. The left eye with the amber filter receives the cross-spectrum colour information and right eye with the blue filter sees a monochrome image designed to provide the depth effect. The human brain fuses both images to perceive a 3D view. The UK television station Channel 4 [20] broadcast a series of programmes encoded using this system during the week of 16 November 2009. It is worth noting that anaglyph generation for solar images is available in "SolarSoft" using IDL, but the license requirements of IDL could restrict the public use of some of the functions developed for processing solar data.

Regarding solar image browsers, JHelioviewer is a JPEG 2000-based software developed by Müller et al [21]. This software provides remote access as a client-server application to visualize and manipulate SOHO's image data for the purpose of discovering new phenomena. The Solar Weather Browser (SWB) is a software tool developed by the SIDC (Solar Influences Data analysis Center) [22], for visualizing solar images in combination with any relevant information that can be overlaid on the

images. The Solar Viewer widget [23] allows the viewing of recent images of the Sun on computer desktops. These images come from NASA/ESA's SOHO missions, NASA's TRACE satellite, and the Big Bear Observatory.

## **1.4 Research aims and objectives**

This work is inspired by the following observations regarding the state-of-the-art in this field:

- The continuous increase in satellites data volumes creating the need for efficient computer systems for the automated processing of data.
- The lack of existing systems that could provide data access and comparison for more than one mission.
- The lack of advanced imaging systems that could provide the user with advanced imaging capabilities in the fields of SR and 3D processing.
- The lack of computer platforms which are available in the public domain for the benefit of the scientific community.

This work had several aims, overall to provide a computerized system accessing related data sets from various instruments that are often analyzed in isolation, to help scientists discover new phenomena. The first aim was to create super resolution images from a set of uncalibrated low-resolution images. The enhanced images could then be used to improve the quality of view from anaglyphs. However, for the purpose of working with uncalibrated images, feature detection and matching is first needed to extract correspondences in pairs of solar images. The resulting method has been called STEREO-CPs. To achieve super resolution, sets of images consisting of many overlapping views of a scene are investigated along with how to produce superior images using the information contained within them.

The second aim was to develop automated and efficient technologies for 3D image enhancement and processing. The focus is on reconstructing the discontinuity between homogeneous colour pixels to improve its perceptual quality, and then create anaglyphs from super resolved pairs of images. This also needs feature matching algorithms and several have been investigated and some integrated to achieve the automated techniques presented in this thesis.

The final aim was to make the implementation of all methods presented in this thesis to be available to the public. This should help not only the scientific discovery but also the researchers to do further research without the need to re-implement what already done.

The intended outcomes of this research were mainly enhanced resolution images, near real-time 3-D images (anaglyphs) and an imaging toolkit for STEREO's and SDO's images. The inputs to such a system could be several solar images which can be retrieved in near real-time from the STEREO and SDO satellites.

In summary, the objectives of this research were:

- To implement algorithms able to work on uncalibrated solar images. Working without calibration allows automatic alignment of a set of images (estimating the vertical and horizontal shifts of a sequence of images with respect to a reference image so they can be into the same plane) and avoids transferring any calibration errors into the process of tracking objects. Using the immediately available JPEG files with small size and different resolutions, rather than the FITS files with large size and single resolution, allows near real-time systems to be created efficiently.
- To apply super-resolution technique to view the Sun with a higher image resolution than is available in the original individual images of the sun.
- To implement algorithms for creating 3D images from calibrated or uncalibrated

---

pairs of images able to work near real-time. This will be useful in a few years time for viewing the back-side of the Sun from the earth, when the two STEREO spacecrafts again have a small separation angle.

- Provide efficient tools to browse, select and manipulate specific data sets among the huge data volumes available from STEREO and SDO. Accessing these data efficiently at both high spatial and high time resolution is useful to support scientific discovery.

The original contributions associated with successful evaluations presented in this thesis can be summarised as follows:

- A new technique for the automatic generation of a set of CPs from an uncalibrated pair of STEREO images is introduced. CPs are used to automate the image registration process needed to construct SR images and to build 3D anaglyphs for the input image sequence. Benchmark evaluation techniques are used for performance measurements.
- A new SR technique, which consists of three main stages: image registration, interpolation and filtering, is developed. This novel technique is applied to STEREO and SDO images to view the Sun with a higher image resolution than is available in the original individual images of the Sun. Quality assessment is improved by using both subjective and objective measurements.
- Algorithms to create anaglyphs from uncalibrated and calibrated pairs of STEREO images are introduced. A comparison for the former with the information available in the header FITS files is presented.
- A computer platform called SOLARSTUDIO to provide efficient access to STEREO and SDO images at both high spatial and high time resolution is designed. SOLARSTUDIO is the only tool working with both STEREO and SDO missions,



---

providing standard image processing tools, and offering more highly focused functions on uncalibrated solar images such as AR detection, super resolution and anaglyphs. The comparison involved several related works based on three criteria: the missions covered (SOHO, STEREO and/or SDO); the information required to perform the image processing (e.g. calibrated or un-calibrated data); and the functionalities that are offered by each application. SOLARSTUDIO could be the future of solar imaging.

## 1.5 Outline of the thesis

The remaining chapters and their principal contribution are organized as follows:

- Chapter 2 provides an extended literature review of recent research on STEREO data, feature detection and matching methods, super-resolution techniques, anaglyph generation, and applications providing solar image browsing and manipulating tools.
- Chapter 3 introduces the author's geometric registration techniques which are the essential steps for creating the SR and anaglyph methods presented in chapters 4 and 5 respectively. An automated method of generating a set of corresponding points from uncalibrated pairs of images is introduced. Some experimental results demonstrating the effectiveness of these techniques are also presented.
- Chapter 4 presents the author's method of super resolution including image registration, projection, and filtering. Experimental results to evaluate the performance of the proposed method comparing to existing ones are presented. The comparison is conducted based on ground truth data.
- Chapter 5 introduces methods to automatically create anaglyphs from uncalibrated pairs of images. Automatic techniques for by the processes of rescaling and fitting are introduced with experimental results to show it can be made to work effectively.
- Chapter 6 presents the SOLARSTUDIO, which provides efficient software for

visualizing and analyzing STEREO and SDO data.

- Concluding remarks and recommendations for future work are presented in Chapter 7.

# CHAPTER TWO

## 2 LITERATURE REVIEW

The review in this chapter covers six distinct areas of research, which in order are the generation of solar data used in this thesis, the geometric registration techniques which enable the super resolution and anaglyph methods presented in later chapters, the segmentation of active regions, the implementation of super resolution techniques, the creation of anaglyphs and the browsing and processing tools for solar images.

### 2.1 Solar Data

The Sun is of fundamental importance to life on earth and is studied by scientists from many disciplines. It exhibits phenomena on a wide range of sizes, timescales and wavelengths and due to technological developments there is a continuing increase in the rate at which solar data is made available for study, which presents both opportunities and challenges.

Two recently launched satellites to observe the sun are STEREO (Solar TERrestrial RELations Observatory)<sup>2</sup>, launched at the end of 2006 to provide simultaneous views from widely spaced locations and SDO (Solar Dynamics

---

<sup>2</sup> <http://stereo.gsfc.nasa.gov>, last access: 2010.

Observatory)<sup>3</sup>, which officially began its five-year science mission on 14 May 2010 to study the solar atmosphere at small size and time scales and at many wavelengths. The STEREO and SDO missions are providing huge volumes of data at rates of about 15 GB (initially it was 30 GB) and 1.5 terabytes per day respectively.

The data from STEREO is available through the STEREO Science Center (SSC) archive and is utilised in many science investigations. Currently it is used through the Space Weather Browser from the Royal Observatory of Belgium, the “SolarSoft” Latest Events service maintained by the Lockheed-Martin Solar and the Astrophysics Laboratory as mentioned in [24]. The National Space Weather Prediction Centre (SWPC) that is the laboratory and service centre of the National Oceanic and Atmospheric Administration (NOAA) serves the STEREO Beacon data via a website and provides near-real-time data from the STEREO mission, but NOAA cannot create products that rely on STEREO data because of the limited lifetime of the STEREO mission [25].

Each spacecraft in STEREO has four instrument packages [26] mounted as shown in Figure 2.1, and each instrument provides information as follows: SECCHI<sup>4</sup> observes the solar corona and inner heliosphere from the surface of the Sun to the orbit of the Earth; SWAVES<sup>5</sup> provides observations of the generation of CMEs, their evolution, and their interaction with the Earth’s magnetosphere; IMPACT<sup>6</sup> is a suite of seven instruments that samples the 3-D distribution of solar wind plasma electrons and records the characteristics of the solar energetic particle (SEP) ions and electrons;

---

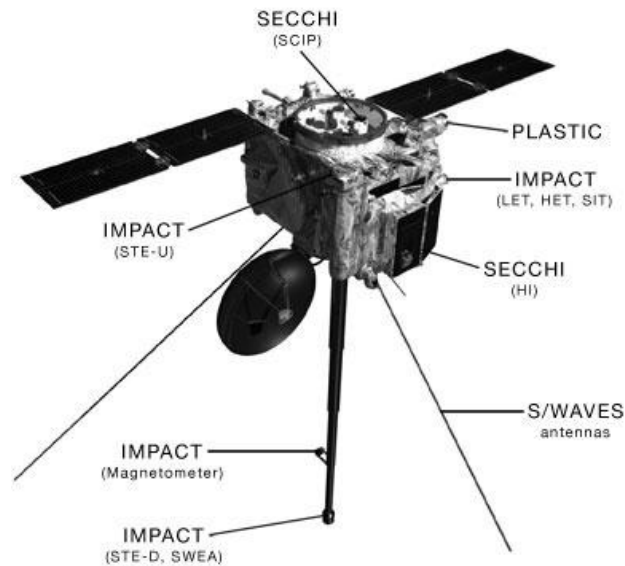
<sup>3</sup> <http://sdo.gsfc.nasa.gov>, last access: 2010.

<sup>4</sup> SECCHI: Sun Earth Connection Coronal and Heliospheric Investigation

<sup>5</sup> SWAVES: STEREO Waves Investigation

<sup>6</sup> IMPACT: In-situ Measurements of Particles and CME Transients Investigation

PLASTIC<sup>7</sup> samples solar wind and supra-thermal particles, providing measurements of kinetic properties and composition.

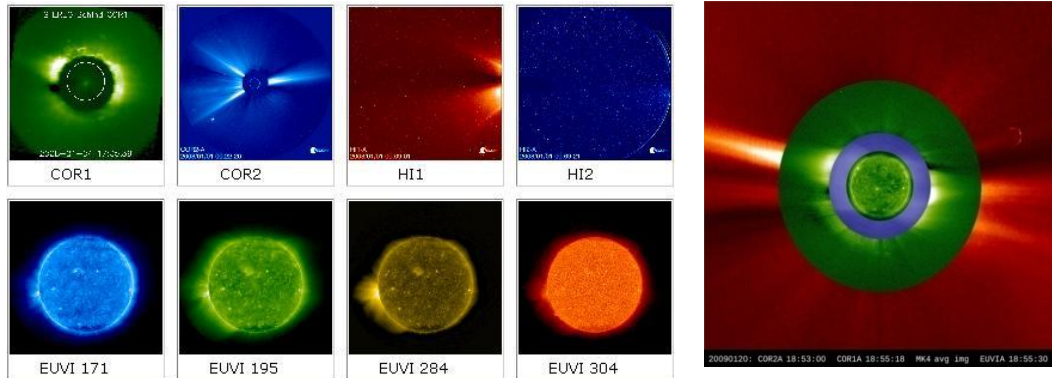


**Figure 2.1 STEREO satellite showing mounted instrument packages.**

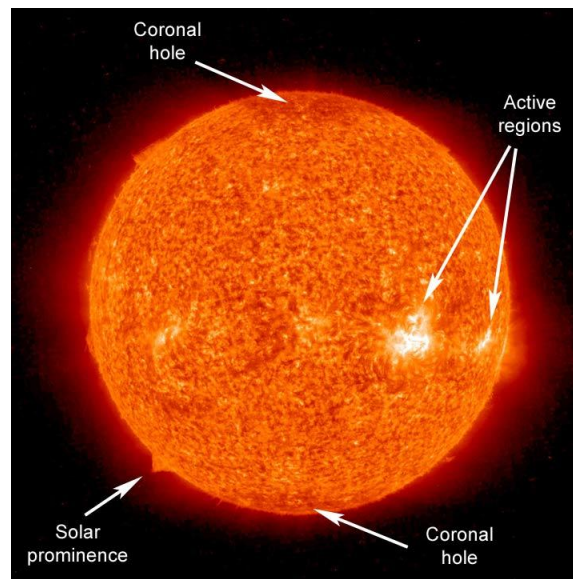
The instrument packages can be divided into two classes, two remote-sensing (SECCHI, SWAVES) and two in-situ sensing (IMPACT, PLASTIC) [27]. SECCHI is a suite of remote sensing instruments consisting of five telescope packages: two white light coronagraphs (COR1: 1.5–4  $R$  (Solar Radii) and COR2: 2.5–15  $R$ ); two new designs of Heliospheric Imagers (HI-1: 15–84  $R$  and HI-2: 66–318  $R$ ); and an extreme ultraviolet imager (EUVI: 1–1.7  $R$ ), which will image the solar corona from the solar disk to beyond 1 AU as shown in Figure 2.2. As the human eye cannot see ultraviolet light directly, the colours of these images are just ways of showing the features of the sun and to differentiate different wavelengths. Different colours have been assigned to particular EUV wavelengths, so usually 195 Å images are green, 304 Å images are orange, etc. Feature such as active regions, prominences or coronal holes are prominently imaged in the EUVI, as shown in Figure 2.3. All these features may last

<sup>7</sup> PLASTIC: PLAsma and SupraThermal Ion Composition Investigation

weeks or even months, providing the opportunity to watch them move across the face of the Sun as it rotates. The first CME was observed using SECCHI COR STEREO-Ahead, during its earliest instrument open-door operations in December 2006 [28].



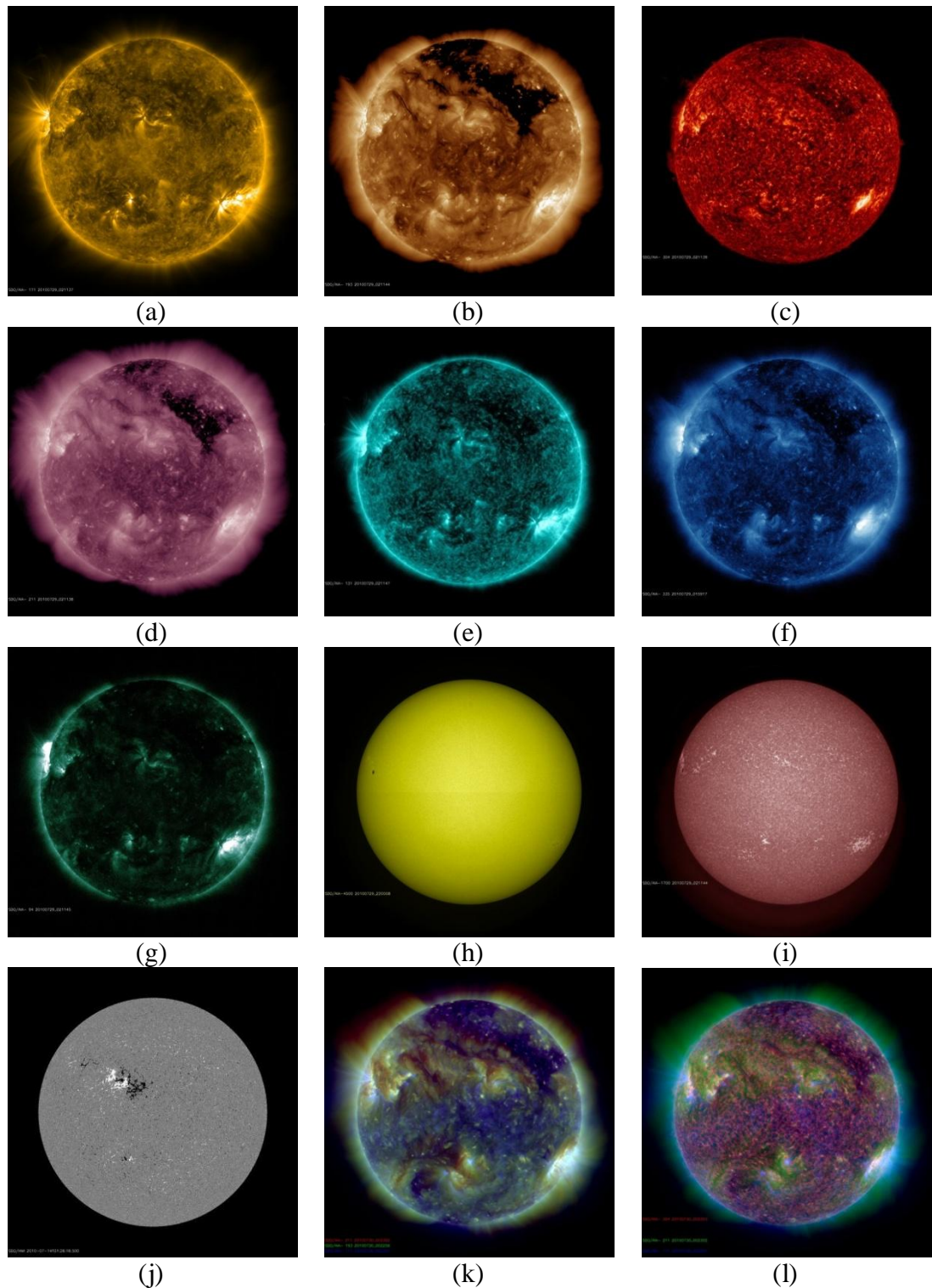
**Figure 2.2** Examples of STEREO images that are provided by the SECCHI instrument package. The right image shows how SECCHI can image the solar corona from the solar disk to beyond 318 R.



**Figure 2.3** The Sun at 304 Å displaying active regions, coronal holes, and prominences which may last weeks or even months. Light at this wavelength is emitted by He II (helium ionized once) at a temperature between 60,000 K - 80,000 K; NASA.

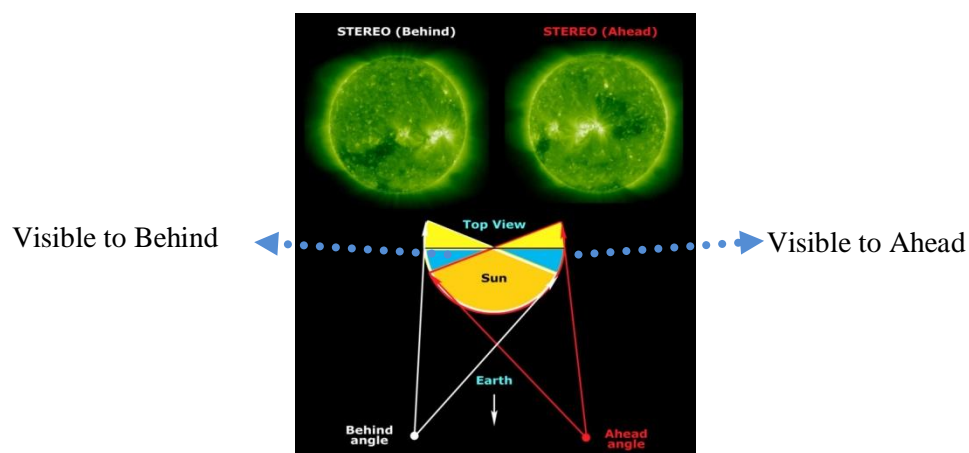
The SDO's [29] Atmospheric Imaging Assembly (AIA) observes the solar corona in ten wavelengths, also mainly in the UV. Some examples of images from AIA and from the Helioseismic and Magnetic Imager (HMI), which measures the Sun's

magnetic field, are shown in Figure 2.4.



**Figure 2.4 SDO images taken on 29/07/2010 (a) AIA 171 (b) AIA 193 (c) AIA 304 (d) AIA 211 (e) AIA 131 (f) AIA 335 (g) AIA 094 (h) AIA 4500 (i) AIA 1700 (j) AIA HMI Magnetogram (k) AIA Composite of 211, 193, 171 wavelengths (l) AIA Composite of 304, 211, 171 wavelengths.**

The twin STEREO satellites have been separating as the mission proceeds with the angle between them subtended at the Sun increasing by 44 degrees a year [3]. Therefore, for the first time, real 3D images and movies of the Sun can be generated (when the angle is not too large). An advantage of a wide angle is that more of the Sun can be seen at one time, as shown in Figure 2.5, whereas, before the STEREO mission, the Sun was watched only from the Sun-Earth line of sight, by SOHO, SDO or Earth based observatories.



**Figure 2.5 The separation angle between the two spacecraft and the Sun, STEREO-B views the events on the far side of the Sun that launch particles toward the Earth at the first time; NASA.**

The STEREO mission enables scientists to view the 3D structure of the Sun when the angle is small, but with increasing angle, leading to most of the solar surface being visible simultaneously, the possibilities for 3D reconstruction decreases. One of these satellites (STEREO-B view) will provide early views of ARs, before they come around to face the Earth, which should help in space weather prediction. Also, the ability to view most of the Sun will help to track solar events from their initiation to termination.

The EUVI instrument doors of the Ahead and Behind spacecraft were opened on Dec 4, 2006, and on Dec 12, 2006, respectively and the two spacecrafts started to



slowly separate at the end of January 2007, as shown in Table 2-1 (collected from [26]). Positions of both STEREO Ahead and Behind spacecrafts with their separation angles can be determined at any time through the SSC website as shown in Table 2-2.

**Table 2-1 Spacecraft separation angle per month.**

Date	Separation Angle
2007 Feb 1	0.6°
2007 Mar 1	1.2°
2007 Apr 1	3.0°
2007 May 1	6.1°
2007 Jun 1	10.6°

**Table 2-2 Positions of A and B STEREO satellites on Jun 1,2008 12:00 [30].**

	STEREO-B	Earth	STEREO-A
Heliocentric distance (AU)	1.050801	1.014183	0.956956
Semi-diameter (arcsec)	913.234	946.208	1002.792
HCI longitude	150.602	175.515	204.018
HCI latitude	-3.852	-0.569	3.080
Carrington longitude	84.746	109.659	138.162
Carrington rotation number	2070.765	2070.695	2070.616
Heliographic (HEEQ) longitude	-24.913	-0.000	28.503
Heliographic (HEEQ) latitude	-3.852	-0.569	3.080
HAE longitude	226.140	251.245	279.968
Earth Ecliptic (HEE) longitude	-25.105	-0.000	28.723
Earth Ecliptic (HEE) latitude	-0.277	-0.000	0.113
Roll from ecliptic north	-0.591		-0.207
Roll from solar north	-6.905		-6.828
Separation angle with Earth	25.106		28.724
<b><u>A and B Separation angle</u></b>		<b><u>53.829°</u></b>	

The first 400 days of the STEREO mission provided data for small-angle stereoscopy ( $< 50^\circ$ ), which are best for making rapid-cadence high resolution 3D images of coronal structures [31], and for direct 3D viewing with anaglyphs (see chapter 5), but when the angle is between  $50^\circ$  and  $110^\circ$  (days 400 to 800) it is more suitable for determining the trajectory and the true dimensions of the observed CMEs by performing

triangulation. When the angle of separation is greater than  $90^\circ$ , features that start on the far side and become more complex as they move to the front side and could produce events affecting Earth, are visible (for the first time).

Data compression (ICER8 algorithm<sup>9</sup>) is applied on the instrument [32] before sending data to the ground. Artefacts of the lossy compression algorithm are not visible in bright image regions, especially not in active regions with bright coronal loops [33], but perhaps there is some loss of useful information [34]. The Compression Factor (CF) is given in the FITS<sup>10</sup> headers of images as shown in Table 2-3.

There are two separate STEREO telemetry streams coming from each spacecraft, the space weather beacon and the science recorder playback telemetries. The beacon telemetry transmits 24 hours per day providing the most recent data and images. The STEREO Science Centre is providing this real-time data stream for processing by a volunteer network of antenna stations around the world. The images are compressed by large factors because the beacon telemetry rate is very low[35].

Data of much higher quality than the beacon data transmitted by the STEREO spacecrafts are written to the on-board recorder and sent to the ground using the NASA Deep Space Network. This high quality data needs a few days to arrive at the STEREO Science Centre website as illustrated in [35]. Therefore, the most recent images on the STEREO Science Centre browser tools are beacon images. The full quality versions become available to replace the temporary beacon images, generally about 2-3 days later. However, it is worth mentioning that the beacon images are recognized by writing

---

<sup>9</sup> Incremental Cost-Effectiveness Ratio (ICER) algorithm is an image data compressor designed to fulfil the needs of deep-space applications while achieving state-of-the-art compression effectiveness, and can provide lossless and lossy compression

<sup>10</sup> FITS stands for 'Flexible Image Transport System' and is the standard astronomical data format endorsed by both NASA and the IAU

the digit “7” near the end of the filename, for example in STEREO Behind “n7euB”, while the full resolution images write the digit “4” in that position.

**Table 2-3 Some parameter values that can be obtained from FITS header files.**

<b>FITS header descriptor</b>	<b>STEREO-A image</b>	<b>STEREO-B image</b>
FILENAME	20070509 204045 n4euA.fts	20070509 204045 n4euB.fts
OBSRVTRY	STEREO A	STEREO B
INSTRUME	SECCHI	SECCHI
DETECTOR	EUVI	EUVI
DATE-OBS	2007-05-09 20:40:45.006	2007-05-09 20:41:29.966
BITPIX	16	16
NAXIS1,NAXIS2 [pixels]	2048	2048
WAVELENGTH [Å]	171	171
DATAMIN [DN]	692.000	664.000
DATAMAX [DN]	8261.00	6837.000
DATAAVG [DN]	947.927	856.703
DATASIG [DN]	354.176	295.418
COMPRSSN	95 / ICER5	95 / ICER5
COMPACT	27.3387 / From file sizes	27.3166 / From file sizes
EXPTIME [s]	4.0020400 / from MEB	4.0053920 / from MEB
CRPIX1 [pixel]	1021.81	1033.69
CRPIX2 [pixel]	926.434	1050.32
CDEL1 [arcsec]	1.58777	1.59000
CDEL2 [arcsec]	1.58777	1.59000

STEREO images can be found online with different resolutions (width×height) 128×128, 256×256, 512×512, 1024×1024 and 2048×2048 pixels, in JPEG format at (<http://stereo-ssc.nascom.nasa.gov/cgi-bin/images>), and with 512×512 and 2048×2048 pixels for the beacon and scientific FITS images respectively, which both are available on (<http://stereo-ssc.nascom.nasa.gov/data/beacon>) and ([http://stereo-ssc.nascom.nasa.gov/data/ins\\_data](http://stereo-ssc.nascom.nasa.gov/data/ins_data)) respectively. In the FITS headers can be found the pixel coordinates of the Sun centre for STEREO images, e.g., in Table 2-3, CRPIX1 = 1021.81, CRPIX2 = 926.434 for image A and CRPIX1 = 1033.69, CRPIX2 = 1050.32

---

for image B, with a solar radius of  $RSUN = 998.966$  for image A and  $RSUN = 912.946$  for image B, where both of FITS files were created on May 09-2007 20:40:45 UT.

## 2.2 Geometric Registration

An essential task for super resolution and anaglyphs is to find accurate point-to-point correspondences between pair of images so the images can be properly aligned. This is known as image registration. After reading and reflecting on the literature, it was noted that the presence of noise and variations in illumination and perspective makes the extraction of true matches from a pair of STEREO images a challenging task. Image registration methods can be classified as either area based or feature based. The former are sometimes called correlation-like or template matching methods. The location of corresponding points is based on the analysis of windows of predefined size about points of interest in the two images. The limitations of using the area-based methods are as follows: firstly, a rectangular window can be transformed to another quadrilateral shape so the same parts of the scene in the reference and sensed images are not covered; secondly, there is a high probability that a window containing a smooth area without any prominent details will be matched incorrectly with other smooth areas in the reference image due to its non-saliency [36]; finally, cross-correlation (CC) methods used for matching, are sensitive to noise and varying illumination and contrast.

Feature-based matching methods are typically applied when the local structural information is transformed to different shapes and orientations in the two images; in this case cross correlation performs poorly in matching. The basic steps are: feature detection, feature matching, mapping function design, image transformation and re-sampling [36]. Pairs of STEREO images have different shifts, scales and angles to the Sun, so this survey has focused on the feature based methods.

---

Features which are locally invariant are widely used for finding corresponding points between two images taken from different viewpoints. In [37], locally invariant regions are achieved by detecting corners and then taking small circular regions around them. Invariance to rotation is achieved using derivatives of Gaussians, while invariance to scale variations is achieved by taking circular regions of different sizes.

In [38], two methods are proposed, one for feature selection to maximize the quality of tracking, and the other for feature monitoring during tracking in order to discriminate between good and bad features based on dissimilarity features. Monitoring feature dissimilarity for tracking has limitations, for example, a bright spot on a glossy surface is a bad (that is, non-rigid) feature but may change little over a long sequence; this may not be detected by dissimilarity measures, in other words, not everything can be decided locally. A method for selecting features known as KLT (Kanade-Lucas-Tomasi) is proposed. The features are tracked through a sequence of video frames by selecting a frame as reference image, and then the active points are detected using gradient values, finally tracking these features in the next frame by finding the transformations between the two frames. The match is achieved if the dissimilarity between the pair features is smaller than a specified residual value (10 is recommended). These provide the new locations for the features of the reference frame in the transformed frame. KLT method is designed to handle translations, and affine transformations but with small change in viewpoints.

An image registration technique for the frames in video sequences, which is based on the use of spatial intensity gradients and a Newton-Raphson iteration, is presented by [39]. This technique can be used to extract depth information from stereo vision systems by making fewer potential matches between two images than techniques which examine the possible positions of registration in some fixed order. The depth

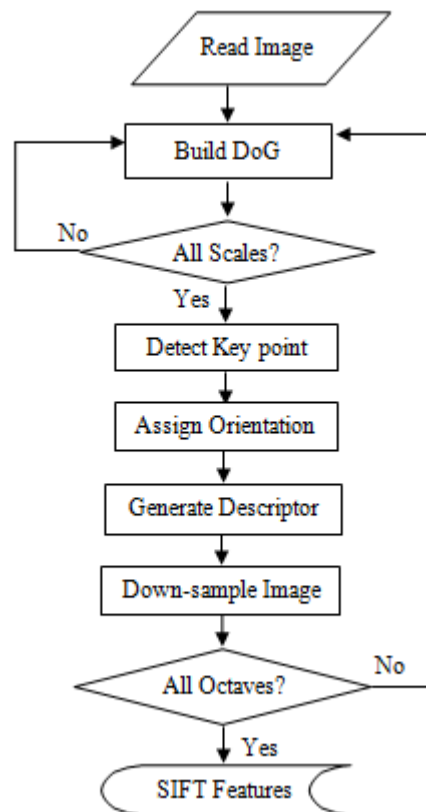
---

information can be obtained in principle by four steps: finding objects in images, matching objects, determining the camera parameters, and determining the distances from the camera to the objects. The presented approach was used to combine object matching to solve the camera parameters and the distances of the objects by using the fast registration technique.

The scale-invariant feature transform (SIFT) algorithm presented in [40] identifies locations in image scale space that are invariant to translation, scaling, rotation, and illumination variations [41]. A flow chart of this algorithm is shown in Figure 2.6. It has four major stages: (1) scale-space peak selection; (2) key localization (3) orientation assignment; (4) key point descriptor. In the first stage, local peaks (maxima and minima of Difference of Gaussian (DoG)) are identified by constructing a Gaussian pyramid in a series of DoG images in multi scales. In the second stage, key localization is achieved to sub-pixel accuracy; also in this stage the unstable candidate key points are eliminated. In the third stage, a dominant orientation is assigned to each key point. Finally, a local descriptor is created by computing a histogram of local oriented gradients around the key point and stores the bins in a 128-dimensional vector (8 orientation bins for each of the  $4 \times 4$  location bins). The matches are determined by finding the 2 nearest neighbours of each key-point from the first image among those in the second image, and the match is accepted, only if the distance to the closest neighbour is less than a predefined threshold (default is 0.8) to that of the second closest neighbour. The threshold can be increased to find more matches or can be decreased to find only the most robust matches.

An alternative method to the SIFT local image descriptor, which is called PCA-SIFT, is introduced in [42]. PCA-SIFT performs the same first three stages of SIFT but the smoothed weighted histogram used in SIFT is replaced using a Principal

Components Analysis (PCA) of normalized gradient patches. PCA-SIFT intends to improve the fourth stage by applying PCA to the local gradient patch, instead of using histograms. PCA-SIFT gives 20 element descriptor, significantly shorter than the 128 element SIFT descriptor. The authors claim that PCA based local descriptors are more distinctive, more robust to image deformation, and more compact than the SIFT descriptor. In [43], the SIFT method is used as a particle filter algorithm for the joint detection and tracking of independently moving objects in stereo sequences recorded by uncalibrated moving cameras. Moving objects entering or leaving the field of view are handled and the method is applied to real world stereo sequences. Object tracking in real scenes using a SIFT based mean shift algorithm is presented in [44]. SIFT features are used to find correspondences among the region of interests across frames. The mean shift is used to carry out similarity search via colour histograms.



**Figure 2.6 Flow chart diagram for the SIFT algorithm.**

In [45], the SIFT approach is used to partially automate the process of estimating the fundamental matrix ( $F$ ) (encapsulating the epipolar geometry of the two camera positions). The key points are identified using SIFT and matched using the L2 distance. Then the fundamental matrix is estimated from this set of matches by using RANSAC.

Mikolajczyk and Schmid [46] introduced an alternative representation to the SIFT algorithm, called Gradient Location and Orientation Histogram (GLOH). This uses the standard SIFT approach, but instead of computing the descriptor on a rectangular grid, the descriptor is calculated on a log polar grid, where the grid is divided into three bins in the radial direction and eight bins in the angular direction. The descriptor vector has length 272, which is reduced to 128 using PCA.

A novel scale and rotation-invariant interest point detector and descriptor method called Speeded Up Robust Features (or SURF) is presented in [7]. The focus is on scale and image rotation invariant detectors and descriptors. Their detector and descriptor do not use colour. They divided their approach into three steps. First, points of interest are selected at distinctive locations in the image using a Fast Hessian detector [47]. Integral images for image convolutions are used to reduce the computation time. Second, the feature vector is generated by constructing a square region centred on the point of interest and then the direction of the Haar wavelet response within the square neighbourhood is used to create the feature vector (the longest vector is the dominant orientation). Finally, a matching pair is detected, if the Euclidean distance between the feature vectors is less than 0.7 times the distance of the second nearest neighbour. The speed of matching is increased by only comparing features having the same type of contrast (sign of the Laplacian).

A data set consisting of a large number of panoramic images with large seasonal changes (snow covered ground, bare trees, autumn leaves, etc.) is compared in [48]



---

using both SIFT and SURF. The results obtained showed that two variants of SURF, called U-SURF and SURF-128 worked better than the other methods in terms of accuracy and speed.

Several approaches to the problem of detecting salient regions are examined in [47] and an approach developed using a combination of spatial and temporal saliency maps. Temporal saliency is computed by finding differences in the motion of particular regions relative to other regions. It was found that SURF was faster and more accurate than SIFT on their data.

Another intensity-based and feature-based approach from different viewpoints is proposed in [49]. The first step extracts salient regions using an algorithm proposed in [50] based on an entropy detector. The next step matches these regions using similarity measures. Finally the efficiency of the algorithm is tested on small medical images of the human brain.

Mikolajczyk [51] introduced an affine point-of-interest detector using a multi-scale Harris detector and an iterative procedure to modify shape and scale over a neighbourhood around the point-of-interest. The shape is then normalized by calculating the second moment matrix (whilst the scale is indicated by local extrema of normalized derivatives over scale). The iterative procedure enables the capture of stable points that are invariant to affine transformations. After getting candidate matches a local descriptor based on normalized Gaussian derivatives is generated for each image patch surrounding the candidate points. Finally a matching scheme is applied to find corresponding points between the set of extracted regions using Mahalanobis distance and to improve robustness cross correlation is applied to verify the matches and the epipolar geometry is estimated using RANSAC.

Corners are detected by a Harris corner detector for modelling 3D objects in

[52]. The matching is achieved by applying normalized cross correlation and the epipolar geometry is recovered from these matches using RANSAC.

Several approaches are considered in [36] for evaluating the performances of the previous algorithms including Alignment Error (AE), Localization Error (LE), CP Error (CPE) and Test Point Error (TPE) methods, consistency checks using multiple cues and visual assessment by experts. AE is the error that is generated from the difference between the mapping model used for the registration and the actual model. This can be evaluated using mean square error. LE is the displacement of the CPs due to their inaccurate detection. It cannot be measured directly on the given image. However, the mean precision of most CP detection methods is known for various image types from computer simulation studies and ground truth comparisons. CPE is generally not a good alignment error measurement [36], because it only measures how well the CP coordinates can be fitted by the chosen mapping model. TPE refers to the CPs that are ignored in the calculation of the mapping parameters. This method can only be used if a sufficient number of the CPs is available.

A method such as RANSAC needs at least 7 inliers. In the consistency check using the multiple cues method, the registered image is compared using an appropriate metric in the image space with the same image registered by another comparative method.

Graphs of recall versus 1-precision are used in another evaluation technique to quantify the results in [42]. Recall and 1-precision are defined in equations 2-1 and 2-2 respectively. The evaluation is carried out on a dataset of images. The key points for all of the images in the dataset are identified using the initial stages of the SIFT algorithm. Matches are identified for key points whose Euclidean distance between feature vectors falls below a chosen threshold. The matches are classified as correct-positives and false

positives. A match is called correct-positive if the key points correspond to the same physical location (as determined either by ground truth for labelled images, or using known image transformations for synthetic image deformation tests), and is otherwise false-positive.

The Quality Factor (QF) is used in [53] to compute the quality of the fundamental matrix F. QF, the mean perpendicular distance between a point and its corresponding epipolar line, is calculated using Equation 2-3. The fundamental matrix describes the geometrical relationship between an uncalibrated pair of stereo images. QF is a basic tool in the analysis of scenes taken from two un-calibrated cameras, and the lower the value of QF the better the quality. Knowledge of the epipolar geometry should facilitate extracting the 3D information for the scene from the images [54].

$$\text{recall} = \frac{\text{number of correct positives}}{\text{total number of positives}} \quad (2-1)$$

$$1\_precision = \frac{\text{number of false positives}}{\text{total number of matches(correct or false)}} \quad (2-2)$$

$$Q_F = \frac{\sum_{i=1}^n (d(p'_i, F_{p_i}) + d(p_i, F^T p'_i))}{2n} \quad (2-3)$$

where

$Q_F$ : Mean distance of points to theirs epipolar lines in the two images.

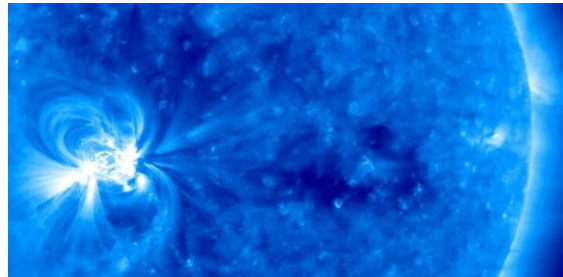
$(p_i, p'_i)$ : Pairs of matched points.

D: Point to line Euclidean distance expressed in pixels.

F: Fundamental matrix

### 2.3 Active region segmentation

Active Regions (ARs) are localized volumes of the Sun's outer atmosphere where a strong magnetic field, emerging from the sub-surface layers, gives rise to various features including sunspots and faculae in the photosphere, and also represents the areas where flares and coronal mass ejection (CMEs) could occur [33]. A prominent AR on December 13-2007 is shown in Figure 2.7. The automated detection of ARs is becoming increasingly important for reliable forecasts of solar activities and space weather.



**Figure 2.7 A prominent AR showing several loops and twisting lines that trace magnetic field lines above it. Captured in EUVI 171 Å radiation on December 13, 2007.**

NOAA has assigned numbers to active regions according to their appearance [55], but unfortunately NOAA will not create products that rely on STEREO data because of the limited lifetime of the STEREO mission [56]. Several papers have investigated AR detection for solar images: In [57] is developed an automated detection of ARs based on the bright areas on a darker background using  $H\alpha$  and Ca KII 3 from the Meudon observatory. This approach segmented a single standardized solar image with a resolution of  $1024 \times 1024$  pixels and a solar disk of radius of 420 pixels with centre at  $511.5 \times 511.5$  pixel. However these specifications are not compatible with STEREO images, because the twin observatories provide several resolutions ( $128 \times 128$ ,  $256 \times 256$ ,  $512 \times 512$ ,  $1024 \times 1024$ , and  $2048 \times 2048$ ), and different coordinates for the solar centre. Measurement accuracy is assessed by comparing the quantitative results of the

automated method and with those obtained manually at the Meudon observatory [58] and NOAA. These accuracies do not reflect comparisons of the shapes of ARs.

In [59] an automated identification of sunspots on full-disk white-light solar images obtained from SOHO/MDI and Ca II K1 images from Meudon is developed. Edge detection is applied to find sunspot candidates followed by thresholding using statistical properties of regions around sunspots. The detection results achieved a high correlation (96%) with manual analysis.

Work in [60] presented a new method for the automatic detection and tracking of solar filaments, addressing problems facing users of existing catalogues. This is done by taking into account structural and temporal evaluation of filaments, differences in intensity, sudden disappearance and reappearance. The problem of tracking is solved by plotting detected filaments on Carrington maps and applying region growing.

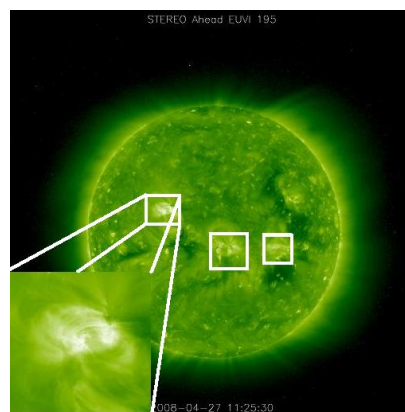
In [61] a new technique to identify the sunspots automatically on full disk solar images is presented. Sobel edge-detection is applied to find sunspot candidates, and then morphological operations are used to filter out noise and define a local neighbourhood background via thresholding. The accuracy assessment is performed by comparing results with the manual synoptic sunspot maps generated at the Meudon Observatory.

## **2.4 Super resolution**

The success of super resolution (SR) methods is highly dependent on the accuracy of each of its three main stages. For example, in [62], if the motion estimated for some of the images is not correct, then the algorithm may degrade the image rather than enhance it. Each stage has potential drawbacks and an error ratio which affects the performance of the SR technique. Poor registration performance causes errors, e.g. the multi frame super resolution problem described in [63], where errors occur in estimating the relative

displacement from the reference image. In interpolation, increasing the size of an image must be performed with minimum visible artefacts such as blurring (which may destroy edges) and/or blocking. In restoration, the characteristics of blurring are assumed to be known [64], such as the point spread function (PSF) of the LR sensor, and the relative motion between the imaging system and the original scene, but if this information is not available it must be estimated, and in this case blurring may appear in the output image due to poor estimation.

Solar images may present several difficulties for applying SR. One problem is the availability of multiple images of the Sun taken at a suitably high cadence rate. Another problem concerns on how to register these images, taking into account the Sun's activity and dynamic magnetic fields [65], which result in shape changes of solar features. However, it is expected that some objects, such as active regions as shown in Figure 2.8, do not change significantly over the short time scales needed for the purpose of registration.



**Figure 2.8 Active regions (ARs) appear bright in the 195 Å wavelength image of Extreme UV light.**

Several researchers have published papers on SR techniques and their techniques may include all or any of SR stages mentioned previously. In [66], a non-uniform interpolation approach is used to perform the reconstruction from samples taken at non-

uniformly distributed locations. This approach performs three stages for SR registration by estimating the relative motions, non-uniform interpolation to produce an enhanced resolution image, and smoothing by applying a de-convolution method to remove blurring and noise. This approach has been investigated in [64]. Its main advantage is the low computational load, making real-time applications possible, on the other hand, it needs a very accurate registration between images, and the blur or noise characteristics should be identical for all LR images. In the restoration step, errors which may have occurred in the interpolation step are ignored.

Another approach to SR uses the frequency domain. Reconstruction can be achieved by relating the aliased discrete Fourier transform coefficients of the LR images to a sampled continuous Fourier transform of an unknown HR image, even in the absence of noise or blurring, as is proved in [67].

Deterministic regularization has been completely discussed in [64] and uses a regularization parameter  $\alpha$  (smoothness constraint) as shown in Equation 2-4 during the reconstruction process in order to solve the ill posed problem in SR image reconstruction. Constrained Least Square (CLS) methods can be used to find the desired image. The desirable solution can be represented by a smoothness constraint, with larger value of  $\alpha$  making the solution smoother. This is suitable when there are a small number of LR images, but if there are larger number of LR images with low noise, then a small value of  $\alpha$  will provide better solution.

$$g = \left[ \sum_{K=1}^P \|Y_k - W_k X\|^2 + \alpha \|CX\|^2 \right] \quad (2-4)$$

where

$g$ : Observed image

$Y_K$ :  $K_{th}$  image

$W_k$ : Represents the additive noise

$X$ : The real scene image

$\alpha$  : Regularization parameter

$C$ : High pass filter

$\|Y_k - W_k X\|^2$ : Estimated shift between  $Y_k$  images with respect to the real scene image.

In [68], a multiple input smoothing convex functional is defined and used to obtain a globally optimal high resolution video sequence where, the regularization parameter is updated at each iteration step from the partially restored video sequence. Most previous work has not provided a way to find the optimal value for  $\alpha$  [69]. The regularization may work well when the scene is strongly restricted, e.g. a binary text image [8].

Projection Onto Convex Sets (POCS) proposed in [70], accounts for the blurring introduced by sensors (PSF) and under-sampling which results in aliased imagery and, consequently, in partial loss of scene information. The resolution of the restored image is limited by the sensor PSF and the sampling rate, but in real applications, the PSF for the imaging system is not always available. Several approaches have used POCS as in [71] and [72] to solve the inverse problem of SR using a full generative image model and arbitrary motion model. POCS based approaches to SR have suffered from slow convergence, and because they optimized a purely constraint-based objective, they do not converge to a unique solution as mentioned in [8].

Optical flow is presented in [73] . It is suitable for images that are non-planar, non-rigid, or which are subject to self-occlusion when rotated. This approach should



---

work well if there is a small amount of noise. Three optical flow methods are discussed in [74]: Least-Squares based flow, consistent flow (CONS) and bundled flow with CONS flow as input.

The Generative Method is proposed in [75]. It tends to restore the HR image using additional information not found in the LR images. This technique relies on strong class based priors to offer more information than simple smooth priors used in existing SR algorithms. The authors claim that the results are better in terms of both subjective and root-mean-square (RMS) pixel error.

The Iterative Back-Projection Approach (IBR) is formulated in [76]. In this approach the HR image is constructed in a similar way to the back projection method used in Computer Aided Tomography (CAT), by back projecting the difference between simulated LR images via imaging blur and the observed LR images. This process is repeated iteratively to minimize the energy of the error rate. A main feature of this approach is that it's easy to understand. However, this approach uses a back projection kernel that is not easy to estimate.

Robust super-resolution is proposed in [62] using a robust median pixel-wise-estimator to discard measurements which are inconsistent with the imaging model by minimizing the error under a norm. Subjective measurements are applied to compare the results of four different algorithms. The experiments were conducted replacing the proposed estimator with two other robust estimators. The first estimator, the Trimmed-Mean, is computed by sorting the errors by their magnitude, and ignoring the top 50%. The second estimator, the Least-Median-Of-Squares (LMeds), is computed on 1-D data. The result of using the median is almost identical to using the mean. Artefacts are introduced using both estimators due to poor estimation.

Registration or motion estimation for each image with reference to one

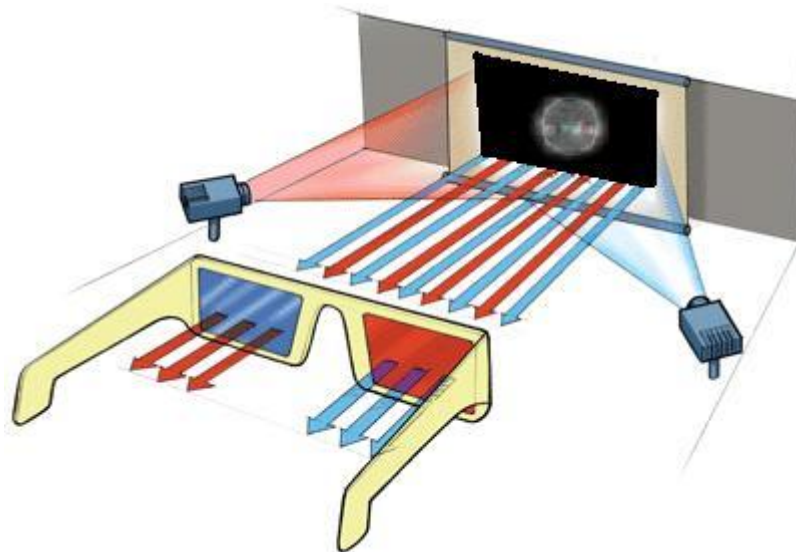
particular image is proposed in multiple registration methods. The work in [77] shows how to compute the images' Fourier Transforms and to determine the 1-D shifts in both their amplitudes. The work in [78] develops a method to estimate the motion using a frequency-domain analysis in order to determine the shift and rotation. The work in [79] demonstrates how to use different down-sampled versions of the images to be analyzed in order to achieve SR by estimating the shift and rotation. The work in [76] shows how the resolution can be improved by estimating the displacements between images accurately.

The method in [77] works well on images with strong frequency content in certain directions. The approach in [75] works well when the blurring process is known. Here, images are represented as two different datasets, frontal images of faces and printed Roman text. The approach in [49] ignores the sensor blurring by mapping the pixels in the observed low resolution frames into a single high resolution frame using the displacements between the frames.

An image enhancement using sub-pixel displacements is presented in [79]. Sub-pixel accuracy with respect to translation and rotation is registered for a sequence of images taken from a moving camera, resulting in image enhancement in the resolution and noise removal. The low resolution images are interpolated and merged onto a finer grid before de-blurring with an inverse blur operator. The method was tested on real noisy images and it was reported that the method worked best when the camera has little or no acceleration. A similar technique is proposed in [80], where a hierarchical block matching is used to obtain a dense optic flow field. The reference frame is interpolated in order to increase its resolution; the other low resolution images are then warped and merged into the reference frame according to the optic flow field. The SR image is then generated by applying a standard single image de-blurring method.

## 2.5 Anaglyphs

An anaglyph is a combination of a stereo pair of images for left and right views of a scene, which contain appropriate offsets with respect to each other, where each image is shown using a different colour in order to achieve 3D perception by users who are wearing the same colour glasses. The first anaglyph image was produced in 1853 by Wilhelm Rollmann [81] in Leipzig and they were used to view 3D still images or 3D movies as shown in Figure 2.9. Anaglyph Maker [82] is a simple application for combining pairs of images taken at slightly different viewpoints on the same horizontal plane into a single anaglyphic image. In this application, two pre-processing steps are required to be performed before superimposition by the user: rescaling and fitting to adjust the image offsets.



**Figure 2.9 Red/Blue glasses filter the two projected images allowing each eye to see only one image.**

Several methods have been proposed to generate anaglyphs. The Photoshop method (PS) [13] is the simplest for implementation. In this method for every pixel in the anaglyph image, the red value is the red colour component of the left image and the blue/green (cyan) value is the blue/green colour component of the right image.

However, for example, if an imaged region is red then it will only be visible to the left eye and will not produce a 3D effect. In the modified Photoshop method (MPS), the original method is followed after first mapping the colour component of the left image to greyscale. This produces a grey anaglyph when corresponding left and right image features have equal intensity. The original PS algorithm and its variant the modified PS method don't take into account the transmission function (percentage of the light at wavelength ( $\lambda$ ) which is passed by the filter) of the filters, as a result the generated anaglyph will be the same regardless of the type of glasses we use.

A least square (LS) projection method was introduced by Dubois [81], which method takes into account two factors. First, the transmission function of the glasses which is used in the computation of the anaglyph. Second, the spectral distribution for estimating the colours in the colour space. The drawbacks of this method are the need for a clipping operation because of the presence of some results (colour components) which are out of the RGB range, and also the resulting anaglyph image is a little dark [13].

Based on the (LS) method, the uniform method (UN) was proposed by Zhang and McAllister [83]. This method takes into account the spectral distribution of the primaries and the transmission function of the filters. They attempted to improve the quality of the anaglyph by estimating the colours in CIE using the Least Square method, with the uniform form instead of the norm form for the length measure. Another difference between the two methods is that Dubois minimizes the square-sum of 6 differences between the typical and real values of colours, while in the uniform method they minimize the maximal value among the 6 differences.

Anaglyphs suffer from several problems including ghosting, binocular rivalry, and colour merging, which may sometimes prevent the viewer perceiving depth in the

scene. This motivated some researchers to look for methods to solve the ghosting problem and generate anaglyphs with better quality.

Another approach called midpoint algorithm for generating anaglyph was introduced in [13], this method is based on calculating a point P in the uniform CIE L\*a\*b\* (or CIELAB) space which is the midpoint of the line connecting the two transmitted colours.

The study presented in [13] demonstrates some of the problems which afflict the generation of anaglyphs with high colour quality. A stereo pair of images of an Indian mother and her daughter of size 443×389 pixels, were used to test the performances of three algorithms: the PS method, the Midpoint method, and the least squares method. Creating an anaglyph using the PS method was the simplest but resulted in a ghosting problem and poor quality colour representation. The application of the midpoint algorithm to generate anaglyphs shows that, there are some resulting colours out of the RGB colour range. For this reason a clipping process is performed. Although this method takes into account the properties of the filters, it still suffers from ghosting. Analyzing the anaglyphs that resulted from the Eric Dubois (Least squares) method shows that, this method requires the clipping process, but on the other hand no ghosting was detected in the tested anaglyph image. While the Midpoint algorithm is the best for forming an anaglyph with high quality colours and good details, it still suffers from ghosting. On the other hand, the least square method produces an anaglyph image which is a bit dark with fewer details, and this can be solved by applying gamma correction, but the advantage of this method is that, there is little ghosting. From the previous comparison it appears that none of the previous described methods can produce colour anaglyphs without any ghosting or region merging.

In [84], three methods are proposed to produce anaglyphs with high quality and

---

minimize the undesired ghosting artefacts. This was achieved by employing the following three methods: Stereo Pair Registration, Colour Components Blurring, and Depth Map Manipulation and Artificial Stereo Pair Synthesis.

Alkhadour et al. [85] presented a simple and flexible method for generating a monochrome and a colour anaglyph. The algorithm is designed to allow the user to choose the level of compromise between the amount of colour and amount of ghosting by simply modifying the colour saturation to improve the 3D visualization of the scene.

## **2.6 Visualizing and Manipulating Solar Images**

In this section, several applications and web-browsing tools associated with working on solar images of interest gathered from SOHO, STEREO and SDO satellites are introduced.

JHelioviewer is a JPEG 2000-based visualization and discovery software for SOHO's image data developed by Müller et al. [21]. This software provides remote access as a client-server application for compressed images using the lossy compression mode of JPEG2000, a compression technology system defined in ISO/IEC 15444-1[86]. The Joint Technical Committee of Photographic Experts (JPEG) has developed the international standard for interactivity with JPEG2000 files called JPEG 2000 Interactive Protocol (JPIP). JHelioviewer uses JPIP and OpenGL. JPIP is used to minimize data transfer by streaming image data in a region-of-interest and quality-progressive way by exploiting the multi-resolution and spatially random access properties of JPEG2000, making a smart dissemination of the data for client-server communication. This was briefly discussed by Taubmana and Prandolinib [87]. OpenGL allows rapid hardware acceleration of image processing and rendering (see, <http://www.opengl.org/about/overview>). JHelioviewer was implemented in Java and

---

supports users creating movies streaming between two dates/times, applying frame-by-frame basic image processing, overlaying unlimited number of images or movies under adjustable transparency levels, and locating solar events data.

The Automated Solar Activity Prediction system (ASAP) [88], identifies and classifies sun spots in near real-time to make predictions of the likelihood of solar flares. The active region candidates are detected from SOHO/MDI magnetogram images, while the sunspots candidates are detected from MDI continuum images. Region growing and neural network techniques are applied afterwards to combine both candidates to determine precise boundaries of sunspot groups. A new visualisation system for viewing 3D solar features and solar loops [89], was introduced recently to work under ASAP.

The Solar Weather Browser (SWB) is a software tool developed by the SIDC (Solar Influences Data analysis Center) [22], for visualizing solar images in combination with any relevant information that can be overlaid on the images. The structure of the SWB includes: the SWB-server, SWB-user interface and SWB download and user support website. The server side uses highly compressed formats of solar images and context data that can be accessed by the client side on the user machine. Background images (e.g EIT) can be interactively combined with overlays (e.g. sunspot or filament locations) on the client side. This feature can be useful for viewing the results of automated solar image recognition/processing chains. It is also useful for the distribution of solar image archives playing the role of a quick-look viewer. SWB provides data related to SOHO and STEREO. A method for CME detection called CACTUS [22] (A software package for Computer Aided CME Tracking) is also available in SWB. A screen shot of the SWB is shown in Figure 2.10.

CACTUS was developed to detect CMEs in image sequences from LASCO

(Large Angle and Spectrometric Coronagraph) C1 and C2 coronagraphs. The LASCO instrument is on board the SOHO satellite. The output of this software is a list of events similar to the CME catalogues as shown in the SOHO/LASCO CME catalogue (e.g. date, time and speed of CMEs), with principal angle, angular width and velocity estimation for each CME. The first steps in the CMEs detection are to merge the C2 and C3 images, and clean, enhance and reformat them to improve the CME contrast and detection. Motion pattern extraction for the CME's bright features moving outward from the Sun is applied afterwards. The performance of this method was evaluated by comparing its output with the visually assembled CME catalogues which exist on <http://lasco-www.nrl.navy.mil/cmelist.html>. The success rate was about 75%. In addition, this technique revealed CMEs that were not listed in the catalogues.

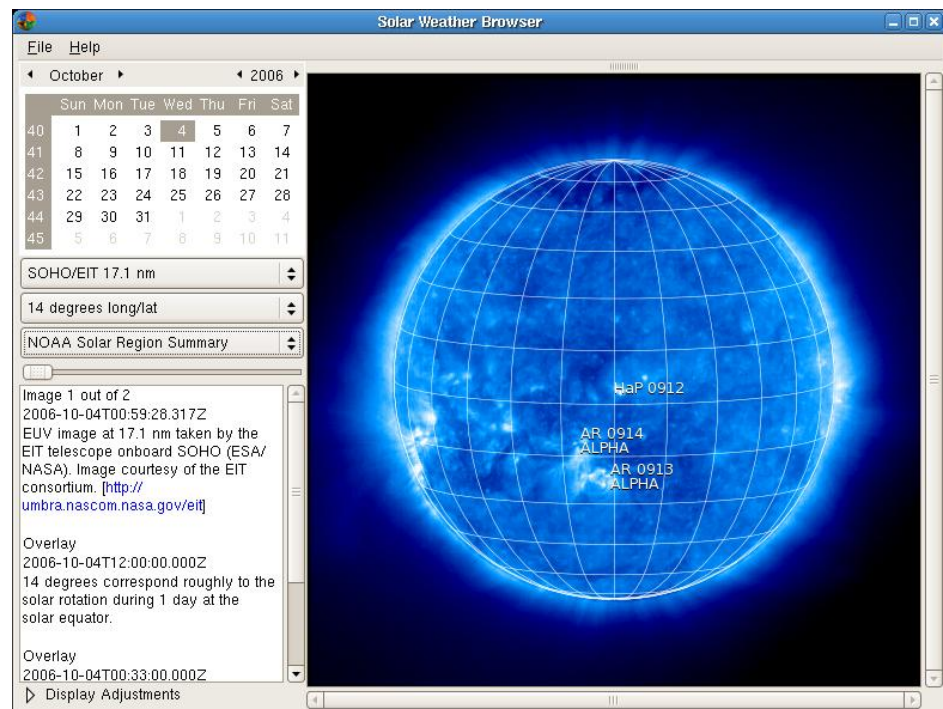


Figure 2.10 Screen-shot of the SWB tool.

## 2.7 Discussions and Summary

In the literature review, the author's contributions can be viewed as making a brief assessment of existing SR techniques, creation of anaglyphs methods and the browsing



and/or manipulating tools for solar images. The success of SR approaches is dependent on the accuracy of individual SR stages. Precise alignment, interpolation and smoothing are the major keys to generate an enhanced SR model. It is clear that there have been several studies for SR techniques that are biased towards their own images. Also it is clear that applying SR on solar images is poorly investigated or achieved although these kinds of images potentially represent suitable data on which to apply SR techniques. In this thesis, a practical study of solar images taken by the STEREO and SDO spacecrafts is performed.

Also the literature revealed that the existing anaglyphs for 3D viewing of solar images are generated either by manual scaling and fitting [90] or by the STEREO software that is distributed as part of the Solar Software Library which known as “SolarSoft” (to see some examples visit [91]). The links to guide the user to install the SolarSoft library can be found on [92]. Generating anaglyphs using IDL is based on the information in the FITS file headers such as the sun centre and solar radius. The license requirements to use IDL packages could restrict the public use of some of the developed functions for processing solar data. It is worth mentioning that each high resolution FITS file is about 8.3MB in size and only becomes available a few days after the real observation. Also the compressed beacon images suffer from artefacts resulting from the compression factor that is used onboard. Motion estimation between sequences of images taken from same spacecraft at different time is not easy to be estimated based on the information in the FITS file headers. This kind of motion estimation is important to generate SR images. Furthermore, working without calibration on JPEG images enables working in near real-time efficiently and avoids the bandwidth restrictions of the available network infrastructure. For example, creating a 3D video including 1000 frames from STEREO images requires downloading more than 16.6GB of high

---

resolution FITS files and double this if applied to SDO images.

From the previous review it can also be seen that there is a key problem to find true correspondences between two images with differences of scale, rotation, illumination and perspective transformation. Mismatched correspondences might reduce the performance of dependent methods such as transformation with respect to the reference image, scaling and fitting. Hence, the focus first might be on producing correct matches with sufficient number of CP's.

Tracking an AR through a STEREO solar video (this video can be reconstructed from a software written by the author of this thesis by composing sequence of images between two dates/times) should be a useful cue for solar event investigations, e.g. tracing the AR loops between two dates or times would be useful in determining their trajectories and height variation.

Also in the literature, the number of data browsing tools available for STEREO and SDO is limited and each tool provides rather limited functions. For example, the web browser for the official STEREO website [2] provides JPEG images in five resolutions:  $128 \times 128$ ,  $256 \times 256$ ,  $512 \times 512$ ,  $1024 \times 1024$ , and  $2048 \times 2048$  pixels and SDO data in the four resolutions:  $512 \times 512$ ,  $1024 \times 1024$ ,  $2048 \times 2048$  and  $4096 \times 4096$  pixels. On the official sites; these data are used to create screen animations with basic movie control functions. One of the restrictions when accessing STEREO and SDO images is the limit on the number of images per query. For instance, no more than 2000 images can be queried per instrument between two dates (time is not included which may not be convenient when the cadence rate is high) in the STEREO browser. The images of interest can be displayed with one of three options: List (just file names), images, or slideshow. On the SDO official site, no more than 400 images per query are allowed, generated as still images, movie, or archive (zipped file).

Considering the previous work it becomes obvious that user's ability to process data is still limited. For example, existing software packages do not enable users to create 3D visual models of the regions of interest, create videos and SR. However, it is found that several applications have been developed to view solar images including: STEREO-GSFC, SDO-GSFC, SWB, and JHelioviewer. Major challenges still exist when studying the solar atmosphere at different size scales, time scales and wavelengths. Firstly, limited functionalities are offered by the official browsers tools for both STEREO and SDO. Secondly, there exist restrictions on the number of images queried per user. Thirdly, there is a serious lack of developed systems that enable users to access multi-wavelength images from more than one satellite at the same time. Finally, license requirements to use the IDL programming language could restrict the public use of some of the functions developed for processing solar data. To tackle some of these challenges, SOLARSTUDIO has been developed.

# CHAPTER THREE

## 3 GENERATING SETS OF CORRESPONDING POINTS FROM UNCALIBRATED PAIRS OF IMAGES

### 3.1 Introduction

In this chapter, a new technique for the automatic generation of a set of Corresponding Points (CPs) from an un-calibrated pair of images taken from the two STEREO spacecrafts is introduced. The ability to extract accurate CPs automatically is useful for several reasons. They are needed to match sequences of image to investigate time and spatial variations. They can also be used to automate the image registration process needed to construct super resolution images and to build 3D anaglyphs for the input image sequence. The main objective of this chapter is to generate a set of robust and accurate CPs for every pair of uncalibrated STEREO images that lies in a specified range. Working with STEREO images without calibration avoids transferring any calibration errors into the process of tracking objects. Moreover, using the immediately available JPEG files, rather than the FITS files, allows near real-time systems to be created efficiently.

This chapter is organized as follows: Section 3.2 presents a performance comparison between standard algorithms using STEREO images. Section 3.3 presents problems observed with the SURF and SIFT methods. An automated method to reduce the number of mismatches in corresponding points is described in Section 3.4.

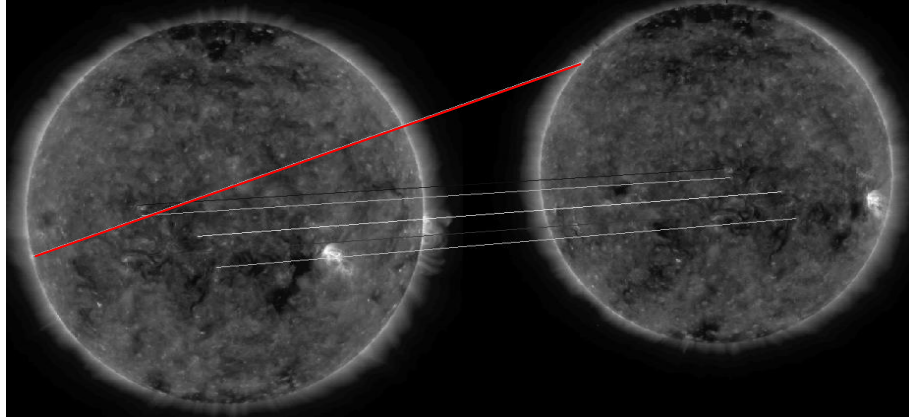
Experimental results are presented in Section 3.5. Conclusions on the results are provided in Section 3.6.

### **3.2 Comparisons between SIFT, SURF and KLT Algorithms**

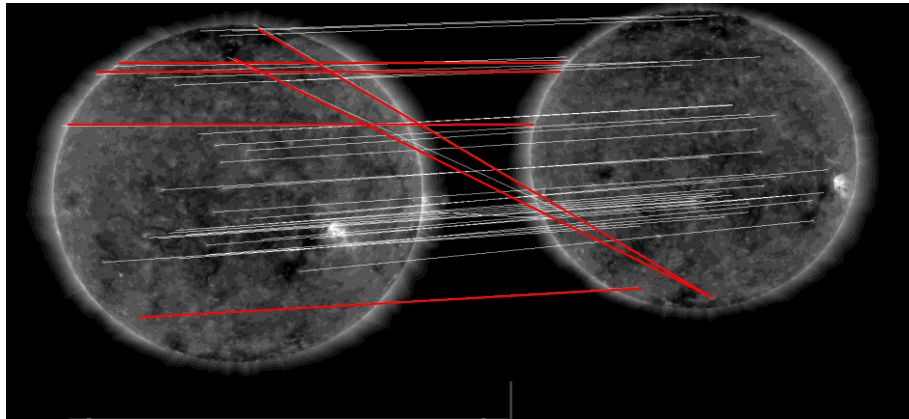
The implementations of the methods compared were collected from the following resources: SIFT from [93], SURF from [94] and KLT from [95]. The standard parameter values recommended by the authors are rarely optimal for any given image, but they work well on average collections of different images. The aims here are to optimise these parameter values to evaluate the performance of the corresponding methods. Consequently, the method that works best on the test images can be selected to generate the initial CPs. One of the novel aspects of this work is to enhance the quality of the CPs found initially.

The evaluation methods used to quantify the results are the Quality Factor (QF) and visual confirmation. The former is used to monitor the number of incorrect matches and minimize the number of mismatches which need to be visually detected. Following Ke [42], the performances of the different methods were measured by examining all pairs of key points. A true match occurs when the pair of points corresponds to the same physical location. This is determined by tables of ground truth data for labelled images as illustrated in Figure 3.1 and Figure 3.2.

Several STEREO images of different sizes taken from different views have been tested using the SIFT, SURF and KLT algorithms. From these tests it has been observed that the number of true matches increases with increasing algorithm threshold, but this also increases the number of mismatches. Examples of the performance of the SIFT algorithm at different thresholds ranging from 0.1 to 0.8 are shown in Table 3-1 and Table 3-2.



**Figure 3.1 SIFT (Threshold 0.50) is applied to the pair of STEREO images (Ahead and Behind) EUVI 171 Å taken at 20070905\_000600 with a separation angle of 29.169°. One mismatch indicated by red line is evident.**



**Figure 3.2 SURF is applied to a pair of images taken from STEREO spacecrafts at a separation angle of 29.169° and a threshold of 0.80, resulting in 37 CPs with 6 mismatches indicated by red lines. The calculation time was 0.925 s with the system described in the text.**

Another example used EUVI-171 Å STEREO images taken from Ahead and Behind spacecrafts at 19-05-2007 00:06:30. No matches were retrieved at the threshold of 0.10, and 308 CPs were retrieved at the threshold of 0.80 but 9 of them were mismatches.

The CPU time was measured for each test. The experiments were conducted on a PC computer with an Intel T93001 Dual core processor running at 2.50 GHz, 6 MB

Level 2 cache and 3 GB of main memory. As expected, the results show that the CPU time increases as the size of images increases. The threshold value has almost no effect on the time. For example, SIFT takes 5.91 s and 5.88 s to be applied to a pair of STEREO EUVI images of size 792×792 pixels for thresholds 0.1 and 0.8 respectively. On the other hand, it requires 6.99 s and 6.97 s to be applied to a pair of STEREO of Ahead and Behind images of sizes 920×920 and 914×914 pixels respectively for thresholds of 0.4 and 0.8 respectively.

The thresholds recommended by the authors of SIFT, SURF and KLT are 0.7, 0.8 and 10.0 respectively. However, the experiments on pairs of STEREO images revealed that SIFT provides correct matches with sufficient numbers of CPs with a threshold of 0.6. For example, for a pair of STEREO Ahead and Behind images at the separation angle of 8.554°, one mismatch was observed from a total of 170 CPs. The number of mismatches increases gradually above this threshold value as illustrated in Table 3-1 and Table 3-2 which present the SIFT performance on STEREO image pairs at the two separation angles 8.554° and 16.780°. In another example, for STEREO EUVI 195 Å image pairs taken with Ahead spacecraft at 19-May- 2007 00:06:30 UT and Behind spacecraft 30 minutes later, there are no mismatches at the threshold 0.6 but the number of mismatches increases gradually with greater threshold values. The same behaviour has been observed in all the experiments.

The same experiments are performed with the SURF and KLT methods; the best threshold for each method on the tested images is found to be 0.8 for SURF as shown in Table 3-4 and 10 for KLT (maximum residue). The KLT algorithm returned no matches when applied to pairs of images taken from the two spacecrafts. However, it sometimes provided matches on pairs of images taken from a same spacecraft with a small separation time (150 seconds) but with mismatches. The Harries detector also returned

poor results on the tested images. SIFT and SURF both provided better results than the KLT and Harries detector algorithms.

**Table 3-1 SIFT performance for a pair of STEREO EUVI-171 Å images taken at 19-05-2007 00:06:30 UT with sizes 731×731 for Ahead and 761×761 for Behind. The numbers of key points resulting from these images before the matching process are 702 and 620 respectively. The separation angle is 8.554°. A null value appears when the number of matches is less than 8 which are required by the 8-points algorithm to estimate the QF value. QF is estimated based on Equation 2-3.**

Threshold	Number of matches provided	Number of correct matches	Number of mismatches	QF
0.10	0	0	0	Null
0.20	2	2	0	Null
0.30	20	20	0	1.97
0.40	65	65	0	2.10
0.50	124	124	0	1.22
0.60	170	169	1	3.26
0.70	256	232	4	8.90
0.80	308	299	9	15.06

**Table 3-2 SIFT performance for a pair of STEREO EUVI-171 Å image taken from Ahead and Behind spacecraft at 05-07-2007 00:06:30 with sizes 792×792 pixels. The numbers of extracted key points from each image are 623 and 576 respectively. The separation angle is 16.780°.**

Threshold	Number of matches provided	Number of correct matches	Number of mismatches	QF
0.10	0	0	0	Null
0.20	0	0	0	Null
0.30	3	3	0	Null
0.40	9	9	0	0.5
0.50	32	32	1	2.08
0.60	50	45	5	5.68
0.70	85	77	8	24.66
0.80	137	116	21	59.57

The results of the comparisons of SIFT and SURF presented in Table 3-3 and Table 3-4 produced two observations: firstly, SURF is always faster and sometimes more accurate than SIFT and KLT. This result was mentioned in [47] for a different



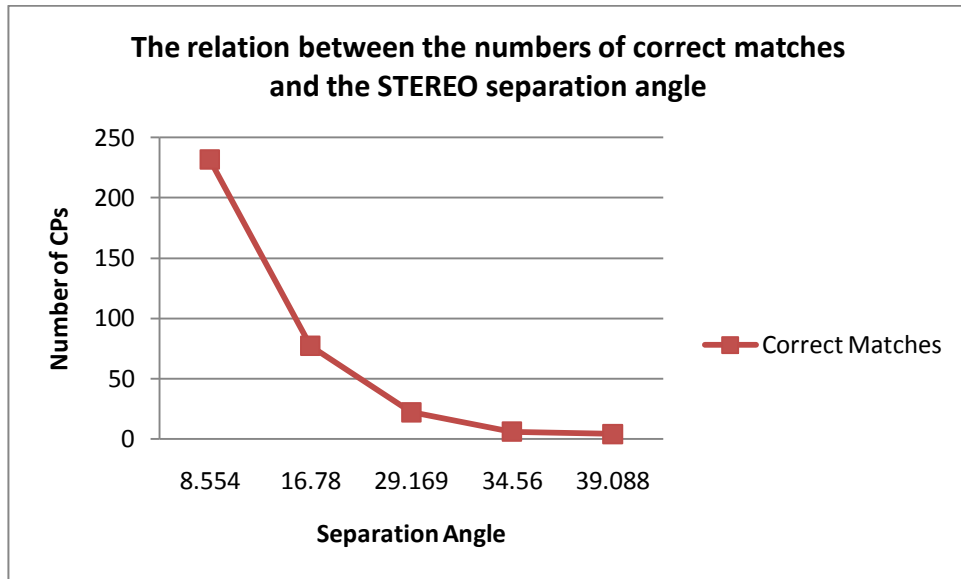
dataset. SIFT provided satisfactory results but was slower and provided fewer CPs compared with SURF. The second observation is that the number of correct matches decreases as the separation angle between the two spacecrafts increases and vice versa as demonstrated in Figure 3.3.

**Table 3-3 The performance of SIFT on several pairs of images taken from STEREO Ahead and Behind at different separation angles. The standard SIFT threshold of 0.7 is used. It can be seen that the numbers of matches decreases with increasing separation angle.**

Date/Time of capture DD-MM-YY SS:MM:HH	Separation Angle ( $\theta$ )	Number of matches provided	Number of correct matches	Number of mismatches	QF
19-05-2007 00:06:30	8.554	236	232	4	8.9
05-07-2007 00:06:00	16.780	85	77	8	24.66
05-09-2007 00:06:00	29.169	30	22	8	31.52
05-10-2007 00:06:00	34.560	8	6	2	Null
05-11-2007 00:06:00	39.088	13	4	8	Null

**Table 3-4 The performance of SURF on several pairs of images taken from STEREO Ahead and Behind at different separation angles. The standard SURF threshold of 0.8 has been used.**

Date/Time of capture DD-MM-YY SS:MM:HH	Separation Angle ( $\theta$ )	Number of matches provided	Number of correct matches	Number of mismatches	QF
19-05-2007 00:06:30	8.554	133	133	0	3.80
05 -07-2007 00:06:00	16.780	83	81	2	5.55
05-09-2007 00:06:00	29.169	35	32	5	22.83
05-10-2007 00:06:00	34.560	25	7	18	75.32
05-11-2007 00:06:00	39.088	25	5	20	80.20



**Figure 3.3** The variation of numbers of correct matches with separation angle for the SIFT method applied to pairs of STEREO images.

### 3.3 The observed problems

This section describes several experiments performed to automatically find the CPs within two images. The SIFT and SURF algorithms are designed to be insensitive to scale, translation, and rotation variations as demonstrated in [40], [47], [7] and [41]. However, the experiments with STEREO images revealed several problems which are listed below.

Sometimes the SIFT and SURF algorithms provide redundant corresponding points as illustrated in Figure 3.4. In this figure, the SIFT algorithm provides 20 corresponding points, but three of them, labelled A, refer to the same location. Unchecked, this could affect the performance of functions that require a minimum number of CPs, such as the 8-point algorithm and RANSAC (7-point algorithm).

With both SIFT and SURF, sometimes more than one point in the left image corresponds to the same point in the right image as illustrated in Figure 3.4 by rows labelled B; these are called conflicting points.

The default parameter values recommended by the authors of the previous works

may not be optimal for particular types of images. For example, using the default parameters sometimes provides too many correspondences which are mismatches. An example showing false CPs after using the default threshold for SIFT is shown in Figure 3.5. A methodology to reduce mismatches is presented in Section 3.4.

	CPs in the left image		CPs in the right image	
a. Redundant CP's.	292.440000	319.480000	318.610000	318.390000
	292.440000	319.480000	318.610000	318.390000
	292.440000	319.480000	318.610000	318.390000
	225.960000	314.900000	254.670000	310.530000
	435.230000	417.500000	446.640000	405.820000
	177.870000	392.470000	208.880000	387.260000
	246.760000	316.870000	274.610000	316.030000
	552.650000	373.910000	545.090000	365.340000
	389.160000	287.780000	404.000000	288.720000
	510.520000	386.870000	510.790000	377.620000
	480.510000	380.220000	485.160000	371.150000
b. Two CP's correspond to the same point in the right image.	287.300000	338.490000	313.370000	335.240000
	415.310000	526.360000	423.250000	505.380000
	220.050000	410.400000	248.980000	402.720000
	220.090000	410.540000	248.980000	402.720000
	168.330000	411.440000	199.440000	405.490000
	198.490000	401.780000	228.020000	395.750000
	346.000000	339.130000	367.970000	336.490000
	251.860000	346.920000	280.410000	343.960000
	206.020000	300.200000	234.210000	303.210000

Found 20 matches.

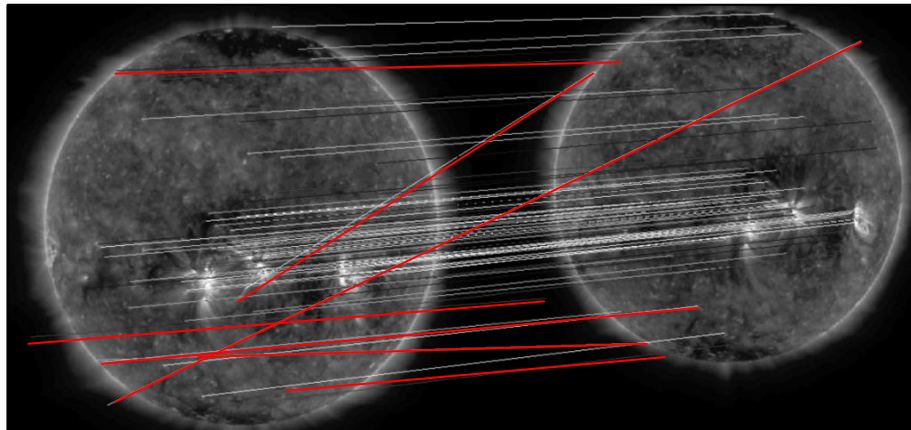
**Figure 3.4 CPs generated from SIFT applied on a pair of STEREO Ahead and Behind images taken at 09 May 2007 000630 UT. Redundant CPs are observed. (A) Triply redundant CPs. (B) Two different CPs correspond to the same point in the right image.**

### 3.4 An automated method for mismatches reduction

Due to the effects of mismatches in image registration resulting in artefacts in super resolution images [96] and distortions in 3D views (see Section 3.5), it is very important to understand the main causes of mismatches as discussed in Subsection 3.3, in order to eliminate them. This section describes an automated algorithm that has been developed to generate sets of high-quality CPs for pairs of STEREO images, which is called STEREO-CPs.

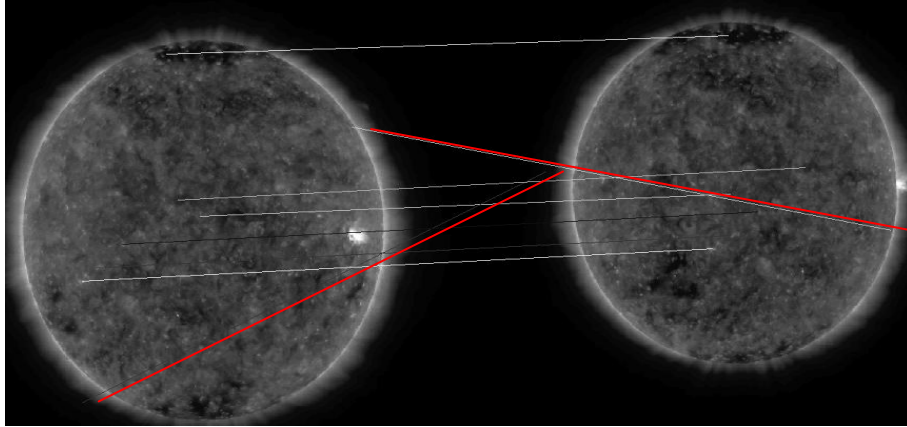
The experiments revealed that the standard thresholds of SIFT and SURF rarely worked well on the test images. Figure 3.5 and Figure 3.6 show two examples of

applying SIFT using its default threshold on pairs of STEREO images. It was noted that the number of mismatches increases with increasing threshold value for both SIFT and SURF methods. Decreasing the threshold value decreases the number of mismatches and also the number of correct matches, perhaps causing insufficient number of high-quality CPs to be obtained. A method to decrease the number of mismatches by integrating the SIFT and SURF algorithms is proposed. The SURF algorithm is used to generate initial CPs and the number of mismatches is reduced by applying the SIFT method to the areas surrounding every pair of initial points.



**Figure 3.5 SIFT algorithm (Threshold = 0.70) is applied on STEREO pair images (from Ahead and Behind) EUV 171 at a separation angle of 16.78°. Several mismatches indicated by red lines are visible.**

This section is organized as follows: tackling the redundant or conflicting CP pairs is presented in Subsection 3.4.1. In Subsection 3.4.2, the mismatches are reduced by method using SIFT after SURF then thresholding the median of difference of pairs of coordinates.



**Figure 3.6** Two mismatches (indicated by red lines) from applying SIFT to a pair STEREO images are visible. The SIFT threshold is 0.7, the images were taken at 05-10-2007 00:06:00 and  $\theta$  is  $34.56^\circ$ .

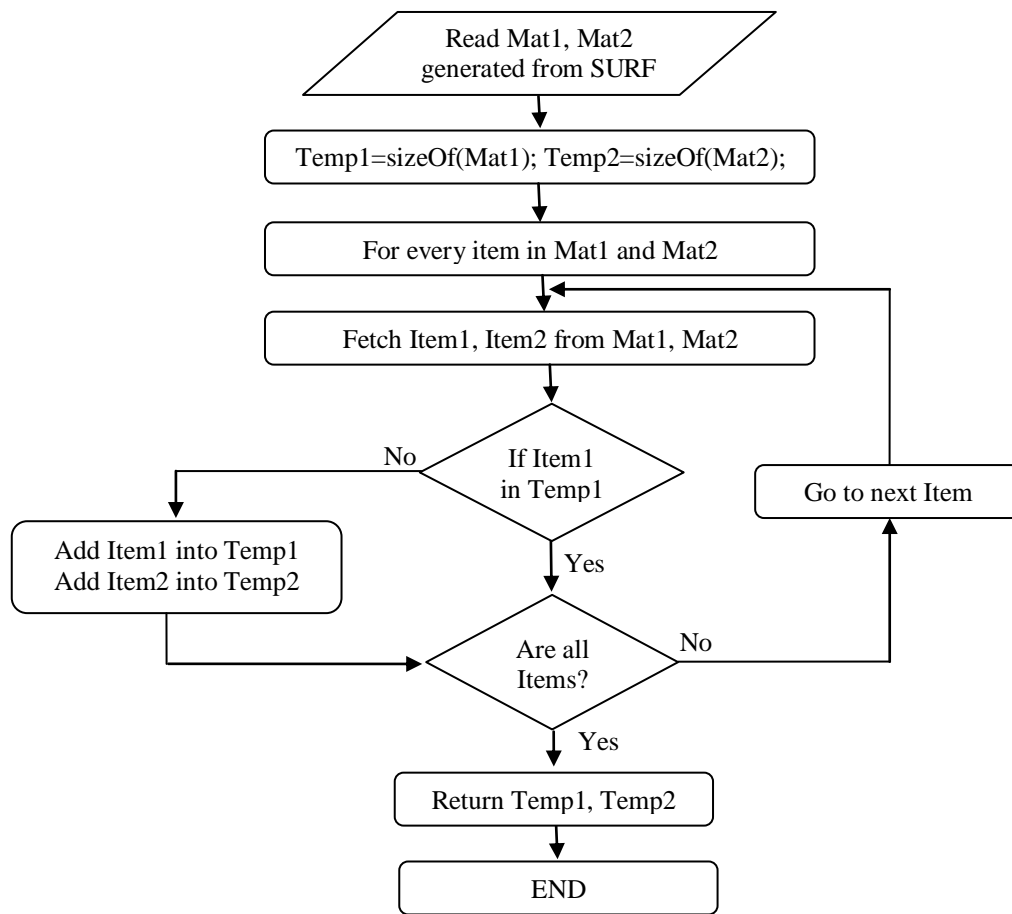
#### ***3.4.1 Removing redundant and conflicting CPs***

Redundant and conflicting CPs in the initial set generated by the SURF algorithm are removed by the algorithm shown as a flow chart in Figure 3.7.

#### ***3.4.2 Mismatch elimination***

The number of generated mismatches can be minimized by discarding the extreme deviations from the median of all the pairs coordinates. This can be achieved by going through the following steps:

- The values of  $\Delta X$  and  $\Delta Y$  can be calculated by applying the equations 3-1 and 3-2.
- The averages of  $\Delta X$  and  $\Delta Y$  ( $\overline{\Delta X}$  and  $\overline{\Delta Y}$ ) are calculated by applying equations 3-3 and 3-4.
- The medians  $\mu_x$  and  $\mu_y$  for  $\overline{\Delta X}$  and  $\overline{\Delta Y}$  respectively are founded by applying equations 3-5 and 3-6.



**Figure 3.7** Flow chart diagram for removing redundant CPs in the results from SIFT and SURF algorithms.

- The differences of  $\alpha_x$  and  $\alpha_y$  with their medians ( $\mu_x$  and  $\mu_y$ ) are calculated by applying the equations 3-7 and 3-8.
- Then outliers are detected if  $\alpha_x$  is greater than the threshold\_x defined in Equation 3-9, or  $\alpha_y$  exceeds the threshold\_y defined in Equation 3-10, as specified in Equation 3-11.

The thresholds are used to identify the mismatches from the distribution of true matches, by discarding the pairs of points that have extreme deviation from the median. It was found that these thresholds work well in several experiments with pairs of STEREO images. A flow chart of this method is shown in Figure 3.8. The example in **Table 3-5** uses the CPs for pairs of STEREO Ahead and Behind images that are shown

in Figure 3.9, with outliers indicated in red texts in columns  $\alpha_y$  and  $\alpha_x$ . Another example is the three mismatches clearly visible in Figure 3.10 and represented by a plot diagram as shown in Figure 3.11.

$$\Delta x = |\sum X1_i - \sum X2_i| \quad (3-1)$$

$$\Delta y = |\sum Y1_i - \sum Y2_i| \quad (3-2)$$

$$\overline{\Delta x} = \frac{\Delta x}{\sum \Delta x} \quad (3-3)$$

$$\overline{\Delta y} = \frac{\Delta y}{\sum \Delta y} \quad (3-4)$$

$$\mu_x = \text{Median}(\overline{\Delta x}) \quad (3-5)$$

$$\mu_y = \text{Median}(\overline{\Delta y}) \quad (3-6)$$

$$\alpha_x = |\mu_x - \overline{\Delta x}| \quad (3-7)$$

$$\alpha_y = |\mu_y - \overline{\Delta y}| \quad (3-8)$$

$$\text{ThresholdX} = \left( \text{Median}(\alpha_x) + \frac{\text{Max}(\alpha_x) - \text{Min}(\alpha_x)}{2} \right) \quad (3-9)$$

$$\text{ThresholdY} = \left( \text{Median}(\alpha_y) + \frac{\text{Max}(\alpha_y) - \text{Min}(\alpha_y)}{2} \right) \quad (3-10)$$

$$\text{Outliers} = \left\{ \begin{array}{l} \alpha_{x_i} > \text{ThresholdX} \\ \text{or} \\ \alpha_{y_i} > \text{ThresholdY} \end{array} \right\} \quad (3-11)$$

where:

N: Number of CPs.

X1, X2: X-axis coordinates for the CPs in the left and right images respectively.

Y1, Y2: Y-axis coordinates for the CPs in the left and right images respectively.

$\overline{\Delta x}$ : Percentage difference in the pair X-coordinates for the CPs.

$\overline{\Delta y}$ : Percentage differences in the pair Y-coordinates for the CPs.

$\mu_x, \mu_y$ : Medians of Diffx and Diffy respectively.

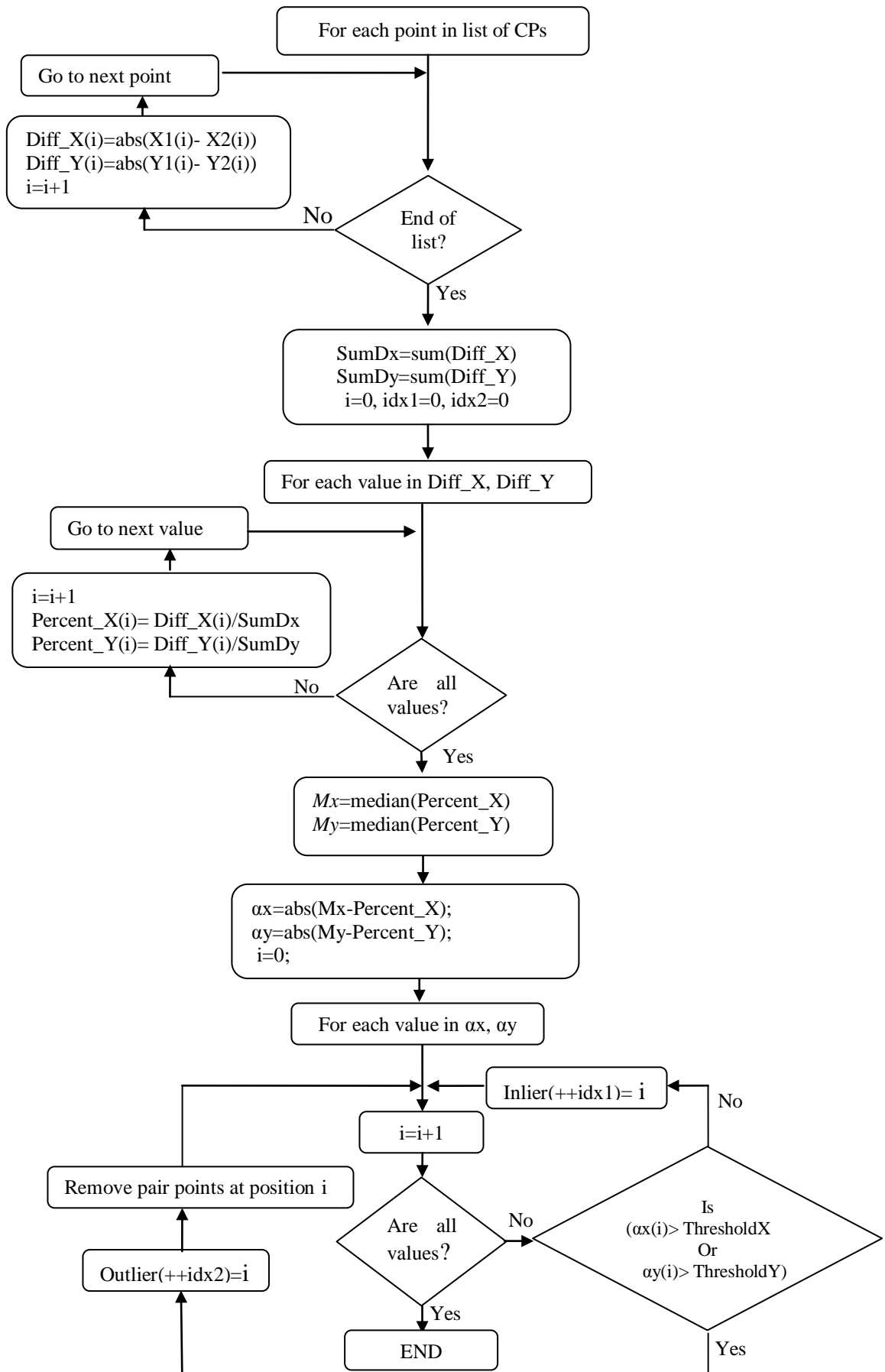
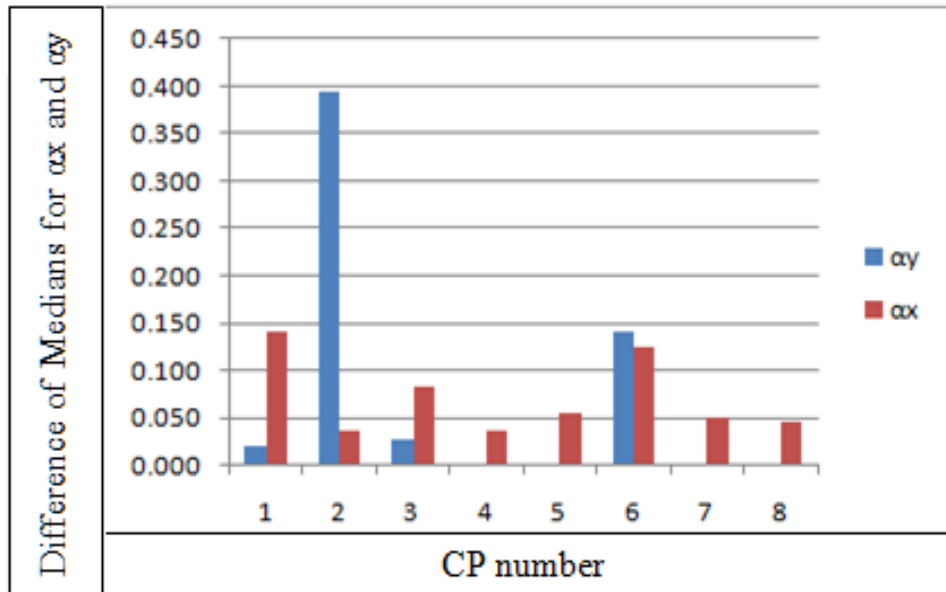


Figure 3.8 The flow chart diagram for reducing mismatches that could result from the SURF method.

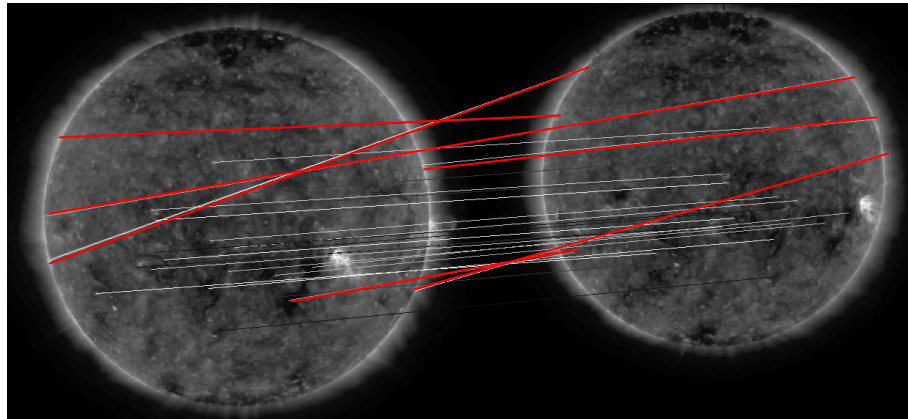


**Table 3-5 Mismatches reduction performed on the pair of images shown in Figure 3.6. The mismatches are marked in red colour for all CPs that have  $\alpha_y$  or  $\alpha_x$  greater than threshold-y and threshold-x respectively.**

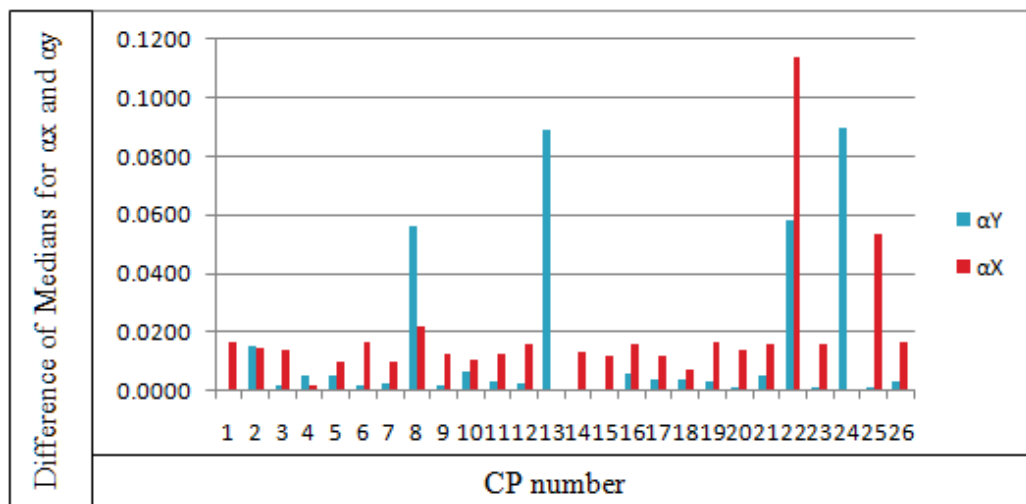
T-True	EUVI Ahead spacecraft		EUVI Behind spacecraft		Differences in coordinates of CPs					
	Y1-axis	X1-axis	Y2-axis	X2-axis	\Delta Y	\Delta X	\Delta Y%	\Delta X%	$\alpha_y$	$\alpha_x$
F	466.22	415.60	428.82	424.27	37.40	8.67	4.44%	0.91%	0.020	<b>0.141</b>
F	776.82	209.27	391.28	102.71	385.54	106.56	45.81%	11.23%	<b>0.394</b>	0.037
T	196.30	357.42	165.42	421.28	30.88	63.86	3.67%	6.73%	0.027	0.082
T	438.73	377.61	385.11	555.26	53.62	177.65	6.37%	18.71%	0.000	0.037
T	512.47	279.78	458.72	473.90	53.75	194.12	6.39%	20.45%	0.000	0.055
F	317.09	681.98	489.19	705.24	172.10	23.26	20.45%	2.45%	0.140	<b>0.125</b>
T	552.38	234.90	498.28	425.63	54.10	190.73	6.43%	20.09%	0.000	0.051
T	574.12	209.77	519.84	394.17	54.28	184.40	6.45%	19.43%	0.000	0.045
<b>Total</b>					<b>841.67</b>	<b>821.53</b>	<b>100%</b>	<b>100%</b>		
<b>Average</b>							<b>12.50%</b>	<b>12.50%</b>		
<b>Median</b>							<b>6.41%</b>	<b>14.97%</b>	<b>0.010</b>	<b>0.053</b>
<i>Threshold-Y and Threshold-X</i>									<b>0.206</b>	<b>0.104</b>



**Figure 3.9 Plot of differences of medians versus CP numbers generated after applying the SIFT algorithm on the pair images represented in Table 3-5. Outliers are identified as having  $\alpha_x$  greater than threshold-X or  $\alpha_y$  greater than threshold-Y.**



**Figure 3.10** Several mismatches resulting from after applying SIFT on a pair of STEREO images. The standard SIFT threshold was used. The separation angle is  $29.169^\circ$ .



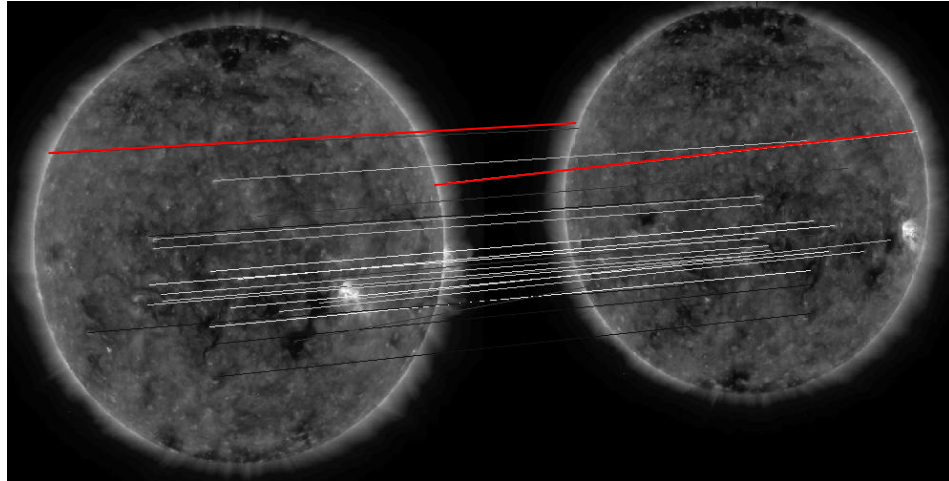
**Figure 3.11** Plot of differences of medians versus CP numbers that were generated after applying the SIFT algorithm on the pair of STEREO images that is shown in Figure 3.10.

The mismatches are identified as having  $\alpha_x$  greater than the estimated threshold-X of 0.0164 and  $\alpha_y$  greater than threshold-Y of 0.0137. Seven CPs were identified as mismatches from a total of 26 CPs.

### 3.4.2.1 Mismatches reduction using a SIFT after SURF method

The previous algorithm still has the drawback that the displacements of some mismatches may be similar to some correct matches as illustrated in Figure 3.12. However, the number of mismatches can often be reduced by using the SIFT algorithm to match the area surrounding each CP provided by the SURF algorithm. SURF is used

to generate the initial CPs based on the results of the comparisons of SIFT, KLT and SURF presented in Section 3.2 which revealed that SURF is always faster and most times provides more accurate CPs than SIFT and KLT on the tested images. The results are evaluated by estimating QF values and the visual assessments on labelled images.

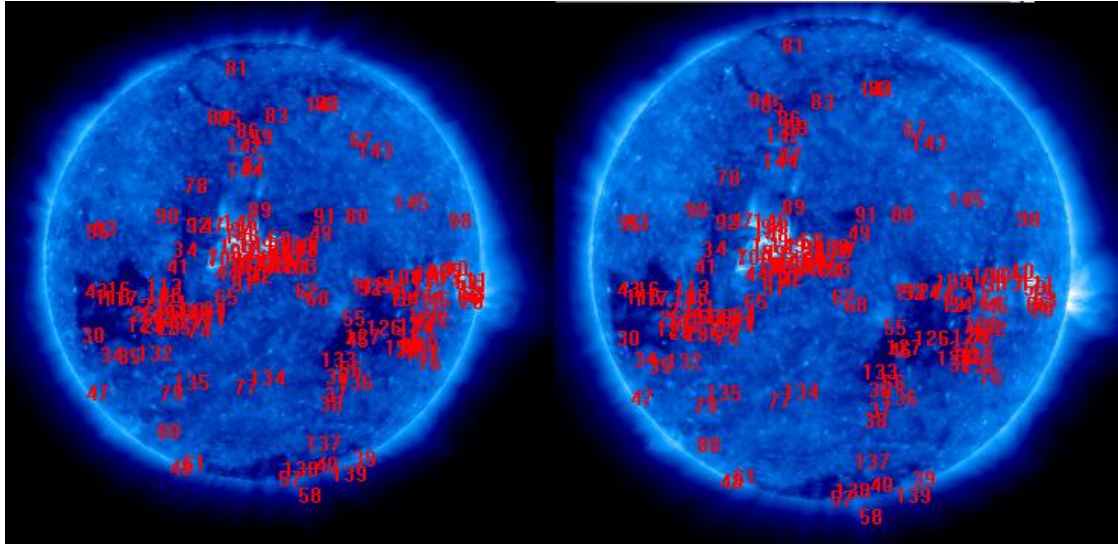


**Figure 3.12 Result from applying the median based method after the SIFT algorithm. The matches before removing the mismatches are shown in Figure 3.10. The remaining mismatches which are indicated by red lines have similar displacements to the correct matches.**

Several experiments have been performed to discard mismatches that result after applying the SURF method to pairs of images. The results have shown that the number of acceptable CPs decreases as the separation angle between the two STEREO spacecrafts increases and vice versa. In most cases the QF value is improved after verification by the SIFT method.

The SURF method was applied with the recommended threshold value to several pairs of STEREO images taken from the Ahead and Behind spacecrafts at different separation angles. At a separation angle of  $8.554^\circ$ , the QF value was equal to 3.85 with a total of 157 CPs using the SURF method. The QF value improved to 1.48 with total of 150 CPs after applying the SIFT method to the areas surrounding the 157 pairs CPs as shown in Figure 3.13. This experiment was repeated with four larger

separation angles with the results shown in Table 3-6. The QF value is improved for most of the experiments, but some mismatches are still associated with the output. For this reason a third technique, combining the previous two methods to minimise the number of mismatches, is presented in the next subsection.



**Figure 3.13** CPs from the SURF algorithm are verified using the SIFT method to discard mismatches. The SURF and SIFT thresholds are 0.7 and 0.6 respectively. The separation angle is  $8.554^\circ$ . The QF value for the resulting CPs improved from 3.85 to 1.48.

### 3.4.2.2 *Integration of SIFT after SURF and the median based methods*

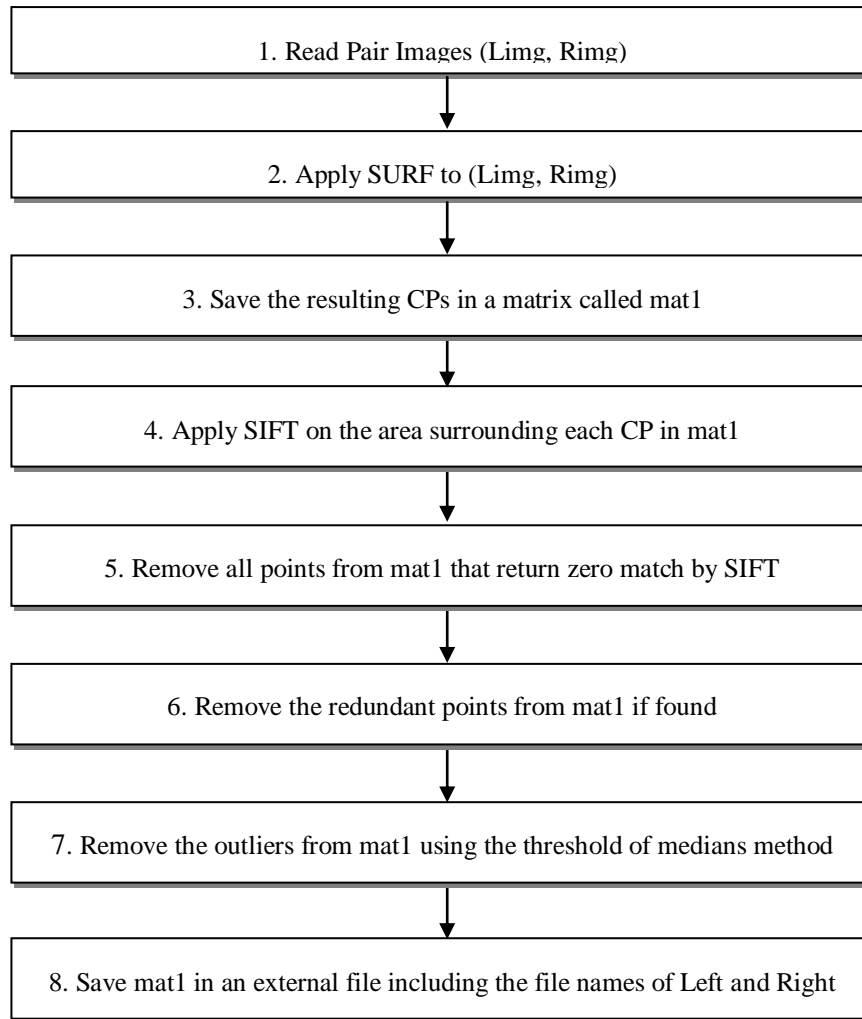
The integration of SIFT after SURF and the median based methods are described by the flowchart shown in Figure 3.14. The input is a pair of images from which the initial set of CPs is extracted by the SURF method. The CPs are verified by SIFT after SURF using surrounding area of size  $100 \times 100$  centred around each pair of candidate CPs. This size has been found to provide enough information about the neighbouring pixels. If SIFT returns no matches for a candidate CP then this CP is discarded. Then the final stage reduces the number of mismatches by discarding CPs which satisfy the thresholding criteria that is described in Subsection 3.4.2.

**Table 3-6 Results from applying SIFT after SURF to STEREO image pairs for five different separation angles. QF is used to show the improvements in the quality of the CPs before and after SIFT validation. The QF values were improved in all experiments except where insufficient number of CPs remained for the 8-points algorithm as shown by the null indicator.**

Number and separation		Image size (width x height)		SURF results before Validation		After SIFT validation		Date/ Time DDMMYYYY SSMMHH UT Comment
	Angle°	Left	Right	Number of CPs	QF	Number of CPs	QF	
1	8.554	761x761	731x731	133	3.85	129	1.48	19052007 000630.
2	16.780	792x792	792x792	83	5.59	74	2.03	05072007 006000.
3	29.169	778x778	748x748	35	22.83	24	7.23	05092007 000600.
4	34.560	920x920	914x914	25	75.32	7	Null	05102007 000600. Four correct matches and three mismatches.
5	39.088	920x920	914x914	25	80.20	2	Null	05112007 000600. No mismatches.

### 3.5 Experimental results

As indicated before, SURF provides better overall performance on the STEREO test images, compared to SIFT and KLT, but also produces significant numbers of mismatches. Therefore, the comparison is based on the results from the SURF method. A comparison among the implementation of the SURF, RANSAC and STEREO-CPs methods is carried out and shown in Table 3-7. This table contains information obtained by averaging the results of more than 100 experiments. These experiments are carried out on test images with separation angles between 0.624° and 39.088° shown in Appendix A. The comparison criteria are based on averaging the QF values, (QF averages the LQb values where LQb is the largest perpendicular distance of a point to its associated epipolar line), and the number of accepted QF values.



**Figure 3.14 Structure of the STEREO-CPs algorithm for generating an improved set of correct matches.**

**Table 3-7 Performance comparison between SURF, RANSAC and the STEREO-CPs methods for experiments carried out on 102 pairs of test images.**

<b>Description</b>	<b>SURF</b>	<b>RANSAC</b>	<b>The STEREO-CPs</b>
Average of QF values	11.28	3.05	1.35
Average of LQb values	131.17	19.78	8.76
Qualified QF values (QF<1)	15.68%	40.19%	59.80%

The results show an improvement in the quality of the remaining CPs using both RANSAC and STEREO-CPs. The average QF value for all the experiments with SURF, RANSAC and the STEREO-CPs are 11.28, 3.05 and 1.35 respectively, so STEREO-CPs gives the best performance of the three methods. The averages of the LQb values are found to be 131.17, 19.78 and 8.76 for SURF, RANSAC and the STEREO-CPs,

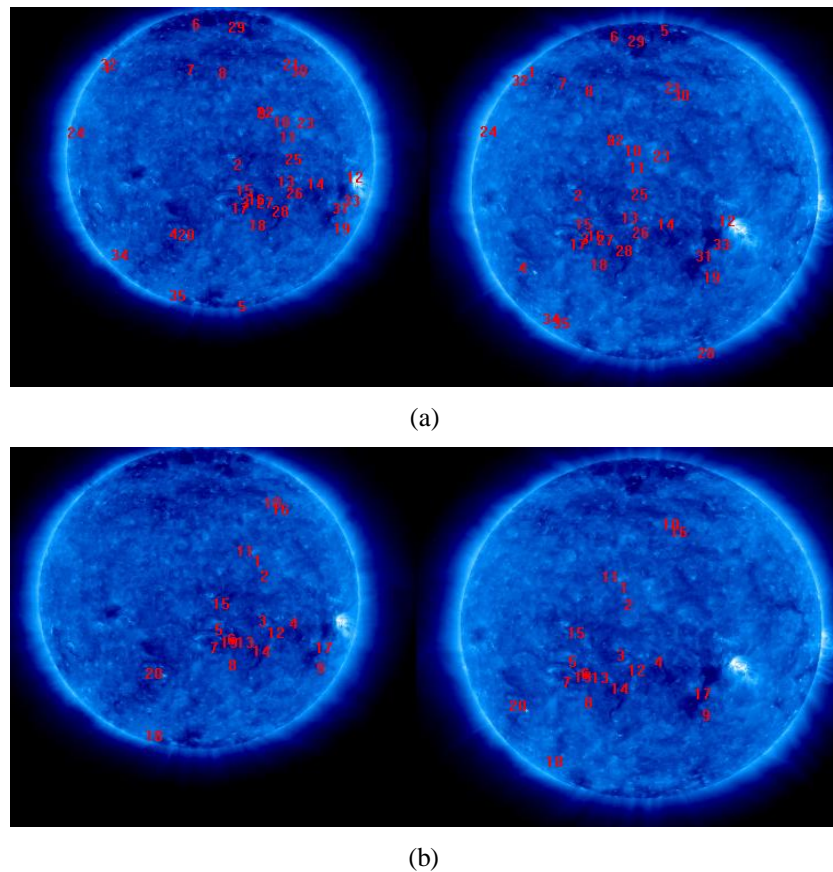
respectively, and again the best performance is from the STEREO-CPs method. Finally, the percentages of the accepted CPs which had QF values less than 1 are 15.68%, 40.19%, and 59.80% for SURF, RANSAC and the STEREO-CPs respectively. Again STEREO-CPs gave the best result of the three.

The null values that appear near the bottom of the Table shown in Appendix A represent 2.94% of the results from the experiments. These indicate that a QF value could not be calculated due to the number of CPs being less than the minimum of 8 needed by the 8-points algorithm used to calculate the fundamental matrix appearing in the definition of QF. This almost always happens when the pair of images is featureless and/or the separation angle is greater than about  $35^\circ$ .

The QF values for the pairs of STEREO images increase when the separation angle between the two spacecraft increases, and vice versa. For example, Figure 3.15 shows how the STEREO-CPs can be used to remove mismatches. For this figure the separation angle is  $29.169^\circ$ , the SURF and SIFT thresholds are 0.8 and 0.6 respectively. The QF value for the SURF's output is 22.83, and when the STEREO-CPs is applied it improves to 4.13. Several mismatches were generated after applying the SURF method as shown in Figure 3.15 (a). The STEREO-CPs method reduces the number of matches from 41 to 20 as shown in Figure 3.15 (b), taking 13.29 s of CPU time. The running time increases as the number of CPs increases and vice versa.

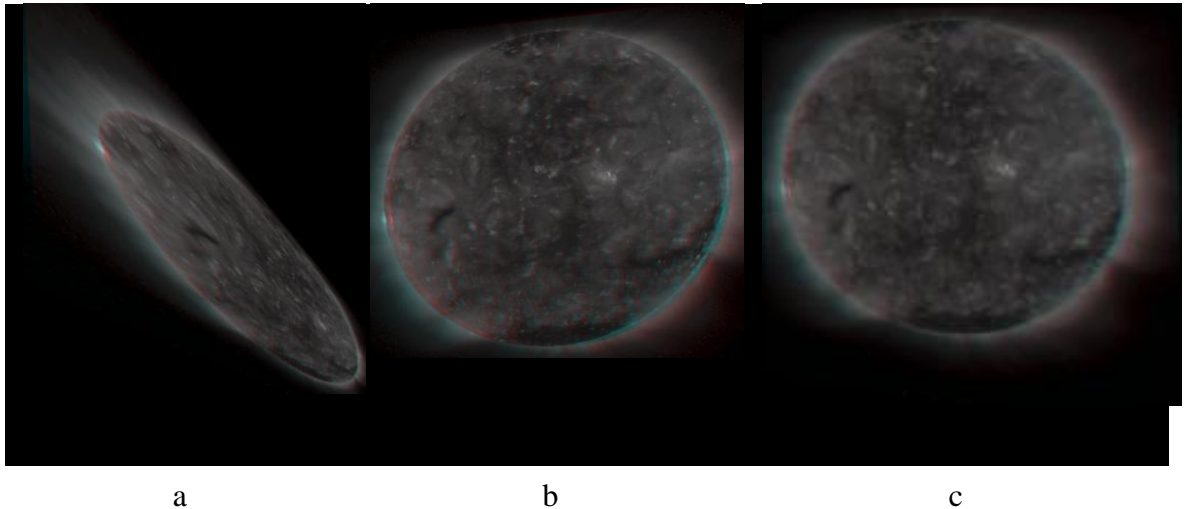
An example of a 3D anaglyph generated using the set of CPs obtained by applying SURF, RANSAC and the STEREO-CPs is introduced to show the resulting distortion generated by the rectification process from an unaccepted QF value, where the minimum distortion can be achieved at the smallest QF value. The same rectification method (called DRUI direct rectification algorithm for un-calibrated images proposed by Al-Zahrani [97]) is used to align the pair of images into the same plane. This

example is shown in Figure 3.16. This pair of EUVI 195 Å images was taken from STEREO Ahead and Behind on March 15, 2007 at 22:15:40 at a separation angle of 1.935°. SURF, RANSAC and the STEREO-CPs provided a set of CPs with QF values of 1.74, 0.46 and 0.35 respectively. The distortion that can be generated using CPs with unacceptable QF value is clearly observed in Figure 3.16 (a). The resulting distortion generated by the rectification process is less at the smallest QF values, as shown in Figure 3.16 (a, b and c).



**Figure 3.15: Comparison of before and after applying the STEREO-CPs method to pairs of STEREO images with a separation of 29.169°. (a) CPs from SURF method including 20 mismatches. (b) CPs remaining after the STEREO-CPs method with 1 mismatch remaining at the pair points numbered 18.**





**Figure 3.16** Anaglyphs generated from an uncalibrated pair of STEREO images, taken in March 15, 2007 at 22:15:40 UT, at a separation angle of  $1.935^\circ$ . The distorted image in the Figure (a) has been generated from a set of CPs extracted from SURF with QF value of 1.74. The Figure in (b) is generated from a set of CPs extracted after applying RANSAC with QF value of 0.46. The Figure in (c) is generated from a set of CPs extracted from the STEREO-CPs with QF value of 0.35.

### 3.6 Conclusions

This chapter presents a method called STEREO-CPs which aims to generate a set of CPs of sufficient quality and number. This technology will represent the corner stone for the advanced imaging applications, introduced in the chapters to follow, such as SR and 3D anaglyphs. To the author's knowledge, this is the first time a study like this has been conducted. This method can be applied to FITS and JPEG images. The work involved uncalibrated JPEG images to run on scenes other than the Sun and to provide efficient algorithms capable for use on near real-time based systems, whereas the FITS files of large size provided in single resolution ( $2048 \times 2048$  pixels) take about 3 days before they become available on the archive. These algorithms will be ready for use when the STEREO spacecrafts meet again. The potential of this technology is huge

because it can be used, for example, to generate anaglyphs, generate super resolution images, or for feature tracking.

One of the major advantages of STEREO-CPs is that it is fully automated and requires no prior information about the processed images. STEREO-CPs is the first CPs algorithm designed for STEREO. Compared to the standard methods in more than 100 experiments, the STEREO-CPs method is more discriminating, leading to significant improvements in the quality set of the CPs in pairs of STEREO images.

The most significant current limitation of the STEREO-CP method is that it works well at separation angles only up to  $35^\circ$ . This is adequate for the early part of the STEREO mission from March to July 2007 which is convenient for the creation of 3D solar images.

Currently, this work is being extended to find matches between images at larger angles, to represent other scenes rather than the Sun, and exploring ways to apply the ideas behind the STEREO-CPs to other related algorithms. STEREO-CPs is used to enhance the performance of the work in later chapters generating SR, anaglyphs and feature tracking for solar images. Creating true 3D solar images (anaglyphs from two different views) from a pair of STEREO images is feasible if the separation angle between the two spacecraft is small. However, STEREO-CPs can be used to create the anaglyph by combining two extreme UV images taken several hours apart by the same spacecraft. This can be possible if the sun has rotated around enough to create a sufficiently separated perspective to create 3D as illustrated on <http://stereo.gsfc.nasa.gov/gallery/item.php?id=3dimages&iid=50>, last access 17 Nov, 2010.

# CHAPTER FOUR

## 4 SUPER RESOLUTION FOR SOLAR IMAGES

### 4.1 Introduction

The fidelity of data gathered by cameras is limited by the quality of the optical and electrical components of the digital imaging system. In other words, the principal work of a camera is to measure scene intensities, and like any other measuring instrument, has a transfer function which may introduce information losses into the measurement process such as: bandwidth reduction and noise which are the common degradations found in imaging system. Therefore, the resulting images are often unable to completely capture the fine details in a scene. Furthermore, artefacts caused by radiation and electronic components can be produced in images from satellites. The sampled images captured by the detectors are limited in their resolution also resulting in the loss of some details from the real scene and possibly aliasing. For example, some details in the real scene projected onto the detector are smaller than the size of the individual cell in the detection array and are averaged out during the image captured process. These details will not be available for other image processing operations such as image sharpening and filtering tools offered by commonly available commercial imaging or graphics packages to be applied on. Finally, the output of digital cameras is often compressed with a JPEG encoder, generating quantization noise. If the coding rate of a JPEG

encoder is not high enough, there appear noticeable blocking and ringing artefacts in the decoded image [98]. Many of these problems could be reduced by using super resolution (SR) techniques.

Several existing SR tools, including Iterated Back Projection (IBP), Projection onto Convex Sets (POCS), Robust SR and QE SR, were tested by applying them on STEREO and SDO images. It was noted that most of these tools are complex and sometimes biased towards their own images, resulting in unsatisfactory results (visible artefacts) with STEREO and SDO images. This could be due to inaccurate solar image registration, failure to recover high resolution details from the tested images and/or inappropriate image filtration. Furthermore, it is clear that applying SR on solar images is poorly offered by a single imaging platform especially designed for solar images. In this thesis, a practical study on real solar images taken by the STEREO and SDO spacecrafts is performed to tackle these problems.

This chapter is concerned with using solar images taken with small shifts between them by a single camera to produce SR. The aims of this, particularly in this thesis, are to provide finer details than are available in the individual JPEG images provided by STEREO and SDO missions, constructing HR enlargements or finer view from a set of LR images. In contrast to image interpolation (e.g., [99] and [100]), new HR details are added to the reconstruction. It has been found that SR can be achieved efficiently from compressed images provided by STEREO and SDO at high cadence rate. SR methods to remove JPEG artefacts are presented in [98] and [101] by reconstructing a map from low quality images (LR or JPEG encoded images) to target high quality images.

No prior information about the camera, such as the locations, focal length, PSF, etc, are assumed and any information needed are gathered from the images themselves, which make the presented SR approach applicable to scenes other than the Sun. Solar

images have been selected to apply this on because of the availability of LR set of images with small shifts (when the cadence rate is high). The method of achieving SR proposed in this chapter includes three steps: firstly, registration of the solar images is achieved by fusing the information derived from multiple, sub-pixel shifted images; secondly, application of a special interpolation technique by projecting and selecting the most appropriate pixels to construct the high resolution grid; and thirdly a smoothing method to smooth the output data.

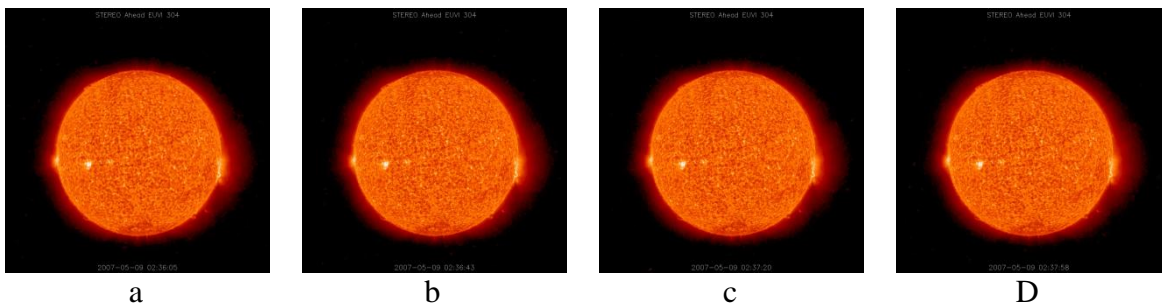
The remaining sections are organized as follows. In Section 4.2 a method to register solar images is introduced. In Section 4.3, a method projecting all LR images onto a HR grid and interpolating only certain excluded pixels is presented. In Section 4.4, a smoothing method based on Gaussian filtering is described. In Section 4.5, three types of objective measurements and benchmark evaluations, to provide quantitative comparisons, are explained. Several experimental results and evaluation with respect to the objective and subjective quality measurements are presented in Section 4.6. Finally, summary and conclusions are presented in Section 4.7.

## **4.2 Registration**

SR algorithms using multiple images are improved by accurate image registration [76]. The ideal scenario, is for the image registration operation to know the displacement between images before the alignment process. With STEREO images, small displacements result from small time intervals between images. STEREO-A and STEREO-B satellites both capture sequences of images of the Sun from different viewpoints. In this research, these images are retrieved automatically with the closest time intervals available. For example a single SECCHI EUVI 17.1 nm image of the Sun, taken by STEREO-A on May 09, 2007 at 02:36:05 UT (hh:mm:ss) is followed by three at 02:36:43, 02:37:20, and 02:37:58 respectively. These images are shown in

Figure 4.1 with an artificial orange colour. It is known that many image features do not change much between images captured at high cadence rates. However, taking images with a low cadence rate will increase the possibility for multiple scale dynamic regions to grow or shrink between images. In this case, improving these features is difficult because of the information loss from the real scene which is viewed in the reference image.

The registration method for solar images introduced in this chapter estimates the shift between images by searching for the most prominent features with little change based on the short time of cadence with respect to a reference image, such as AR or local maxima points. Recognition of ARs is performed by thresholding the differences between neighbouring pixels as explained in subsection 4.2.1. The locations of ARs in the set of LR images are used to estimate the shifts in location with respect to the reference image. The steps to estimate the shifts for solar images are summarised as follows:



**Figure 4.1** Images of the Sun, taken by the SECCHI EUVI 304 on STEREO-A on May 09, 2007. (a), (b), (c) and (d) were taken at 02:36:05, 02:36:43, 02:37:20, and 02:37:58 UT respectively.

- Select the reference image from STEREO-A or STEREO-B satellites and retrieve the nearest set of LR images to the reference image.
- Detect and extract the location coordinates for the centre points of active regions

(see subsection 4.2.1) in each LR image required in the matching process.

- Match the detected regions in the set of LR images with respect to the reference image. Two matching methods are presented in this work. The first uses correlation<sup>11</sup>, by looking for pixels within predefined windows of size 13×13 (this value makes the method work best on the tested images) that are maximally correlated with other windows surrounding each AR centre point. Only pixel coordinates that correlate mostly with each other by the searching window are returned. To maximise the speed of search, a radius of value equals to the greater width or height of the area surrounding the detected AR in the reference image is defined for matching pixels. This area is useful because there is a little disparity between neighbouring images captured at high cadence rates; hence, based on experiments, the shift is not expected to exceed it. This method is relatively simple and fairly fast, but has the limitations that it works well only on solar images with small shifts, and is sensitive to changes in illumination and scale. The second approach uses the CPs resulting from the STEREO-CPs method by finding the  $\Delta x$  and  $\Delta y$  between the resulting correspondences. The STEREO-CPs method proceeds slower than the previous method but can overcome its limitations (see Chapter 3). The results of using both methods on the test images were almost identical because the shift is quite small.
- Estimate the horizontal and vertical shifts  $a_i$  and  $b_i$  by finding the difference between these locations with respect to the reference image.
- Translate the pixels for all LR images toward the reference image based on the estimated shifts, in order to align all LR images in same plane before the

---

<sup>11</sup> <http://www.csse.uwa.edu.au/~pk/Research/MatlabFns/#match>

projection process.

#### 4.2.1 Active Regions Detection

AR detection is applied by recognizing the pixels that are related to the AR based on the difference in intensities between neighbouring pixels as shown in Figure 4.2, where 3D plot diagrams have been used to emphasise the difference between quiet regions (Figure 4.2b with its 3D plot diagram in Figure 4.2d) and active regions (Figure 4.2c with its 3D plot diagram in Figure 4.2e) of the Sun. The presented technique first accepts images or video as input. If the input is a video then segmentation into a stream of images is performed first. A flow chart describing the algorithm is shown in Figure 4.3. The algorithm tries to find the maximum difference between neighbouring pixels based on (Equation 4-1).

$$\text{maxdiff} = (p1 + p2) - (p3 - p4) \quad (4-1)$$

where

$$p1 = \text{pixel}(x, y)$$

$$p2 = \text{pixel}(x + 1, y)$$

$$p3 = \text{pixel}(x, y + 1)$$

$$p4 = \text{pixel}(x + 1, y + 1)$$

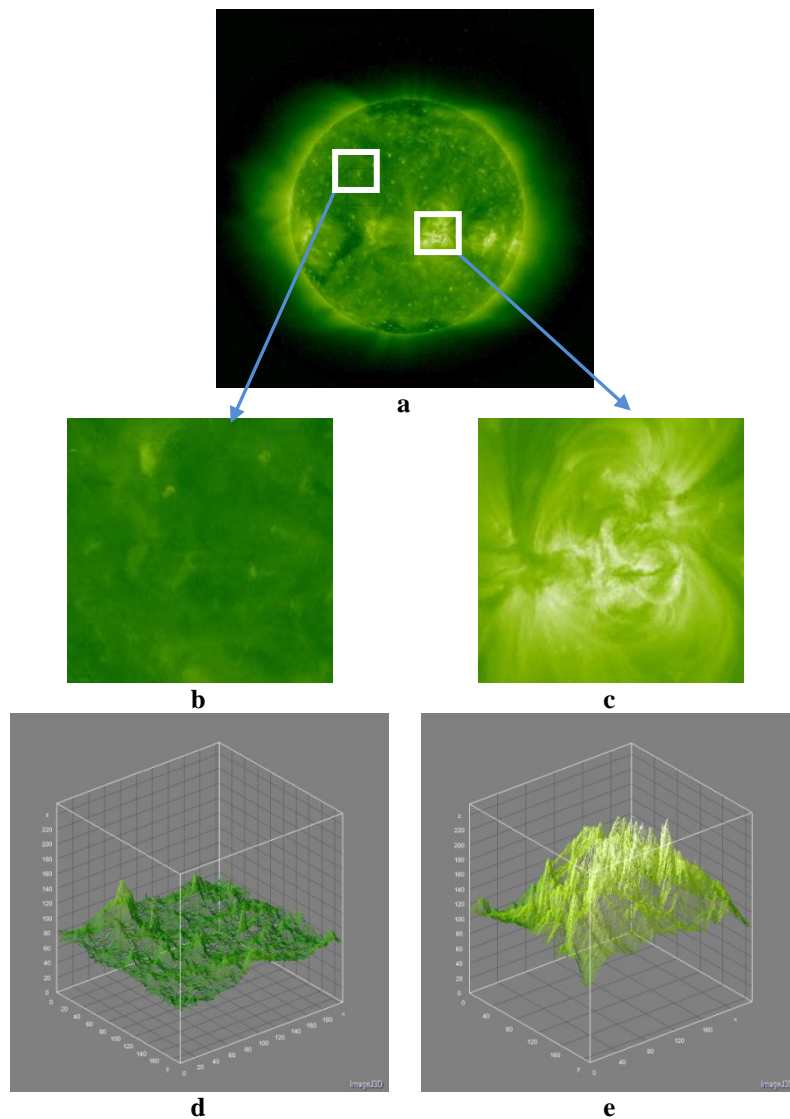
A threshold value is used to determine the intensity range for the pixels of AR; the best value is estimated at 65% based on the intensities determination of the quiet region versus AR of the Sun (see Figure 4.2). The AR pixels are represented as in (Equation 4-2).

$$\text{ARpixels}(x, y) = \begin{cases} \text{pixel}(x, y) & \text{if } \text{pixel}(x, y) > \text{maxdiff} * \text{Threshold} \\ \text{else} \\ \text{setColor(Black)} \end{cases} \quad (4-2)$$

The final part is displaying the shapes of ARs extracted from the red or blue



channel in which the AR is most prominent depending on the wavelength as shown in Table 4-1. In Figure 4.4, the output after thresholding and extracting the blue channel from EUVI 195 is shown in Figure 4.4c, and the red channel from EUVI 171 is shown in Figure 4.4d. The shapes of the detected ARs are enlarged for clarity and displayed as shown in Figure 4.4(e and f). The system determines the type of wavelength by requiring the user to select it before starting the detection process.



**Figure 4.2** Determination of the quiet region versus AR of the Sun, whereas the highest pixels count from a 3D plot surface of a “flattened” solar image. (a) Full-disk solar image, (b) Quiet region cropped image, (c) AR cropped image, (d) Interactive 3D surface plot for the sub-image in (b), and (e) Interactive 3D surface plot for the sub-image in (c).

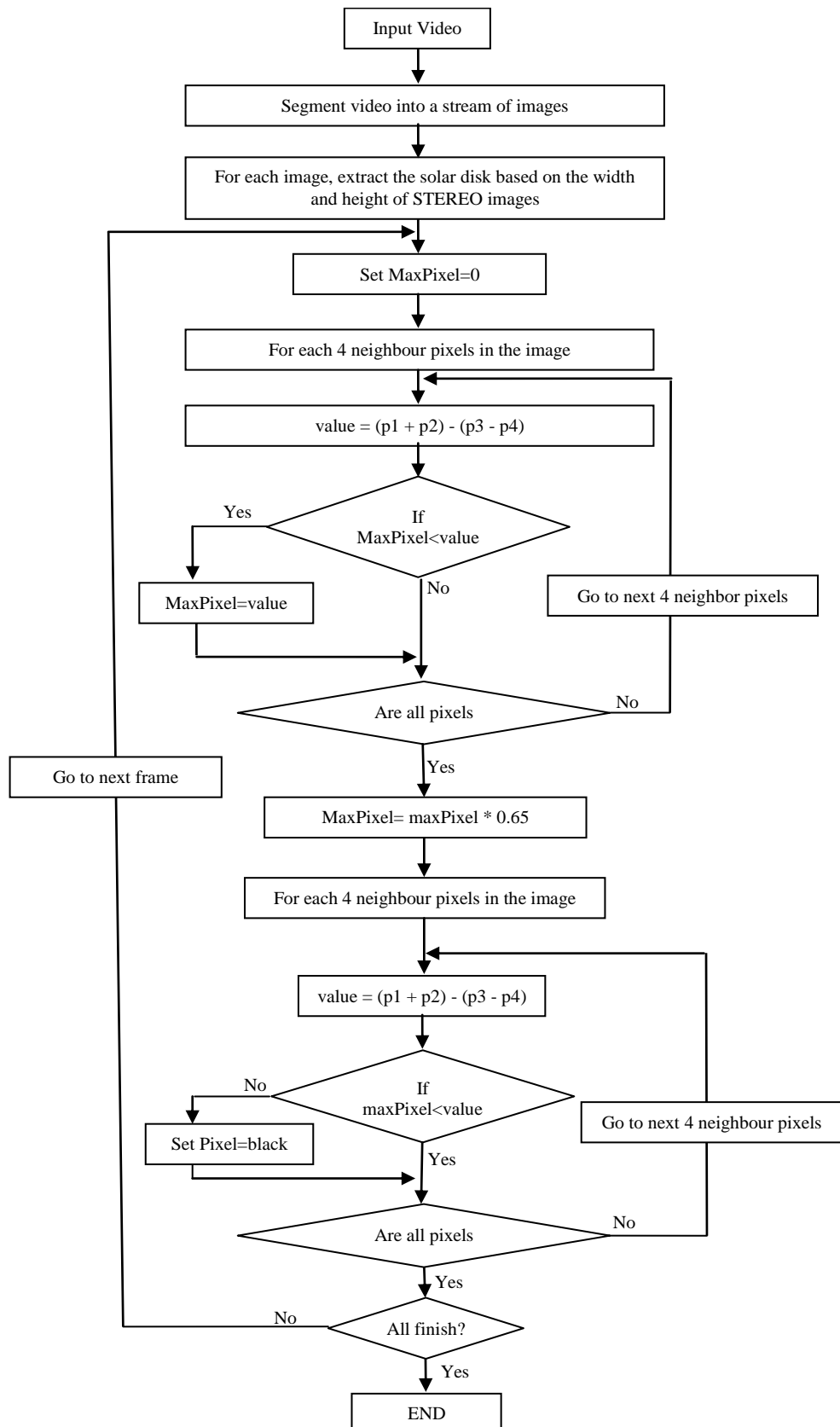
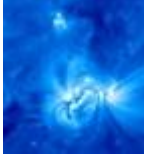
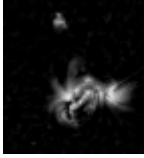
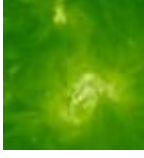
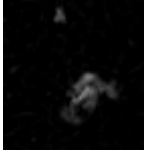
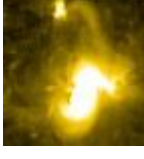

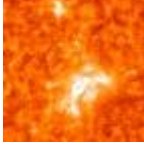
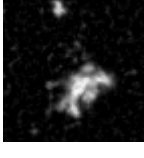


Figure 4.3 Flow chart of ARs detection.

**Table 4-1 Highlight ARs in EUVIs images based on colour extraction.**

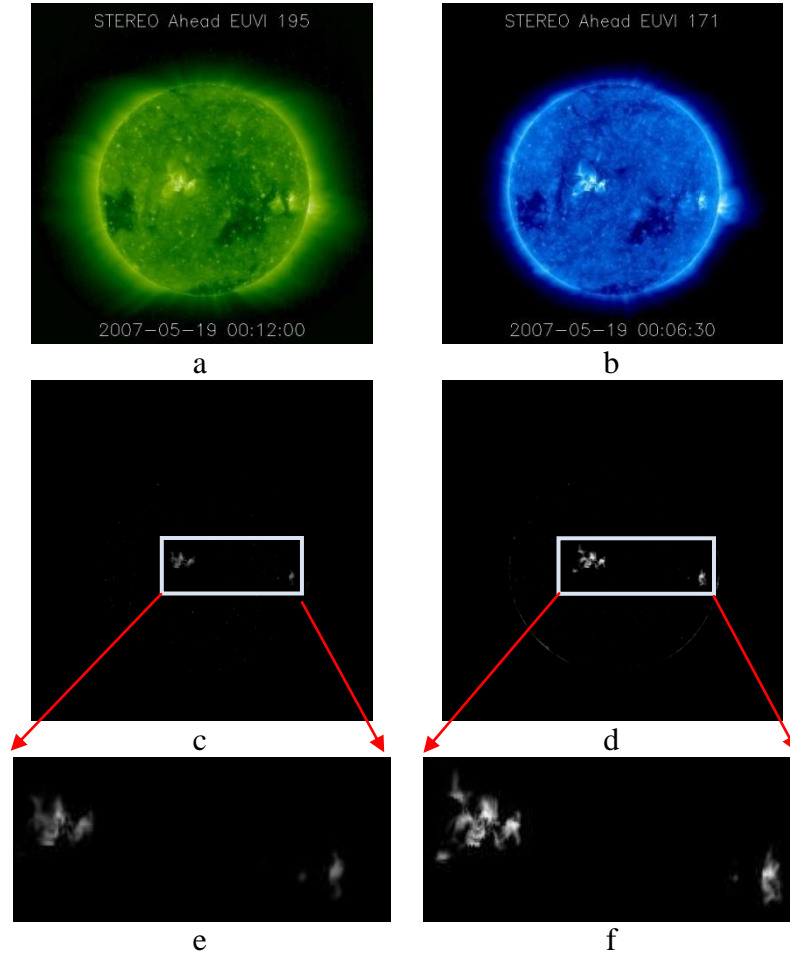
EUVI type	Colour to be extracted	EUVI Sub-image	Channel extraction
171	Red		
195	Blue		
284	Blue		
304	Blue		

This algorithm has been tested on several images and videos from STEREO-A and STEREO-B. The tests are based on subjective measurement and not data provided by NOAA, because NOAA only provides the locations of ARs and not their shapes.

#### ***4.2.2 Translation and Error Estimation***

Generally, the horizontal shift  $a$ , vertical shift  $b$ , and the rotation  $\phi$ , relating two LR images 1 and 2 are estimated as indicated in Equation 4-3 [76]. In the STEREO and SDO missions, the spacecrafts provide multiple frames and at this stage of research when the cadence rate is high the shifts are small and rotation is ignored as shown in Equation 4-4 where the proposed interpolation method in Section 4.3 can prevent contributions from unrelated pixels. Expanding  $Y_1$  to the first order in a Taylor's series, gives Equation 4-5 representing the shift between two LR images. Then the observation model can be represented by relating the HR image to the LR (observed) images as in Equation 4-6. The input signal  $f(x,y)$  denotes the HR image in the focal plane co-

ordinate system  $(x, y)$ . The motion is represented as translation  $\sigma_k$  obtained from applying equations (4-7, 4-8, and 4-9) (see next paragraph). The next consideration is the effects of the physical dimensions of the LR sensor associated with the blurring kernel  $B$ . Finally, the addition of noise  $n_k$  yields the  $k^{th}$  LR image per observation.



**Figure 4.4 AR detection; full solar disk image of STEREO-A observed on 2007-May-19. a) At 00:12:00 UT in EUVI 195 Å; b) At 00:06:30 UT in 171 Å; c) Detected ARs from image (a); d) Detected ARs from image (b); e) Enlarged detected ARs from image (c), and f) Enlarged detected ARs from image (d).**

$$Y_2(x, y) = Y_1(x \cos \phi - y \sin \phi + a, Y \cos \phi + x \sin \phi + b) \quad (4-3)$$

$$Y_2(x, y) = Y_1(x + a, y + b) \quad (4-4)$$

$$Y_2(x, y) \approx Y_1(x, y) + a \frac{\partial Y_1}{\partial x} + b \frac{\partial Y_1}{\partial y} \quad (4-5)$$

$$Y_k(m, n) = \sigma_k(B f(x, y) + n_k(x, y)) \quad (4-6)$$

where

$Y_k$  :  $k_{th}$  observed image

$B$  : blurring kernel

$f$  : original scene

$n_k$  : an additive noise

$\sigma_k$  : translation of  $k$  LR pixel spacing estimated in next paragraph.

$(m, n)$  : the observed location

$(x, y)$  : the scene location

Among the approaches investigated in the literature for sub-pixel motion estimation, the one indicated in [76] has provided satisfactory results. The error function between two images  $Y_1$  and  $Y_2$  after accounting for any integer pixel shifts is denoted by  $E(a, b)$  and represented in Equation 4-7. This error could be recovered by computing its derivatives with respect to  $a$  and  $b$  and setting them to zero, that should also minimize the difference between the image  $Y_1$  and the image  $Y_2$ , which is warped by  $a$  and  $b$  as shown in equations 4-8 and 4-9, which are built only to resolve the small displacements. This algorithm works well when the shifts do not exceed 1 pixel in both x and y axes so should be suitable for use with STEREO or SDO images with short interval times.

$$E(a, b) = \sum \left[ Y_1(x, y) + a \frac{\partial Y_1}{\partial x} + b \frac{\partial Y_1}{\partial y} - Y_2(x, y) \right]^2 \quad (4-7)$$

$$Y_x Y_t = \sum Y_x^2 a + \sum Y_x Y_y b \quad (4-8)$$

$$Y_y Y_t = \sum Y_y^2 b + \sum Y_x Y_y a \quad (4-9)$$

where

$$Y_x = \frac{\partial Y_1}{\partial x} : \text{Horizontal shift ratio};$$

$$Y_y = \frac{\partial Y_1}{\partial y} : \text{Vertical shift ratio}$$

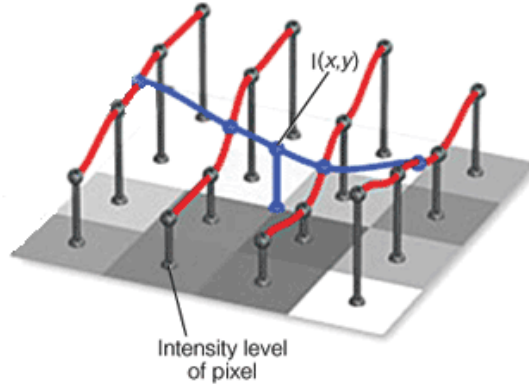
$$Y_t = Y_2 - Y_1 : \text{The difference between two images}$$

### 4.3 Projection and Interpolation

STEREO images are available online with different dimensions. An empty grid of appropriate size must be created for the purpose of projecting the pixels from the registered set of LR images. The grid dimension will represent the size of the output image (SR image), so it will be called the HR grid. In this work, the HR grid is usually reconstructed with size equal to  $2^n$  of the size of the input images, where  $n$  is a positive integer number, e.g. if  $n=0$  then the output size is equal to the same size of the input image. The double size ( $n = 1$ ) is useful to compare the generated SR image with an original HR image if that is available. The HR grid samples are projected from the available  $Y_n$  images rather than from just a single image which does not provide any additional information. All pixels from these images are mapped from the registration step by warping the shifted pixels into the HR grid and are called contributing pixels.

The contributing pixels from each image can be represented as in Equation 4-10, and the HR grid samples can be projected from all LR images as shown in Equation 4-11. The interpolation is applied to all pixels which satisfy the threshold based conditions defined in Equation 4-12. These conditions reduce the number of interpolation calculations, because the interpolation is needed only if a noticeable deviation between warping pixels is detected. The interpolation technique implemented is Bicubic interpolation which uses  $4 \times 4$  neighbourhoods of known pixels (for a total of 16 pixels)

to interpolate the unknown pixels as shown in Figure 4.5. The threshold value  $T = 2$  is used to adjust the level of interpolation and has been found to improve the output. The threshold prevents extreme contributions having higher or lower values than the average, projecting onto the HR grid.



**Figure 4.5 Bicubic interpolation based on the closest 4×4 neighbourhoods of known pixels at position (x,y).**

$$CP_k(x, y) = \sum_{k=1}^N Y_k(x, y) \tag{4-10}$$

where

$CP_k(x, y)$  : contributed pixel for the location  $(x, y)$  in LR image  $k$ .

$Y_k$ : Stands for the  $k_{th}$  LR image.

$N$ : Number of LR images.

$$HR(H, W) = \sum_{k=1}^N \sum_{x=0}^{H-2} \sum_{y=0}^{W-2} \sum_{i=0}^1 \sum_{j=0}^1 CP_k(x + i, y + j) \tag{4-11}$$

where

$HR(W, H)$  : is the HR grid of size  $H \times W$  before filtration.

$$IP(x, y) = \left\{ \begin{array}{ll} \overline{CP_N(x, y)} - \sigma_N(x, y) - T > Y_{k(x,y)} & \\ I(x, y) & \text{Or} \\ \overline{CP_N(x, y)} + \sigma_N(x, y) + T < Y_{k(x,y)} & \\ HR(x, y) & \text{Otherwise} \end{array} \right\} \quad (4-12)$$

where

$P(x, y)$  : represents the pixels in SR grid.

$I(x, y)$  : is the interpolated pixel based on Bicubic interpolation method.

$\overline{CP_N(x, y)}$  : is the average for all CPs in  $Y_N$  images.

$\sigma(x, y)$ : is the standard deviation for the  $CP$  at position  $x$  and  $y$ .

$T$ : Threshold value.

The outputs from this stage usually contain artefacts which need be resolved; these artefacts are handled in subsection 4.4. The computational load for this method should be lower than those of the standard Bilinear and Bicubic interpolation as the information about the surrounding pixels is utilized only under the conditions indicated.

#### 4.4 Smoothing

In order to smooth and reduce any artefacts from the previous step, a Gaussian filter method is used to enhance image structures at different scales. The automated construction of a suitable 2D-Gaussian kernel is represented in Equation 4-13. The kernel with elements depending on their distance and on the adjustable parameter ( $A$ ) can be obtained from Equation 4-14, where  $A$  is defined by Equation 4-15. Applying these equations produces a surface whose contours are concentric circles with a Gaussian distribution about the centre point. The kernel matrix using the values from the Gaussian distribution is then convolved with the HR grid samples producing the SR



image as shown in Equation 4-16. Each new pixel value is a weighted average of its neighbouring pixels. The original pixel value receives the greatest weight and neighbouring pixels receive smaller weights as their distance from the original pixel increases.

This means that the Point Spread Function (PSF) is a Gaussian. The imaging PSF is typically determined entirely by the imaging system (that is, camera or telescope and sensor), which produced the LR images, but if the imaging system is unknown, then it can at least be assumed to be a low-pass filter. In the technique presented, a Gaussian filter with the adjustable parameter ( $A$ ) offered the highest objective measurement values, as shown in Section 4.6, compared with box or median filters.

$$Kernel[N, N] = \sum \sum e^{-\frac{\sigma^2}{A}} \quad (4-13)$$

where

$Kernel[N, N]$  : is the quadratic Gaussian kernel

$N = 3$  for the convolution  $3 \times 3$  matrix

$\sigma$ : Estimated distance between elements as shown in Equation 4-14

$A$ : is used to adjust the width of the e-function and can be estimated as shown in Equation 4-15.

$$\sigma = \sqrt{\sum_{x=0}^{w-m-1} \sum_{y=0}^{H-m-1} (x-m)^2 + (y-m)^2} \quad (4-14)$$

where

$W * H$ : the size of the image

$m$ : is equal to either kernel's height or width dividing by 2.

$$A = \begin{cases} 1 & \text{if } N \leq 3 \\ -2 \frac{\left(\frac{N}{2}\right)^2}{\log(0.01)} & \text{otherwise} \end{cases} \quad (4-15)$$

$$SR(x, y) = HR(x, y) \otimes Kernel[N, N] \quad (4-16)$$

where

$SR$ : is the image after the convolution.

$HR$ : is the image before the convolution

$\otimes$ : is a convolution operator.

## 4.5 Quality Measurements

From the survey of the literature in Chapter 2, it seems that most previous researchers relied on subjective measurement, which uses the human eye, to assess their outputs. Quality assessment is improved by using both subjective and objective measurements. Examples of the objective measurements are Signal to Noise Ratio (SNR), Mean Square Error (MSE), Peak Signal to Noise Ratio (PSNR), and Structural Similarity Index Matrix (SSIM). As indicated in Table 4-2, the most commonly used method for presenting results is subjective visual quality followed by MSE, and PSNR objective quality assessments. Several quality measurements methods are discussed in the next subsections.

### 4.5.1 Mean-Squared Error (MSE)

MSE is a quality metric for comparing two images  $Y(x, y)$  and  $Y'(x, y)$ , and is defined in Equation 4-17. MSE has a significant problem in that it relies on the image intensity scaling without which it does not guarantee providing an accurate indication.

$$MSE = \frac{1}{MN} \sum_{x=1}^M \sum_{y=1}^N [Y(x,y) - \hat{Y}(x,y)]^2 \quad (4-17)$$

**Table 4-2 Measurements of super-resolution accuracy that have been used in some of the previous works.**

SR Method	Performance Measurements			
	Subj	SNR	MSE	PSNR
Vandewalle, Susstrunk et al. [77]	√			
Baker and Kanade [75]	√			
Irani and Peleg [76]	√			
Huang, Sun et al. [49]	√		√	
Zomet, Rav-Acha et al. [62]	√			
Clark, Palmer et al. [66]	√			√
Alexey Lukin [102]	√	√	√	√
Hong, Kang et al. [68]	√			√
Tekalp, Ozkan et al. [70]	√			
Huang, Sun et al. [49]	√			
Elad and Feuer [103]	√		√	
Capel [8]	√			

#### 4.5.2 Peak Signal to Noise Ratio (PSNR)

PSNR resolves the intensity scaling problem of MSE by scaling the MSE according to the image range as shown in Equation 4-18. PSNR is measured in decibels (dB), and is good for comparing the restoration results for the same image. However, neither MSE nor PSNR are well matched to perceived visual quality [43].

$$PSNR = 10 \log_{10} \frac{(Max_i)^2}{MSE} \quad (4-18)$$

where

$Max_i$ : the maximum possible pixel value of the image.

Typical values for PSNR are between 30 and 50 dB in the degraded image,

where the higher the number the better. If the two images are identical, then MSE returns zero and PSNR returns infinity.

### 4.5.3 Structural Similarity (SSIM)

SSIM is used to measure the similarity between two images and is designed to improve the assessment of visual image quality over MSE and PSNR. The measurement process for the SSIM is based on the luminance [43] as defined in Equation 4-19. The result is a decimal value between -1 and 1. If the result is equal to 1 then the two images should be identical.

$$SSIM(X, Y) = \frac{(2\mu_x\mu_y + C_1)(2cov_{xy} + C_2)}{(\mu_x^2 + \mu_y^2 + C_1)(\sigma_x^2 + \sigma_y^2 + C_2)} \quad (4-19)$$

where

$\mu_x, \mu_y$  :average of  $x$  and  $y$  respectively.

$\sigma_x^2, \sigma_y^2$  :variance of  $x$  and  $y$  respectively.

$cov_{xy}$ : covariance of  $x$  and  $y$ .

$c_1 = (k_1L)^2, c_2 = (k_2L)^2$ : two variables to stabilize the division with small denominator.

$L$ : Dynamic range of the pixel values (typically this is  $2^{\#bits \text{ per pixel}} - 1$ )

$k_1 = 0.01$  and  $k_2 = 0.03$  by default

In summary, MSE, PSNR, and SSIM are mathematical methods of quality measurements, but these metrics may give inconsistent results. In [104], a performance test of MSE and SSIM metrics based on certain benchmark images is described which finds that SSIM gives better indication than MSE. In this work, both subjective and

objective quality assessments (PSNR and SSIM) are used for evaluation. From the literature review it seems this use of SSIM is unique in SR testing. The known HR images have been used to compare the real performance of the selected SR methods.

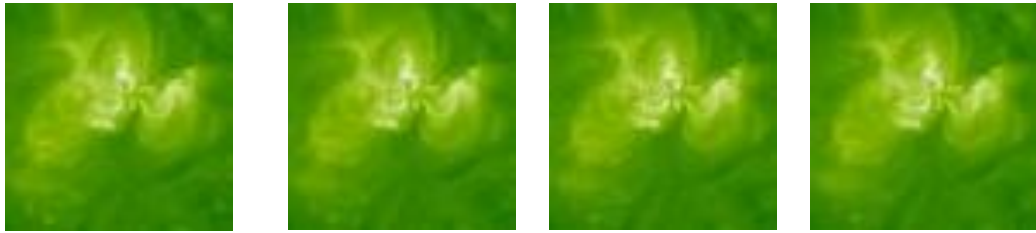
## 4.6 Experimental results

Comparisons using SSIM and PSNR have been performed against several SR approaches including Iterated Back Projection (IBP), Projection onto Convex Sets (POCS), Robust SR and QE SR. The implementations of IBP, POCS, and Robust SR methods were obtained from the authors of [105] and the QE SR from the authors of [106]. Two types of experiments were performed; the first depends on the objective quality measurements to compare the resulting enlarged SR image of size equal to double the size of the reference (LR) image with the known HR image. The second uses the subjective quality measurement to judge the finer details in the SR image with respect to the reference image without enlargement.

### 4.6.1 Enlarged super resolution images

Several experiments have been conducted on sets of EUVI 195 Å and EUVI 171 Å LR sub-images. A set of LR sub-images were cropped from a set of EUVI 195 Å LR images of size 512×512 pixels taken at 10 minutes separation saved with the JPG file format and 24 bits depth as shown in Figure 4.6. The output is shown in Figure 4.7 after enlarging the reference image by a factor of two using several SR methods. The original sub-image cropped from the known HR image size of 1024×1024 pixels before down sampling is shown in Figure 4.7a. The aim here is to create a SR image double the size of the input images. Hence, the result most similar to the original image is considered the best. In this experiment, none of the resulting SR methods show the same details of the original sub-image, because the cadence rate is about 10 minutes per image, which

means, the features have slightly changed.



a. LR1 (Reference image)

b

c

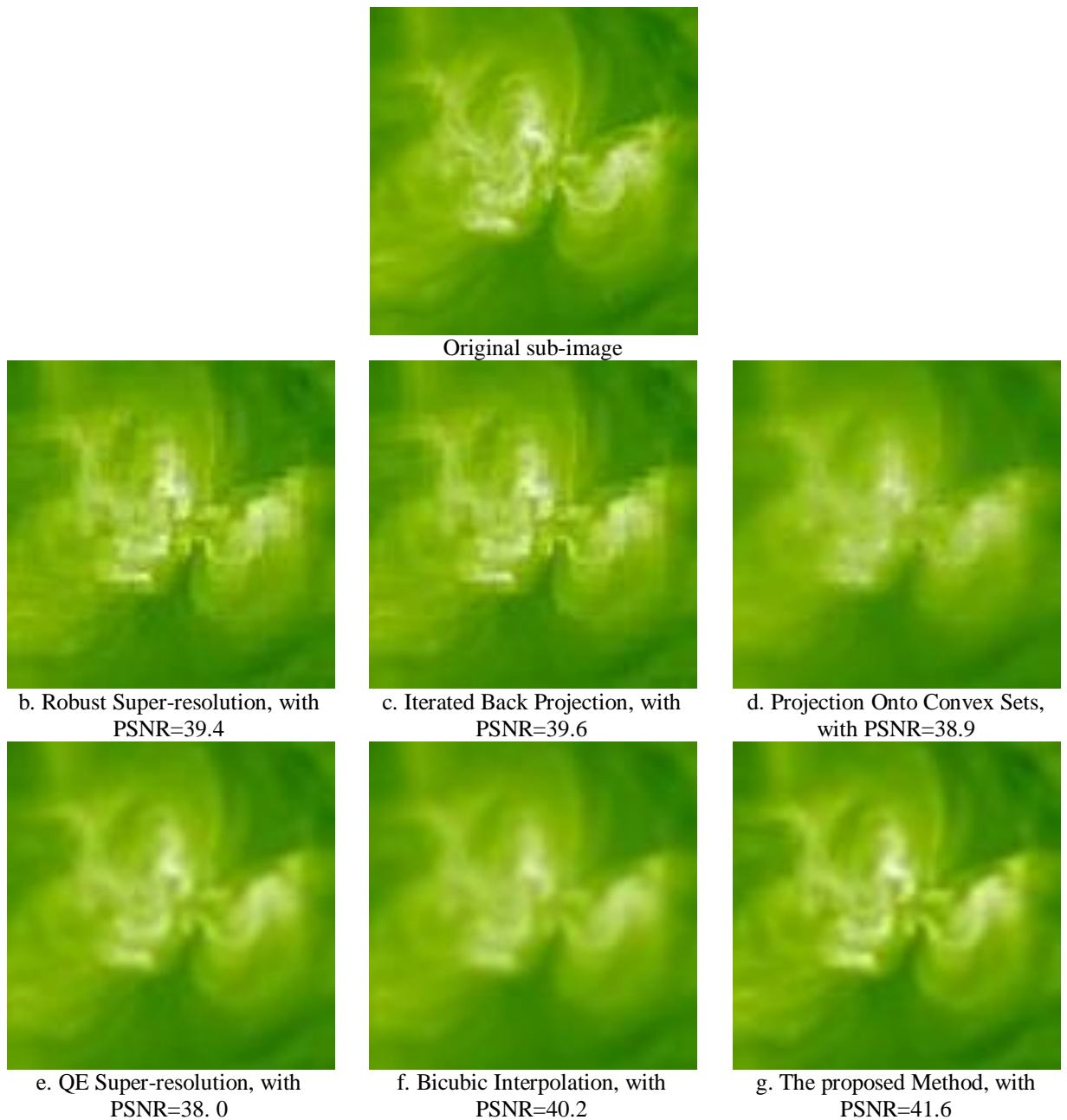
d

**Figure 4.6 Four LR Sub-images are cropped from STEREO-A image of size 512×512 on May-19-07 at 00:12:00, 00:22:00, 00:32:00 and 00:42:00 (a, b, c and d respectively), that are required to generate SR image. (a) LR1 (the reference image), (b) LR2, (c) LR3 and (d) LR4.**

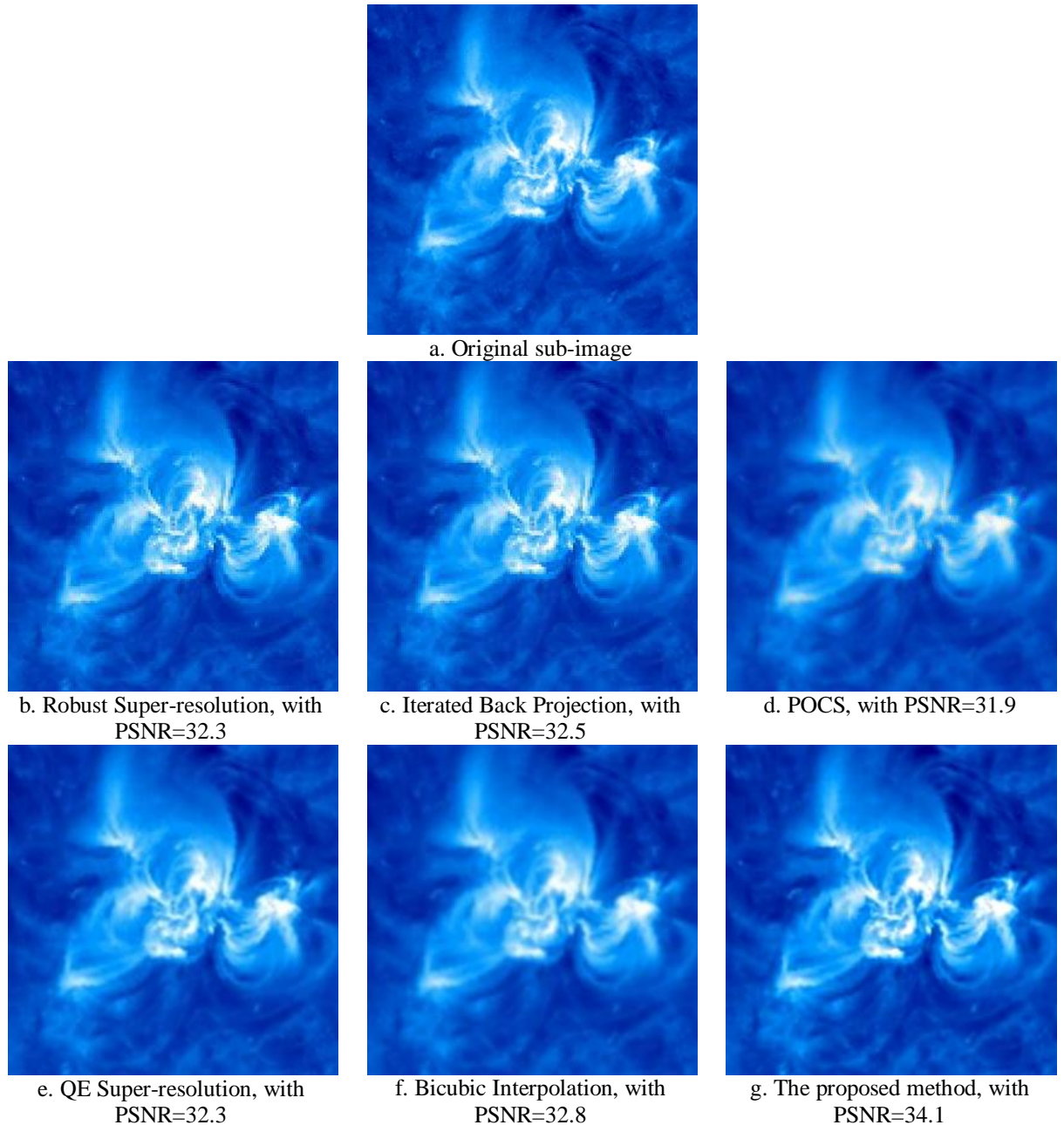
The output from the Robust SR is shown in Figure 4.7b with PSNR = 39.4 dB, Figure 4.7c is the output for IBP which has PSNR = 39.6 dB, Figure 4.7d is related to POCS with PSNR = 38.9 dB, Figure 4.7e is for the QE Super-resolution with PSNR = 38.0 dB, Figure 4.7f is for the Bicubic interpolation (standard resize method), with PSNR = 40.2 dB, and in Figure 3.5g is the output of the proposed method with the highest PSNR value which equals to 41.6 dB. Using SSIM, the results of SR methods are sorted based on the similarity with the original sub-image from low to high as follows: POCS, IBP, Robust SR, Bicubic interpolation, QE SR and then the proposed method as shown in Table 4-3.

Another test has been performed using EUVI 171 Å solar images of size 2048×2048 pixels and a set of LR images of size 1024×1024 pixels. The sub-images were cropped around the area of the active region that resides in the solar disk as shown in Figure 4.8. The SR results shown seem closer to the original than those in Figure 4.7 because the set of LR images were taken at the higher cadence rate of about 2.5 minutes per image reducing the change between them. The proposed method scores the highest PSNR value with 34.1 dB, followed by Bicubic interpolation, IBP, QE SR, Robust SR,

and then POCS. Also the proposed method scores the highest SSIM value with 0.96 followed by QE, IBP, Bicubic, Robust SR, and then POCS.



**Figure 4.7 SR sub-images, (A) Original sub-image cropped from STEREO-B image of size 1024x1024 on May-19-07 at 00:12:00, (B) Robust Super-resolution, (C) Iterated Back Projection, (D) Projection Onto Convex Sets, (E) QE Super-resolution, (F) Bicubic Interpolation, and (G) Proposed method.**



**Figure 4.8 SR sub-images , cropped from STEREO-A EUVI 171 Å images on May-19-07**

**at 00:06:30 of size 2048x2048 pixels, (a) Original, (b) Robust Super-resolution, (c) Iterated Back Projection, (d) Projection Onto Convex Sets, (e) QE Super-resolution, (f) Bicubic Interpolation, and in (g) The proposed SR method.**

Further experiments have been performed on 10 different wavelength sets comprising 40 LR sub-images taken by STEREO-A of size 1024×1024 pixels on May-19-2007 between 00:06:30 and 01:46:30 (hh:mm:ss). The enlarged SR images of size factor 2 of the reference images are compared with their related original images of size



2048×2048. The results are averaged and shown in Table 4-4. The proposed method has the highest PSNR value with 35.3 dB, followed by Bicubic, IBP, QE, Robust SR, and then POCS. Also the proposed method has the highest SSIM value followed by QE SR, Bicubic interpolation, IBP, POCS, and then Robust SR method.

**Table 4-3 Comparing SR images with the original image of the same size based on SSIM and PSNR. The solar LR images of STEREO-B EUVI 195 Å of size 512x512 and EUVI 171 Å of size 1024×1024 have been used, captured on May-19-2007 at 00:12:00.**

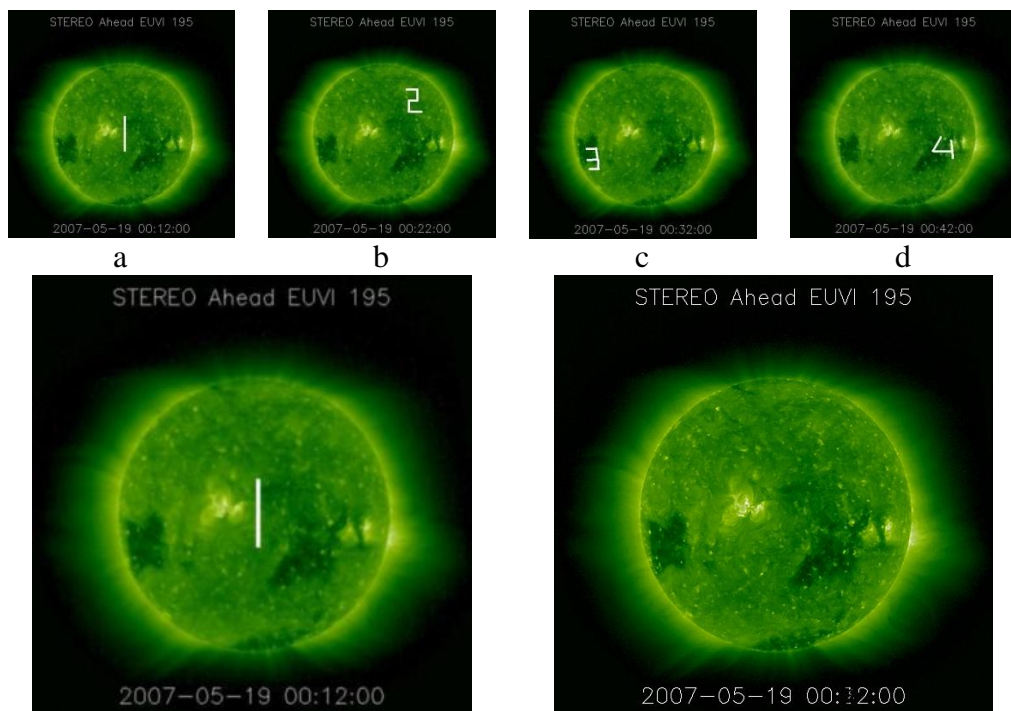
SR Method	Quality Measurements Sub-images cropped from SR of size 1024×1024 of EUVI 195		Quality Measurements Sub-images cropped From SR of size 2048×2048 of EUVI 171	
	SSIM	PSNR	SSIM	PSNR
QE SR	0.968	38.0	0.961	32.3
POCS	0.963	38.9	0.947	31.9
Robust SR	0.965	39.4	0.955	32.3
Iterated Back Projection	0.968	39.6	0.957	32.5
Bicubic Interpolation	0.971	40.2	0.956	32.8
Proposed method	0.975	41.6	0.963	34.1

**Table 4-4 Performance comparisons based on SSIM and PSNR. 40 LR sub-images have been cropped from STEREO-A images of size 1024x1024, in May-19-2007 between 00:06:30 and 01:46:30 (hh:mm:ss) and colapsed in 10 sets.**

SR Method	Quality Measurements	
	SSIM	PSNR
QE SR	0.946	33.9
POCS	0.928	33.6
Robust SR	0.926	33.8
Iterated Back Projection	0.934	34.1
Bicubic Interpolation	0.942	34.5
The proposed Method	0.947	35.3

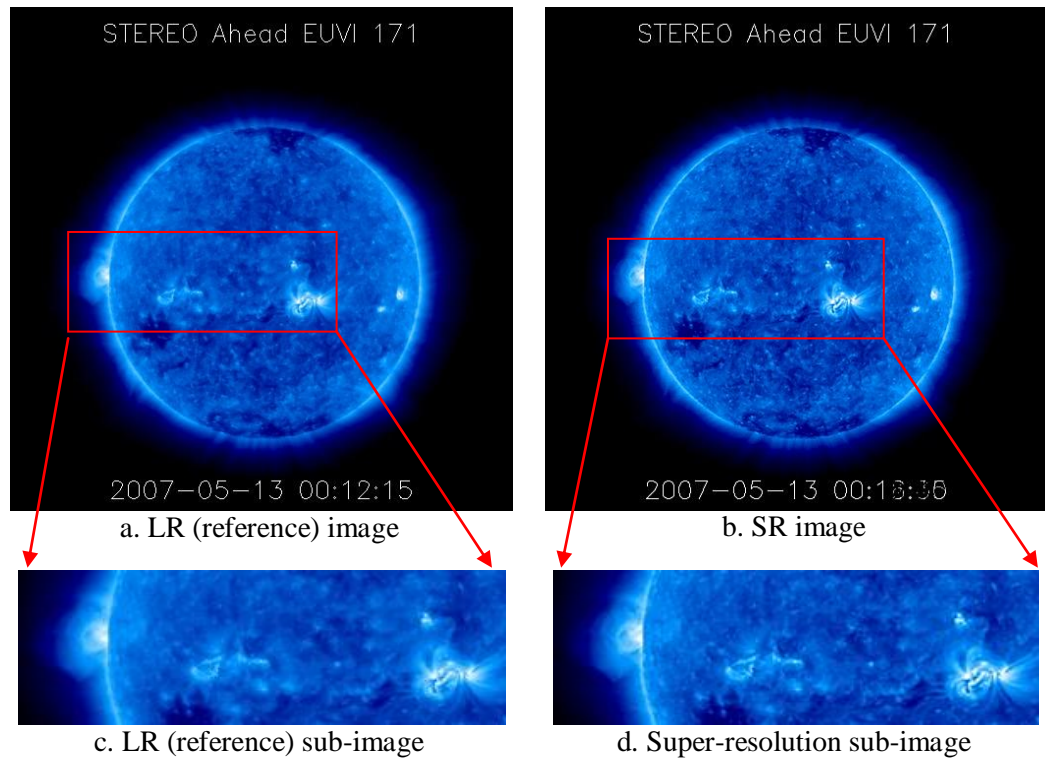
Another experiment involves images with superimposed numeral which are removed by the proposed method which excludes pixels that are higher or lower than the thresholded average (Interpolation Performance). A set of full disk solar LR images for STEREO-A EUVI 195 Å have been downloaded, and then different labels have been added to each LR image in different locations as shown in Figure 4.9 (a, b, c, and d). This experiment aims to show how much information can be obtained from all LR images to produce a more similar image to the original, and to show the performance of

the presented interpolation by excluding the pixels that exceed the thresholded average. The comparison was made between QE SR and the proposed method, because QE SR has offered better SSIM indication than POCS, IBP, and Robust SR. The result from QE super-resolution is shown in Figure 4.9e, the output looks like the reference image (note the label), but the output from the proposed method is more similar to the original image as shown in Figure 4.9f. The proposed method generates the SR image by selecting the most appropriate pixels among all LR images in the set; the output has no labels as well as being closer to the original image.



e. Result from QE super resolution      f. Result from the proposed method  
**Figure 4.9** Comparison between QE SR and the proposed SR method to show the

interpolation performance. (a, b, c, and d) represent the set of LR images. (e) Result from QE SR. (f) Result from the proposed SR method.



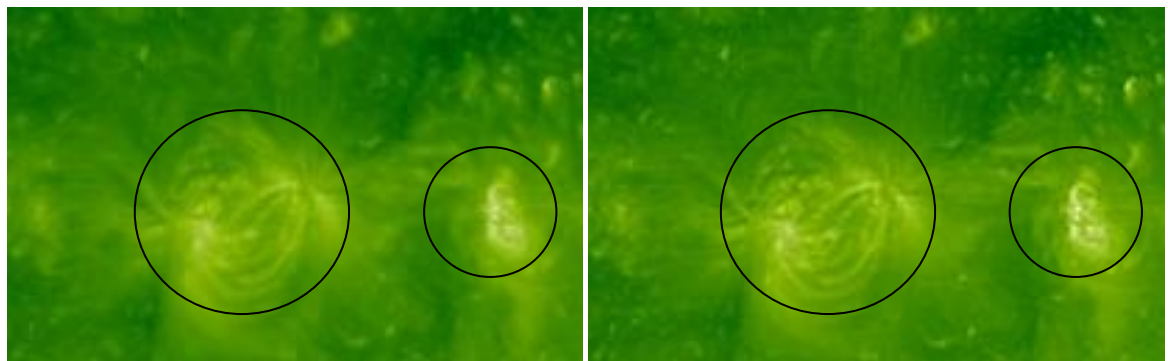
**Figure 4.10** The SR image in the top right shows the full disk of the Sun with finer details than the reference image shown in the top left. The edges of the loops in the active region area are more distinguishable than they appear in the LR image. (a) LR (reference) image. (b) SR image. (c) Sub-image from figure a. (d) Sub-image from figure (b).

#### 4.6.2 *SR image with respect to the reference image without enlargement*

The second type of experiments involves creating SR images of the same size as the reference image. Hence, only the subjective assessments are used, because the resulting SR image has details not available in any individual image, so it is not possible to provide objective quality assessment. Firstly, a set of four LR EUVI 171 Å images taken by STEREO-A on 13th May 2007 at 00:12:15 with a separation time of 75 s and a size of 512×512 pixels was used to generate SR images of the same size. The results, presented in Figure 4.10, show that the edges of the loops and the ARs shapes in the SR images are more distinguishable than in the LR images. Secondly, a set of LR images of EUVI 195 Å of size 2048×2048 taken by STEREO-A on 5th July 2007 at 11:37:00 with

10 s separation time, was used to generate SR image holding the same size. A prominent region is cropped to provide better visual assessment between LR and SR images as shown in Figure 4.11.

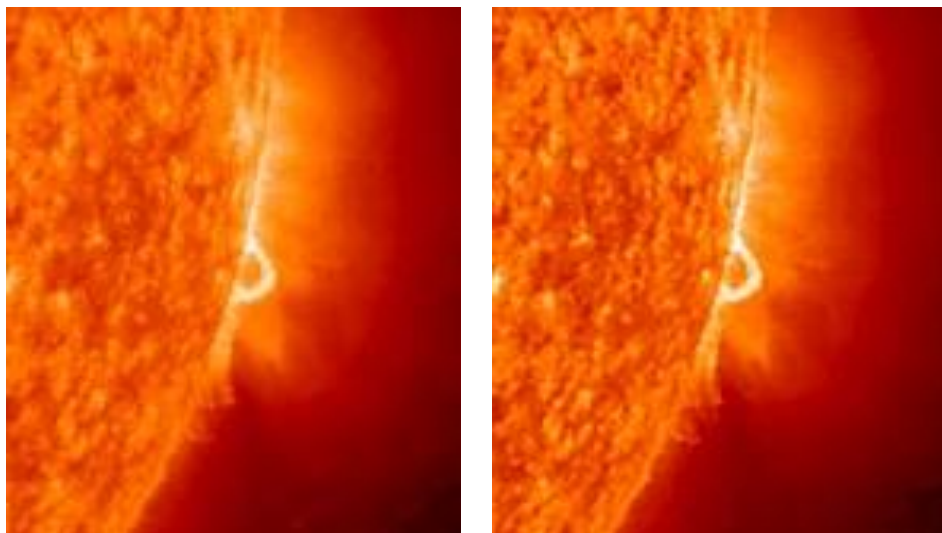
Finally, a set of LR sub-images of EUVI 304 taken by STEREO-A on 9<sup>th</sup> May 2007 at 02:36:05 at a cadence rate 36 s was used to generate a SR sub-image of the same size. The enhancements are clearly visible in Figure 4.12.



a. LR sub-image

b. SR sub-image

**Figure 4.11** The shapes of the active region that marked by a circle appear sharper in SR sub-image than the LR sub-image. The involved images before crop are of size 2048×2048 taken by STEREO-Ahead on 5th July 2007 at 11:37:00 with 10 seconds separation time.



a. LR sub-image

b. SR sub-image

**Figure 4.12** EUVI 304 Å sub-image taken by STEREO-Ahead on 9th May 2007 at 02:36:05 with 36 seconds cadence, shows the loops of an active region that resides on the right side of the solar disk. The edges in SR sub-image look more detailed than the LR sub-image. (a) LR sub-image. (b) SR sub-image.

## 4.7 Summary

The SR approach applied to solar images presented in this chapter includes three major stages. Firstly, image registration of the images is performed based on an automated method for AR detection developed using correlation. This is simple and suitable to match images with small shifts as assumed in this work but is also sensitive to changes in scales and intensities. Hence, the STEREO-CPs method is used to overcome these limitations and provides the ability to run the proposed method on scenes other than the Sun. Secondly, interpolation has been applied based on the Bicubic technique with a threshold parameter, and thirdly smoothing has been done using a Gaussian filter with adjustable parameters. Several practical tests have been performed and the results evaluated using subjective and objective (PSNR and SSIM) assessments. The results show an improvement in the output compared with several competitive SR methods including IBP, Robust, QE, and POCS and in addition, the Bicubic interpolation method. Also it is found that Bicubic interpolation provided results better than those from some SR methods, which could be an indication of: firstly, a failure of the registration step. Secondly, the corresponding SR methods work best on certain images. Finally, the finer details in the tested images were not well recovered from the given set. The output of the presented approach is used to enhance 3D perception by creating higher resolution image pairs to create anaglyphs in Chapter 5.

# CHAPTER FIVE

## 5 GENERATING ANAGLYPHS USING PAIRS OF IMAGES FROM THE STEREO SATELLITES

### 5.1 Introduction

An anaglyph is a combination of left and right images of a scene taken with offset viewpoints with respect to each other, where the images are shown using different colours in order to achieve 3D perception by users wearing glasses with complementary colour filters. The resulting anaglyphs can be used for viewing 3D images or 3D movies.

On the Sun, the depth perception in 3D views is useful because it can reveal features that are not apparent in 2D views. The mission of NASA STEREO provided the first opportunity to view the Sun in 3D using images captured at the same time from two different satellites. The current attempts to create anaglyphs from pairs of STEREO images provided on STEREO-GSFC site are based on manual rescaling and fitting using image processing software such as Adobe Photoshop and Anaglyph Maker<sup>12</sup> as illustrated on <http://stereo.gsfc.nasa.gov/classroom/3d.shtml>, last access 17 Nov, 2010).

---

<sup>12</sup>Anaglyph Maker is a program available at [http://www.stereoeye.jp/software/index\\_e.html](http://www.stereoeye.jp/software/index_e.html), which is used to create interleaved images for 3D viewing using LC-shuttered glasses, from the given stereo photograph pair.

Another example of anaglyph creation from a pair of STEREO images is available from Ian Musgrave<sup>13</sup>. The generation of anaglyphs from pairs of STEREO images using the information available in FITS header files can be performed as described in [33].

Anaglyph creations from calibrated and uncalibrated pair of images are introduced here. The focus is on how to efficiently construct anaglyphs when the separation angle between the spacecraft is small enough to allow 3D perception. The size of the high resolution FITS files is about 8.3 MB provided with single resolution, so creating a video from these high resolution images with 1000 frames would need the download of more than 16.6GB of data. However this overloads the existing Internet and network infrastructures. Furthermore, the wavelength type in FITS is included in its headers only and not in its file names, e.g. 20070513\_002115\_n7eu.fits, so this needs to download extra irrelevant data. However, in JPEG files, the wavelength is included in the file names, e.g. 20070513\_001615\_n4euA\_195.jpg. This is used to optimise the query to determine what data is important before starting the download process.

The main aims of this chapter are as follows. The first aim is to provide methods to create anaglyphs efficiently from pairs of STEREO images, either as still images or videos. For example, if there is a particular time interval required for study, it would be useful to provide a quick-look 3D movie to see if there is anything worth further study. The second aim is to provide methods able to work in near real-time. Both aims can be achieved by working with lossy compressed JPEG images (with no calibration information) rather than the uncompressed FITS files (containing calibration information), which are more suitable for scientific analysis but take about 3 days to become available on the archive. These algorithms will be ready to be used when these spacecrafts meet again. The third aim is to improve the quality of the anaglyphs by

---

<sup>13</sup> <http://astroblogger.blogspot.com/2007/07/stereo-anaglyph-of-sun.html>, last access 21/10/2010.

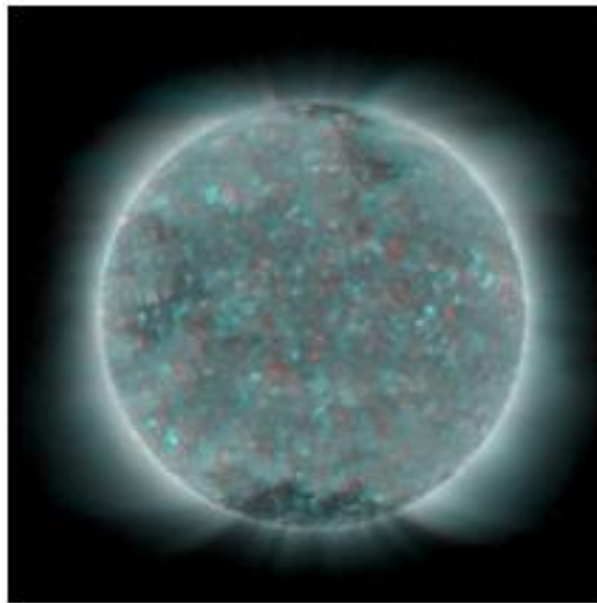
combining left and right images of the scene from SR images which show the surface of the Sun in more details than the LR images. HRA (High Resolution Anaglyph) is a term used here to refer to the anaglyph created from pairs of HR images. HRA is possible during periods of high cadence rates, where the performance of the proposed SR method that was illustrated in chapter 4 is enhanced. After reading the literature, this appears to be the first attempt to enhance the quality of anaglyphs using SR. The final aim is to introduce techniques that could be used for other applications beside solar imaging.

Several points should be taken into account before creating anaglyphs for STEREO images. Firstly, the separation angle between the two spacecraft should be small (less than  $44^\circ$ ) [107]. Secondly, if the angle is larger, between about  $44^\circ$  and  $90^\circ$ , then anaglyph creation is still possible as mentioned in [2] but requires some pre-processing steps, e.g. rotate the Sun on its axis for the left view and/or right view before the combination process). Thirdly, we can work with or without calibration information for both spacecraft. Using calibration information, there is no need to know any information about the scene, but without calibration, some features of interest in the two images must be matched in order to map the corresponding pixels between the pair of images. Finally, when the angle exceeds  $90^\circ$ , it becomes too difficult to construct anaglyphs, because the spacecraft views of the scene are too different. 3D scene reconstruction can then only be done by mathematical analysis and graphic display rather than binocular vision [33].

Anaglyphs can be generated by combining two extreme UV images taken by the same spacecraft at different times. The different viewpoints result from the rotation of the sun (period roughly 28 days), but small-angle stereoscopy is usually all that can be achieved with this technique because solar features change with time. For example, the coronal holes of the Sun on Dec, 2008 (this example is taken from



<http://stereo.gsfc.nasa.gov/gallery/item.php?id=3dimages&iid=46>) are the most prominent features in the anaglyph image shown in Figure 5.1. The SOLARSTUDIO application was used to create this 3D image by combining two extreme UV 171 Å images taken about 12 hours apart on Dec. 19, 2008. Many 3D images and movies generated from STEREO data are offered by STEREO-GSFC and are available online at <http://stereo.gsfc.nasa.gov/gallery/3dimages.shtml>.



**Figure 5.1 Anaglyph of the Sun created from pair of STEREO-Ahead spacecraft on Dec. 19, 2008 with 12 hours apart. The coronal holes are the most prominent features.**

## **5.2 Anaglyphs from calibrated pairs of STEREO images with a significant angle of separation**

Anaglyphs can be created from recorded pairs of STEREO images taken at the same time from two perspectives corresponding to small-angle stereoscopy over the period between March and July of 2007. The steps necessary for creating anaglyphs using calibration data are illustrated in the following example which utilises two extreme UV images taken on May 09-2007 at 20:40:45 at separation angle of  $7.246^\circ$  ( the angle at this date was retrieved from NASA GSFC [30]). A verging stereo anaglyph (camera

optical axes converging at a finite distance) is generated using information provided in the headers of the FITS files as follows:

1. Retrieve the pair of STEREO images with small separation angle. The right image is from STEREO-A and the left image is from STEREO-B.
2. Co-align, rescale, and rotate both images into the same plane (see Figure 5.2) based on the information in the FITS header files, including the pixel coordinates of the Sun centre, i.e., CRPIX1 = 1020.63, CRPIX2 = 926.70 for image A and CRPIX1 = 1035.55, CRPIX2 = 1051.08 for image B, with a solar radius of RSUN = 998.9600 for image A, and RSUN = 913.5800 for image B, as described in [33].
3. The disk of the STEREO-A image can be reduced to the same size as the disk of the STEREO-B image as shown in the following equations:

$$\text{ResizeFactor} = \frac{\text{RSUNB}}{\text{RSUNA}} \tag{5-1}$$

where

RSUNB: Radius of the Sun for STEREO-B image

RSUNA: Radius of the Sun for STEREO-A image

and

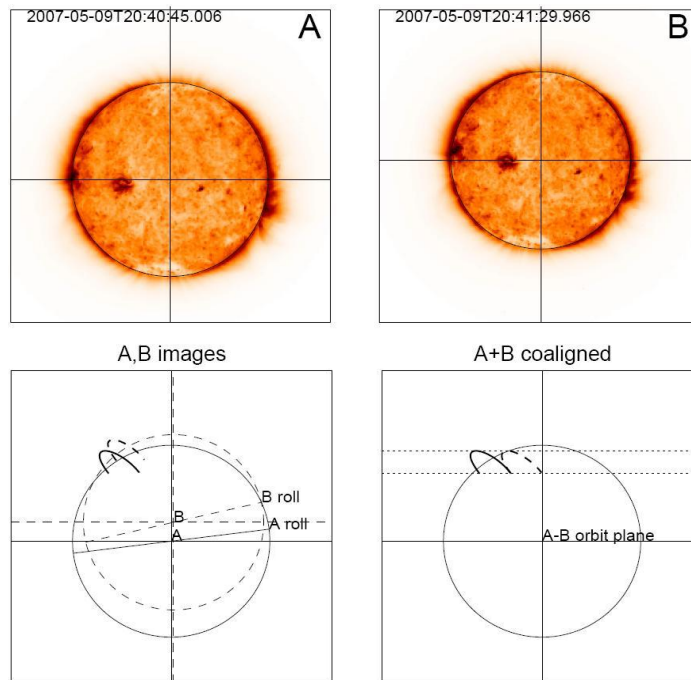
$$\text{NewAheadImg} = \text{Bilinear}(\text{ResizeFactor} \times \text{SizeOfAheadImg}) \tag{5-2}$$

4. Move the solar disk in the left image to a proper offset with respect to the right image based on the central point locations. The new location of the central point in the processed STEREO-A images can be determined as in Equations 5-3 and 5-4 and the alignment is shown in Figure 5.2.

$$\text{NewCRPIX1A} = \text{ResizeFactor} \times \text{CRPIX1A} \tag{5-3}$$

$$\text{NewCRPIX2A} = \text{ResizeFactor} \times \text{CRPIX2A} \quad (5-4)$$

5. Convert the left and right images to grey colour as shown in Figure 5.3(c and d).
6. Extract the red channel from left image and the blue/green channels from right image. It is important that the Ahead and Behind images are the cyan and red filtered images respectively, otherwise the 3D effect will be inverted using standard glasses.
7. Combine the left and right images to generate the anaglyph image as shown in Figure 5.3(e).

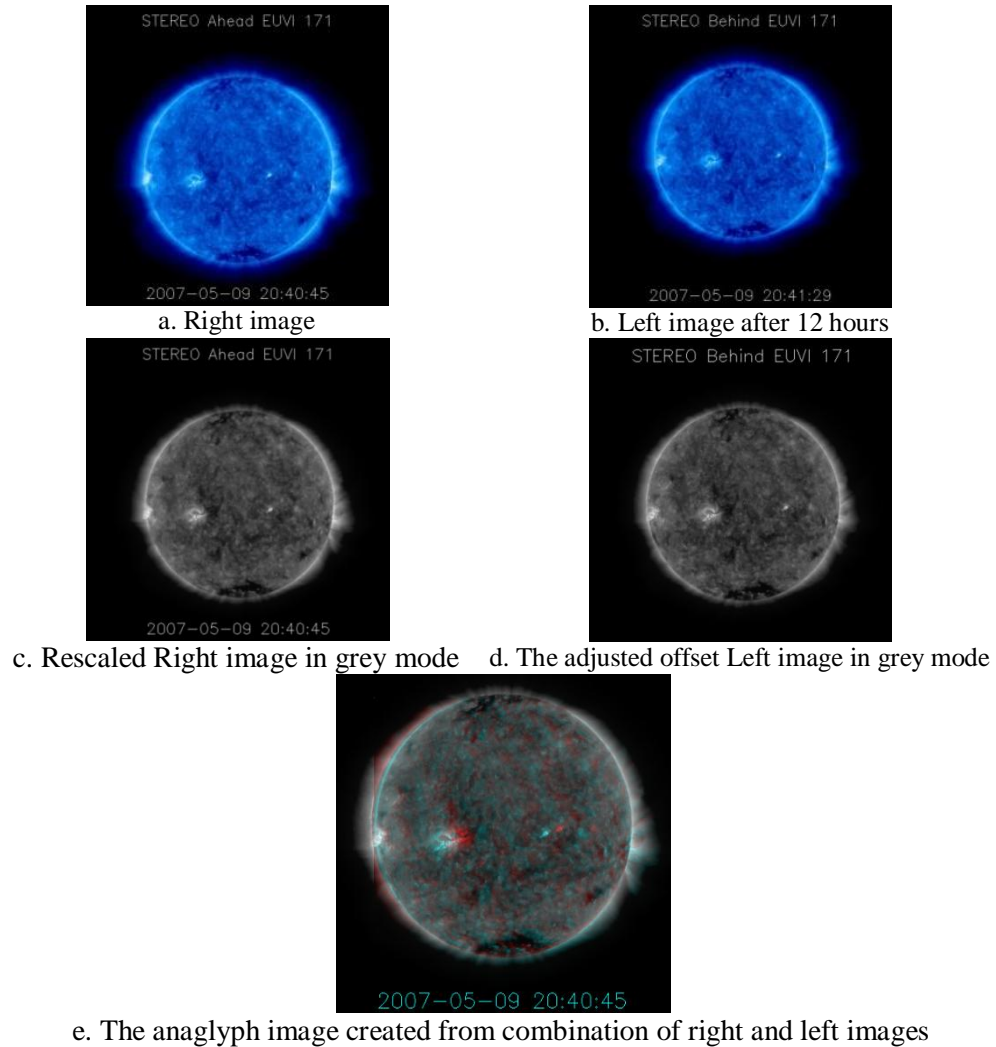


**Figure 5.2 Full disk inverted colour EUV 171 images of STEREO-A (top left) and B (top right). The crossing vertical and horizontal lines show the Sun’s center point. The Coalignment involves centring the Suns’ centers [33] in the images.**

### **5.3 Anaglyphs from uncalibrated pairs of STEREO images with a significant angle of separation**

The steps to create anaglyphs from un-calibrated data are similar to those described in

the previous section except the information taken from the FITS header is obtained from the images themselves. The required data is obtained using STEREO-CPs to find the size ratio between the Sun's disks in the STEREO Ahead and Behind images. Then two methods can be used to create anaglyphs as shown below:



**Figure 5.3 Steps to create an anaglyph. (a) and (b) are the original images, (c) and (d) are the aligned and converted to grey scale images and (e) is the resulting anaglyph.**

### 5.3.1 Boresighted stereo anaglyphs

Image rectification can be used to generate two images with horizontal epipolar lines on the same scan lines from a pair of images of a scene taken from different viewpoints, which facilitates the search for corresponding points. Also it can be used to match an

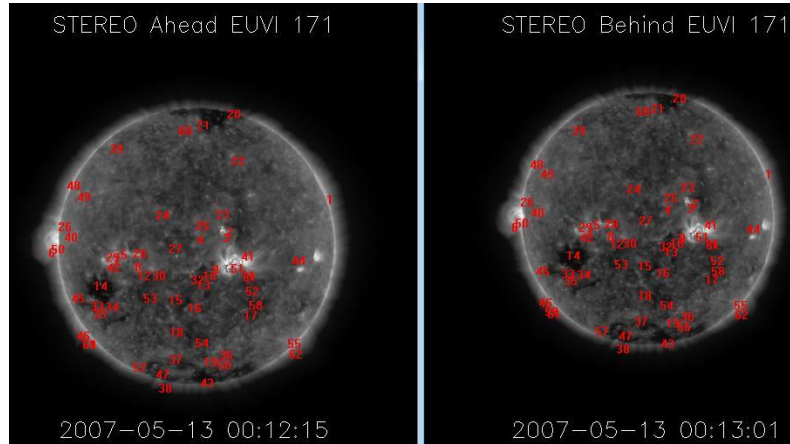
image and a map. Anaglyphs equivalent to those generated from a boresighted stereo system (parallel camera alignment) can be constructed from the resulting pseudo-stereo pair of images. Rectification is achieved by transforming the image planes so that the corresponding space planes coincide [108], in other words, applying transformations which map the epipoles to infinity. It must be born in mind that this image rectification is not possible if either epipole lies inside the image.

The STEREO-CPs method is used to generate the CPs and rectification is performed using the DRUI direct rectification algorithm for un-calibrated images proposed by Al-Zahrani [97]. DRUI is a short closed calculation that is virtually immediate compared with the more time consuming resampling and display of rectified images. DRUI assumes that the fundamental matrix is known and the modified eight point algorithm proposed by Longuet-Higgins and modified by Hartley [109] is used to estimate the fundamental matrix as illustrated in [110]. The modified eight point algorithm is simple and accurate linear method for estimating the fundamental matrix [111]. In Figure 5.4, two un-calibrated STEREO images have been used to create the anaglyph. STEREO-CPs was used to generate the CPs as shown in Figure 5.4a, and DRUI was applied to rectify the images as shown in Figure 5.4b. The resulting anaglyph is constructed by combining the rectified images as shown in Figure 5.4c.

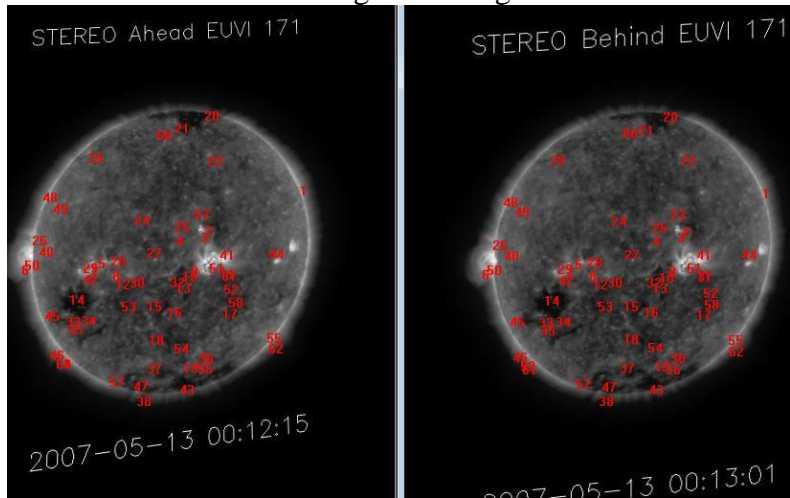
The visual limitation of this method is the resulting distortion of the rectified images from the circular shape. The distortion is limited by including rectify transformations isotropic<sup>14</sup> scaling of the rectified images to make the central epipolar line in each view have equal lengths before and after rectification. The distortion could be minimised by applying appropriate skewing transformation to the images but cannot be eliminated because the epipolar lines are parallel in the pseudo-stereo pair.

---

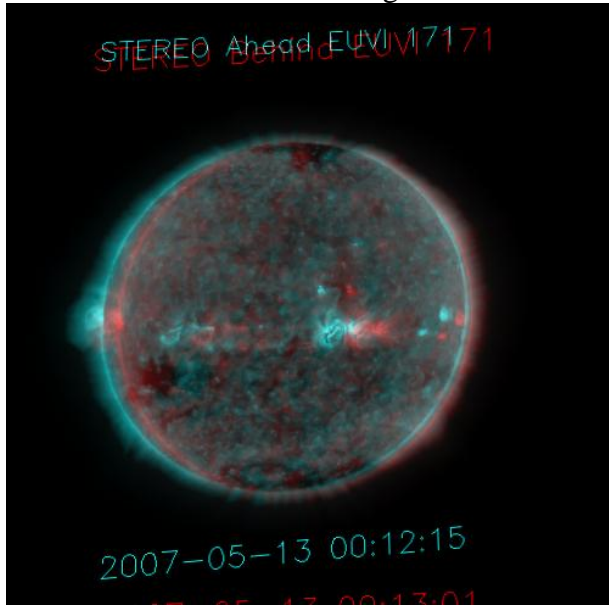
<sup>14</sup> Isotropic means that the intensity of the radiated light is the same in all directions.



a. Image matching.



b. Rectified images.



c. Anaglyph

**Figure 5.4 Anaglyph creation from a rectified pair of un-calibrated images using CPs from the STEREO-CPs method. (a) Feature matching by applying STEREO-CPs. (b) Rectified images after running DRUI on images shown in Figure (a). (c) 3D image of the Sun.**

### 5.3.2 *Verging stereo anaglyphs*

To follow the same processes of alignment as used when the calibration information is available: firstly, the resize factor ratio is estimated by finding the minimum  $x$  and  $y$  coordinates from the set of CPs within the left and right images as shown in Figure 5.5. The resize factor then can be calculated by Equation 5-5. Secondly a reference pair of points is required to fit the pair images with a proper offset which can be  $Lminx, Lminy$  and  $Rminx, Rminy$  in the left and right images respectively. An Euclidean transformation can be used to bring the right image into alignment with the left image based on the geometric relationship between the corresponding points. In this step, the resulting CPs from STEREO-CPs method are fed to a data-fitting function called “cp2tform” which is included in MATLAB to determine the parameters of the transformation needed to bring the image into alignment as shown in Table 5-1. “cp2tform” returns the parameters in a geometrical transformation structure. The Euclidean transformation is determined by passing the “linear” parameter to rotate the image into alignment with the map coordinates.

This technique has been tested on several pairs of STEREO images and efficiently produced visually satisfactory anaglyphs. Figure 5.6 shows four outcomes using images in four extreme ultraviolet wavelengths. The labels on the original images were maintained to identify the processed images before the combination. This technique will be available to generate anaglyphs in near real-time when the two spacecrafts meet again at the behind of the Sun in a few years’ time.

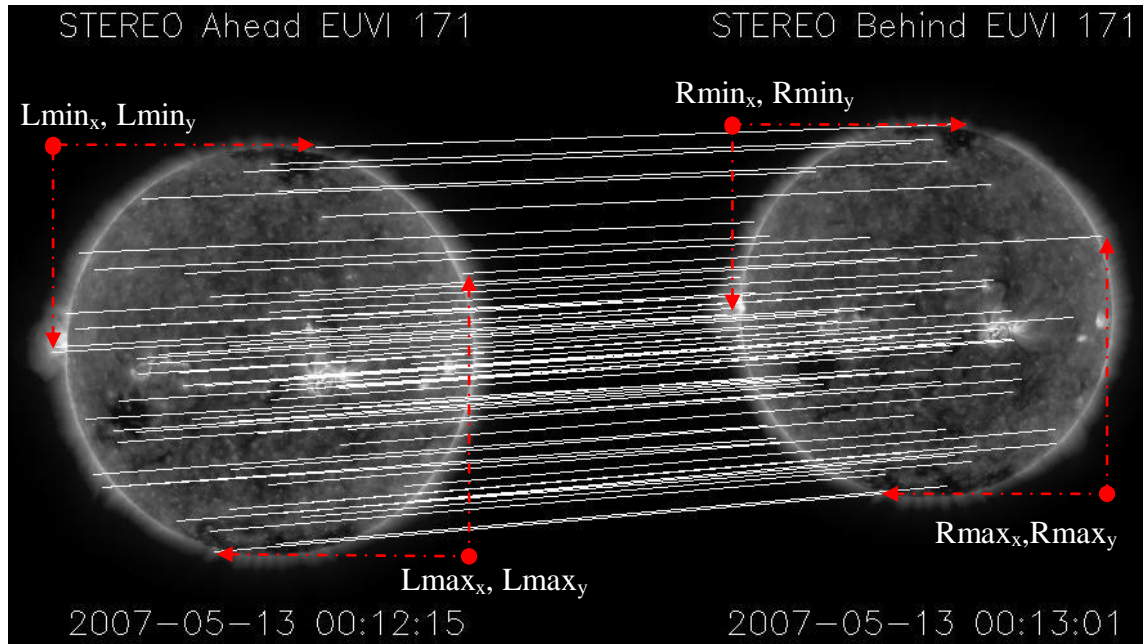


Figure 5.5 The resulting CPs from STEREO-CPs are used to estimate the different sizes of the full solar disk. The top left and bottom right corners of the outbound rectangle for each image is determined by finding the minimum and maximum x, y coordinates of the CPs.

$$ResizeFactor = \left| \frac{Lmax_x - Lmin_x}{Rmax_x - Rmin_x} \right| \tag{5-5}$$

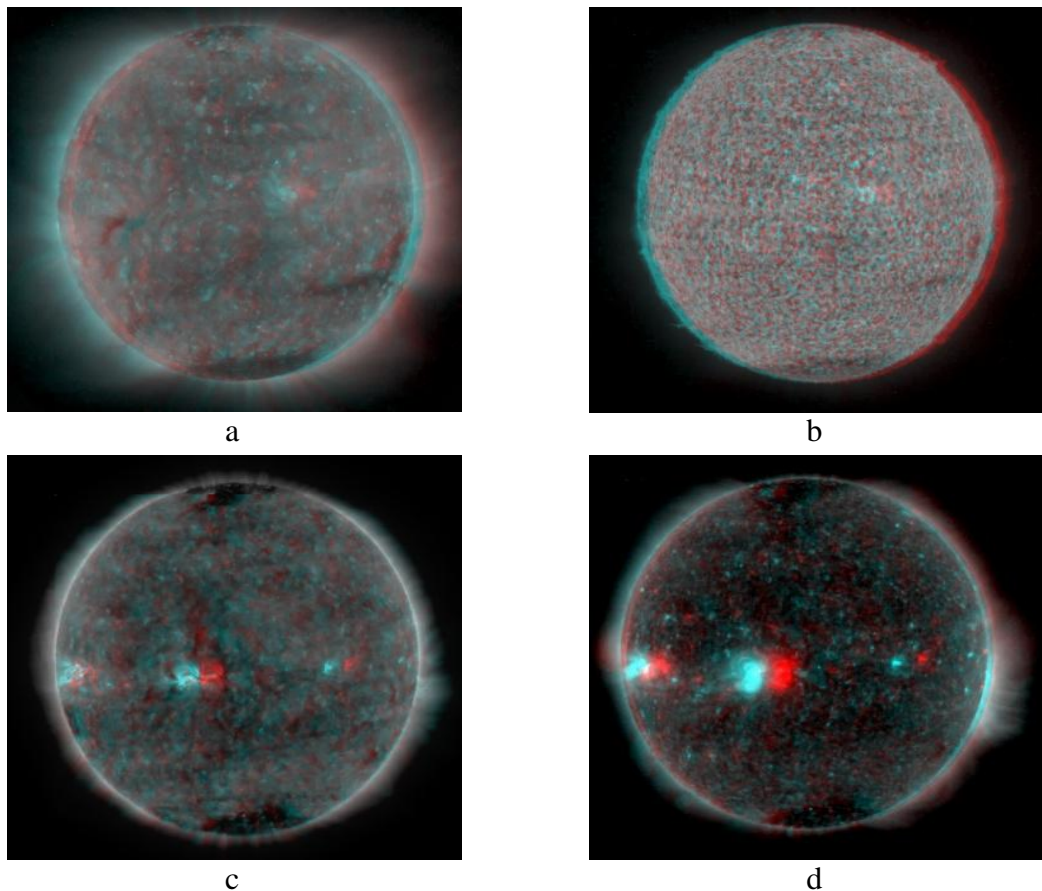
Table 5-1 MATLAB commands to bring two images into alignment using the resulting CPs from STEREO-CPs method.

No	MATLAB Command	Comment
1	<code>[input_points base_points]=STEREO_CPs(file1,file2);</code>	Return the resulting CPs from STEREO-CPs method
2	<code>mytform = cp2tform(input_points, base_points, 'linear');</code>	Return the parameters of the transformation needed to bring the image into alignment. The Euclidean transformation is selected.
3	<code>registered = imtransform(unregistered, mytform);</code>	Bring the image into alignment.

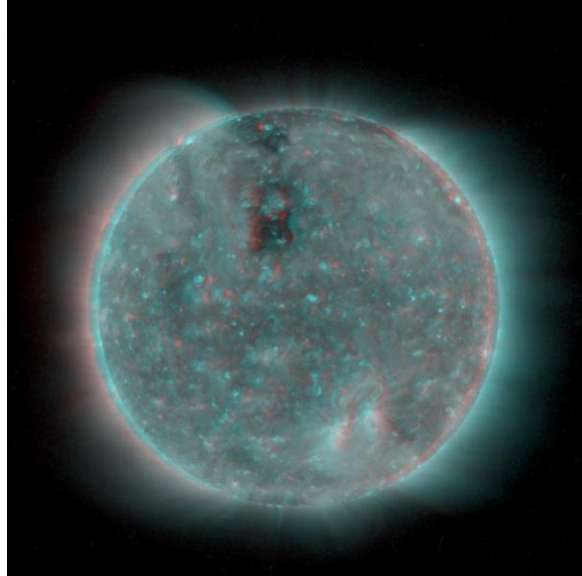


## 5.4 Anaglyphs at large separation angles

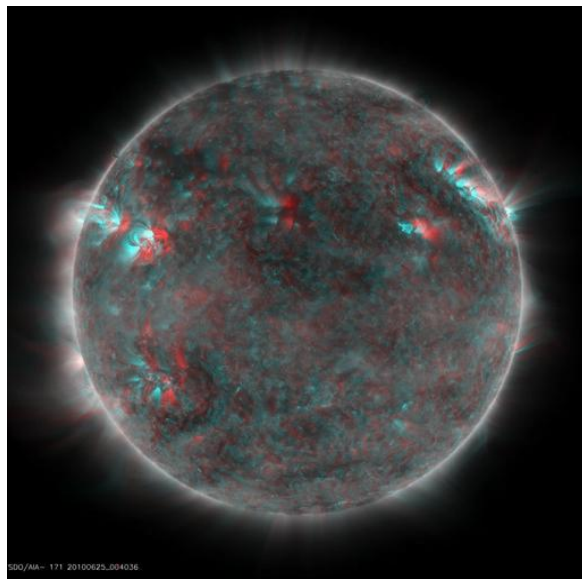
In future work, the process of creating anaglyphs from the STEREO spacecrafts when their separation angle is between 40 and 90 degrees should be considered. A possible solution is to investigate the numerical techniques described in [24]. However anaglyphs can still be created by combining two extreme UV images taken at different times by one spacecraft e.g. two EUV 195 Å images taken 12 hours apart by STEREO Ahead on Aug. 07, 2009 was generated and displayed in [112] as shown in Figure 5.7. Similarly, the SDO mission can be used to generate 3D images of the Sun from a single spacecraft and the anaglyph shown in Figure 5.8 was generated using SOLARSTUDIO to combine two images that were taken in a EUV wavelength about 8 hours apart on Jun 25, 2010.



**Figure 5.6** 3D images for the full disk of the Sun generated from uncalibrated pairs of images. 3D images using EUVI of (a) 195 Å. (b) 304 Å. (c) 171 Å. (d) 284 Å.



**Figure 5.7 Anaglyph of the Sun created by combining two images taken 12 hours apart by STEREO Ahead on August 7, 2009. This figure was included in [112].**



**Figure 5.8 Anaglyph of the Sun combining two EUV images that were taken about 8 hours apart (June 25, 2010) into one 3D image. This image was generated by the SOLARSTUDIO application written by the author.**

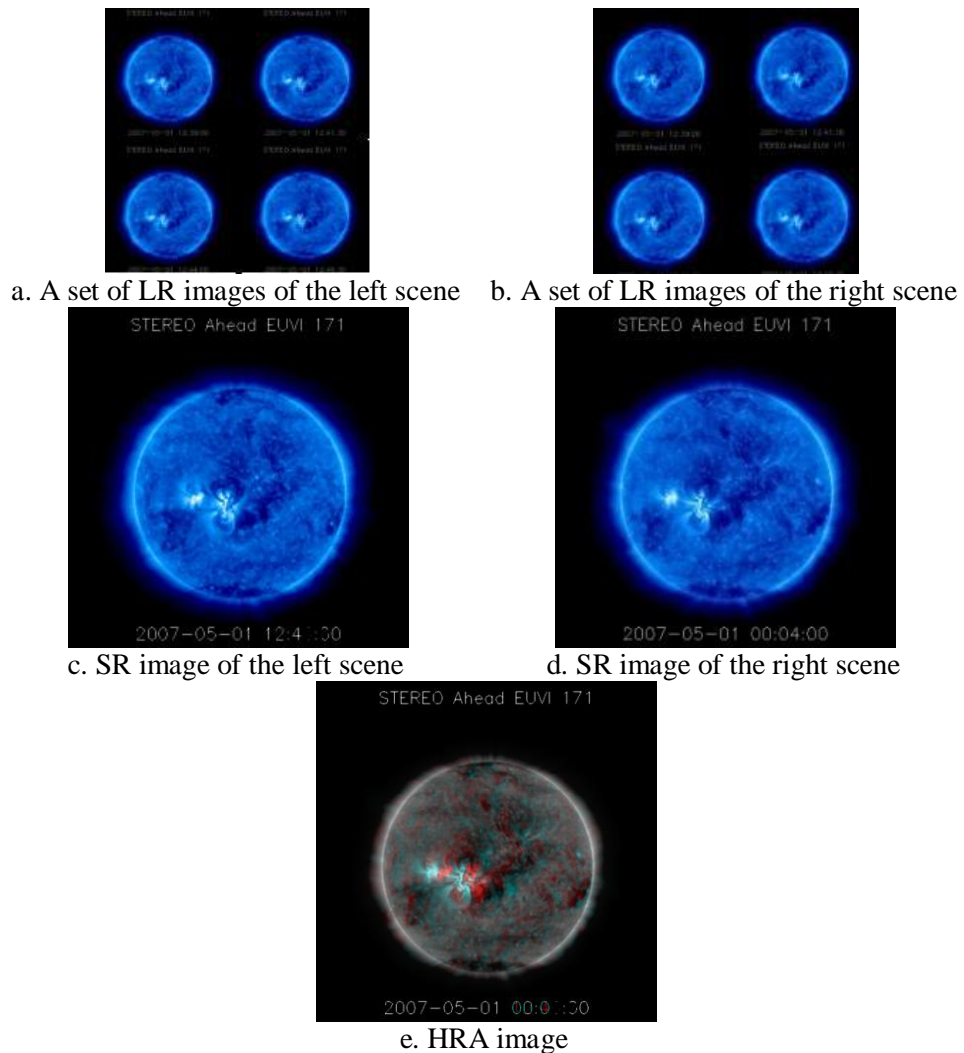
### **5.5 Anaglyphs from pairs of super resolution images**

High Resolution Anaglyphs (HRAs), as the name implies, are anaglyphs created with a higher resolution than the original images. This can be achieved by applying the SR method proposed in Chapter 4 to provide a high resolution (HR) pair of images from

two sets of low resolution (LR) images of both views (left and right) as shown in Figure 5.9.

### 5.6 Evaluation

In order to make quantitative comparisons between the performances of the algorithms of sections 5.2 and 5.3.2 in rescaling the solar disk using the calibration information included in header FITS files and information available in the images, the ratio of the disc sizes in Ahead and Behind images were calculated. The resulting ratios are shown in Table 5-2. The average absolute difference between the two methods for the conducted experiments is 0.45%.



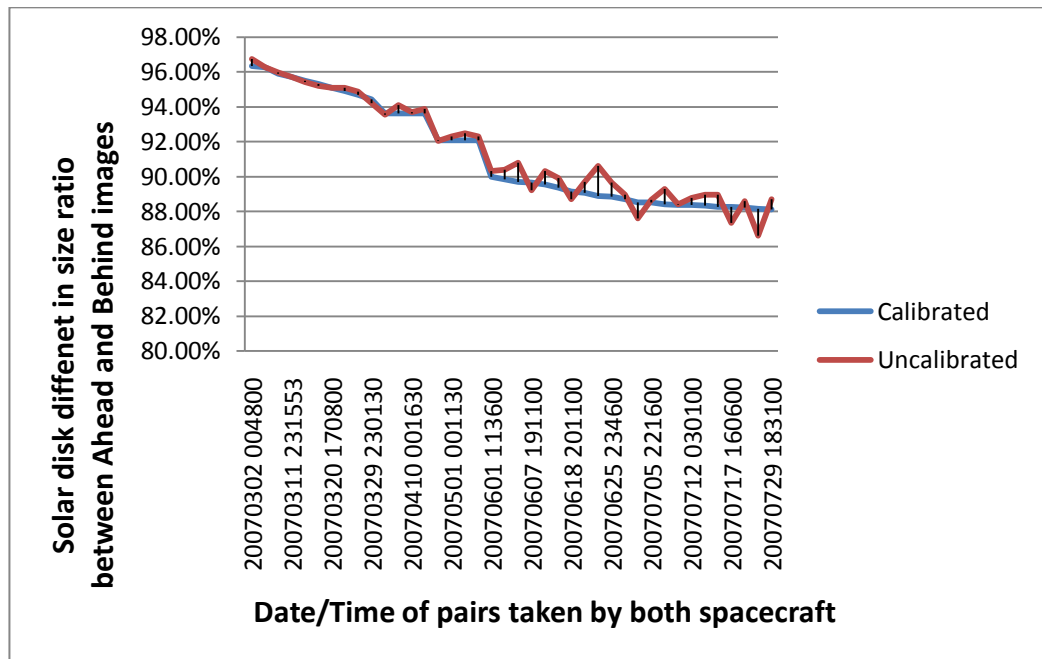
**Figure 5.9 Steps to create the HRA image.**

**Table 5-2 Performance evaluation between rescaling from calibrated and uncalibrated pairs of STEREO images. The ratios are the estimated sizes of STEREO Behind images to STEREO Ahead images. The calibration information and the proposed method are given the abbreviations Cal and PM respectively.**

No.	Date/Time Month DD,YYYY HH:MM:SS	Estimated Size Ratios		Error% Abs(Cal-PM)
		Calibration (Cal)	Proposed Method (PM)	
1	20070302 004800	96.34%	96.74%	0.40%
2	20070303 101800	96.25%	96.27%	0.02%
3	20070308 224553	95.90%	95.99%	0.09%
4	20070311 231553	95.70%	95.71%	0.01%
5	20070314 204800	95.51%	95.44%	0.07%
6	20070317 200800	95.31%	95.19%	0.12%
7	20070320 170800	95.11%	95.10%	0.01%
8	20070323 110800	94.92%	95.10%	0.18%
9	20070326 112800	94.70%	94.89%	0.19%
10	20070329 230130	94.45%	94.20%	0.25%
11	20070410 000400	93.64%	93.54%	0.10%
12	20070410 000900	93.64%	94.10%	0.46%
13	20070410 001630	93.64%	93.71%	0.07%
14	20070410 005900	93.63%	93.87%	0.24%
15	20070501 000400	92.08%	92.03%	0.05%
16	20070501 001130	92.08%	92.32%	0.24%
17	20070501 001200	92.08%	92.47%	0.39%
18	20070501 002900	92.08%	92.30%	0.22%
19	20070601 113600	90.00%	90.33%	0.33%
20	20070604 150100	89.83%	90.40%	0.57%
21	20070606 173600	89.71%	88.37%	1.34%
22	20070607 191100	89.66%	89.22%	0.44%
23	20070610 004830	89.54%	90.32%	0.78%
24	20070613 181100	89.36%	89.93%	0.57%
25	20070618 201100	89.13%	88.72%	0.41%
26	20070619 211600	89.08%	89.69%	0.61%
27	20070624 222600	88.88%	90.06%	1.18%
28	20070625 234600	88.84%	89.66%	0.82%
29	20070629 220100	88.70%	88.95%	0.25%
30	20070704 223100	88.54%	87.60%	0.94%
31	20070705 221600	88.51%	88.66%	0.15%
32	20070709 183100	88.41%	89.28%	0.87%
33	20070711 033600	88.38%	88.43%	0.05%
34	20070712 030100	88.36%	88.77%	0.41%
35	20070713 033600	88.34%	88.98%	0.64%
36	20070716 033600	88.28%	88.98%	0.70%
37	20070717 160600	88.25%	87.34%	0.91%
38	20070719 163100	88.22%	88.59%	0.37%
39	20070723 180100	88.17%	86.62%	1.55%
40	20070729 183100	88.12%	88.71%	0.59%

This error is quite small and seems to have little detrimental effect on the 3D perception. The experiments cover the period between 2nd of March, 2007 and 29th of

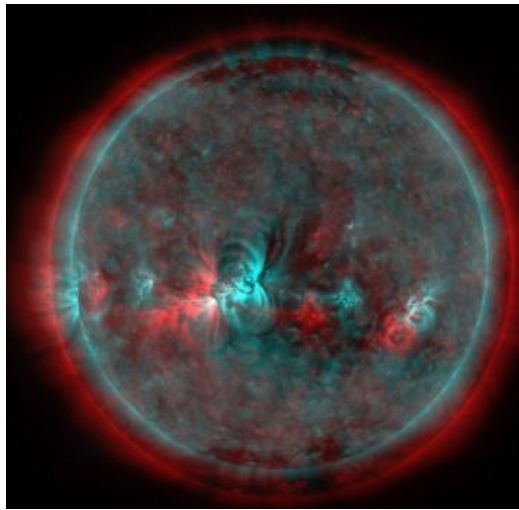
July, 2007 and are presented as a chart in Figure 5.10. This figure shows that the size of the solar disk in STEREO Behind images decreases gradually with respect to the size of STEREO Ahead images as the mission proceeded in this period. It also shows that the error ratio increases gradually when the separation angle between the two spacecraft increases. Note that the size ratio scale and the date/time of images in this chart are arranged to clarify the small error differences. Two images from the samples with 1.34% error are combined to show the difference in the size of full disk of the Sun for a pair of STEREO images taken on 6th of June 2007 at 17:36:00 as shown in Figure 5.11. In spite of this difference, 3D perception is achieved in both cases.



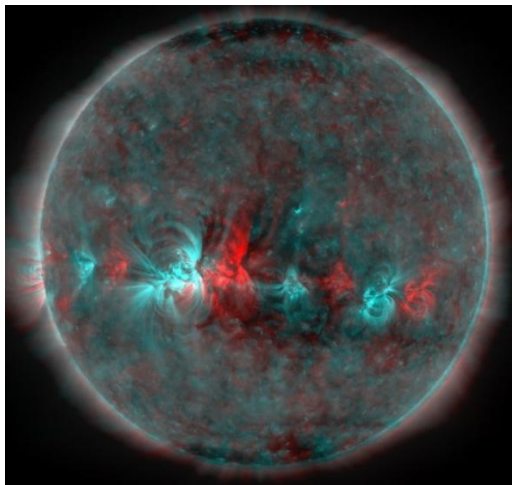
**Figure 5.10 The performance of the algorithm presented in section 5.3 is evaluated compared with the method of rescaling the full solar disk STEREO pairs using the calibration information included in header FITS files.**

A visual comparison between LR anaglyph image and HRA image is shown in Figure 5.12. Zooming into a region of interest with the same scale is used to show the visual enhancement of the HRA anaglyph over the normal one. Another example of HRA image for the full disk Sun is shown in Figure 5.13, no zoom is applied; the HRA

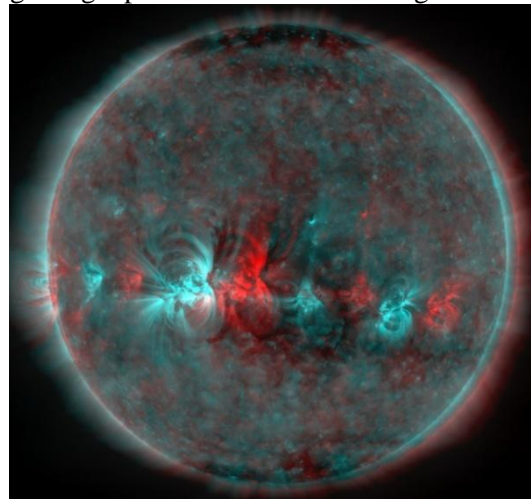
image provides finer details than the normal anaglyph image.



a. Superposition of image without rescaling using a pair of un-calibrated images.



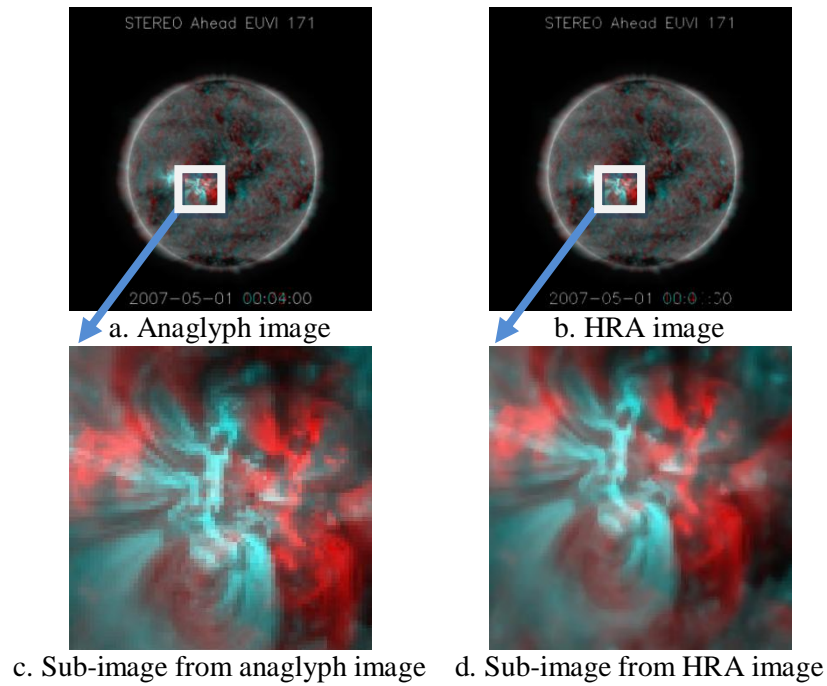
b. Fitted and rescaled image from calibrated pair of images.



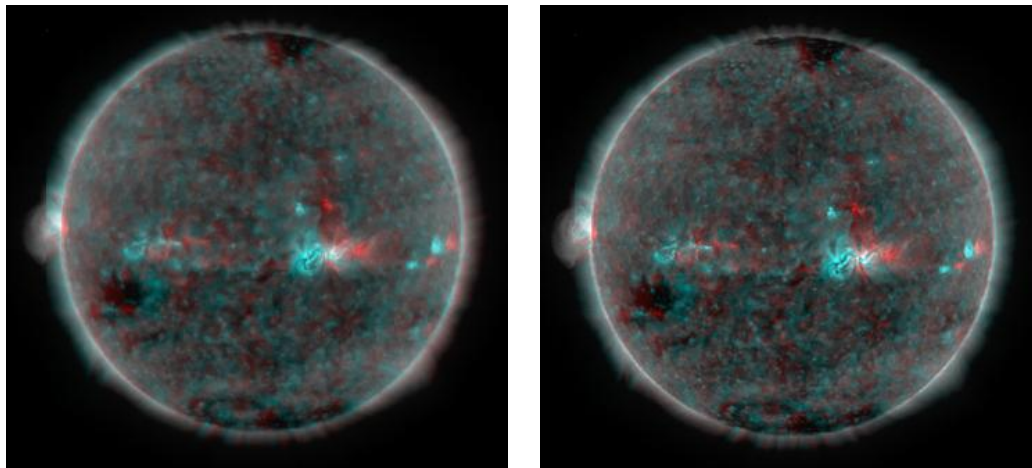
c. Fitted and rescaled image from un-calibrated pair of images with error ratio 1.34%.

**Figure 5.11** Visual comparison to clarify the rescaling process by fitting the full disk of the

**Sun pair of images taken on June, 06 2007 at 17:36:00. (a) Fitting the pair without rescaling. (b) Fitting and rescaling for calibrated pair. (c) Fitting and rescaling for un-calibrated pair using CPs.**



**Figure 5.12 Comparison between anaglyph and HRA.**



a. Low resolution anaglyph      b. High resolution anaglyph

**Figure 5.13 Examples of 3D images of the EUVI 171 Å full Sun. On the left is the 3-D image generated by combining pairs of LR images, and on the right is the 3-D image generated using HR images. The images were taken on May 13, 2007.**

## 5.7 Conclusion

Anaglyphs are a cost-efficient and technically simple way of generating stereoscopic images. Anaglyphs of the Sun can reveal features that are not apparent in 2D images and are obtained by combining a pair of STEREO images using a pair of complementary colours (often red and blue/green for the Ahead and Behind spacecraft

respectively). Currently anaglyphs are created by manual rescaling and fitting by the user or by using IDL methods provided by “SolarSoft” using the information available in the FITS file headers. FITS files only become available a few days after the real observations. Also the license requirements for IDL packages could restrict the public use of some of the developed functions for processing solar data.

To tackle these limitations new techniques are proposed in this research. The first is to efficiently create anaglyphs for the Sun and provide algorithms able to work in near real-time using CPs from STEREO-CPs. This will be useful to view the back side of the Sun in 3D when the two spacecraft next approach each other. The second technique is to enhance the 3D perception by combining a superior pair of images generated by the proposed SR method presented in this thesis rather than LR images. The performance of the proposed rescaling method was compared with the process of rescaling using calibration information included in FITS file headers. The results show that the proposed rescaling method over the tested period gives very similar results to those obtained using calibration data. Advantages of the proposed method are that it is simple, and saves the user time and effort.



# CHAPTER SIX

## 6 SOLARSTUDIO: A TOOL FOR VISUALIZING AND PROCESSING LARGE SETS OF SOLAR IMAGES

### 6.1 Introduction

As explained earlier, STEREO and SDO provide full disk images of the Sun at different cadence rates in different wavelengths with maximum resolutions of  $2048 \times 2048$  and  $4096 \times 4096$  pixels, respectively. It is not an easy process to download, browse and analyze significant areas of interest for these data volumes on a remote server, simply because these processes overload the existing Internet and network infrastructures. Also from a scientist's viewpoint, the process of retrieving large data volumes from even a few repositories, and dealing with immobile data sets poses the problems of searching, browsing and extracting images of interest while avoiding the search for a needle in a haystack problem, as explained in [21]. The SOLARSTUDIO visualizing and analysing software has been developed to tackle these problems.

### 6.2 Motivations for developing SOLARSTUDIO

As explained in Chapter 2, several applications have been developed to view solar images including: STEREO-GSFC, SDO-GSFC, SWB, and JHelioviewer. However, major challenges still exist when studying the solar atmosphere at different scales, times and wavelengths. Firstly, limited functionalities are offered by the official browsers

tools for both STEREO and SDO. Secondly, there exist restrictions on the number of images queried per user. Thirdly, there is a serious lack of developed systems that enable users to access multi-wave length images from more than one satellite at the same time. Finally, the license requirements of the IDL programming language could restrict the public use of some of the developed functions for processing solar data. To tackle some of these challenges, SOLARSTUDIO was developed.

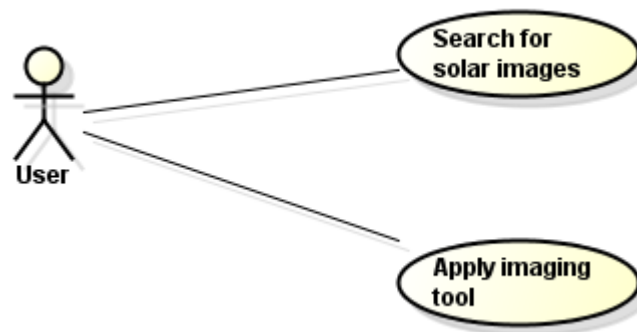
SOLARSTUDIO could help scientists discover new phenomena and link related data sets from various instruments that are often analyzed in isolation. To achieve this, SOLARSTUDIO enables the user to browse images from both STEREO and SDO satellites using a unique GUI (Graphical User Interface). SOLARSTUDIO has a modular object-oriented-based design, which makes it easy to update according to users' feedback. SOLARSTUDIO will be available in the public domain, and users would be able to download it from <http://spaceweather.inf.brad.ac.uk/index.html>, as a standalone application including installation instructions and a user manual.

This chapter is organised as follows: SOLARSTUDIO's operation, image access, architecture and features are described in sections 6.3, 6.4, 6.5 and 6.6, respectively. Comparisons with other systems are introduced in Section 6.7, while conclusions are provided in Section 6.8.

### **6.3 The SOLARSTUDIO Imaging Tools**

The SOLARSTUDIO was developed to download the remote JPEG and FITS images provided by the STEREO and the JPEG images provided by the SDO. Also other compatible images (BMP, TIFF, PNG, and JPEG and FITS files) can be accessed locally. SOLARSTUDIO enables the user to browse these images using a unique GUI (Graphical User Interface). SOLARSTUDIO has a modular object-oriented-based

design, which makes it easy to update according to users' feedback. The UML (Unified Modelling Language) is used to show the architecture of this system as follows: the use case diagram which describes the two main processes (browsing and processing) offered by the SOLARSTUDIO is shown in Figure 6.1. The sequence diagrams for browsing and processing the solar images are shown in Figure 6.2 and Figure 6.3 respectively. Communications between the classes of SOLARSTUDIO are shown in Figure 6.4, where the "Imaging Tool" class is the super class from which the other sub-classes inherit its attributes and operations which are described in Section 6.6.



**Figure 6.1 Use case diagram of SOLARSTUDIO indicating the main two processes: image browsing and applying an imaging tool.**

Currently SDO FITS images are accessed outside the application. SOLARSTUDIO makes it possible to retrieve images from two satellites while maximizing their usability. Accessing these huge data volumes efficiently at both high spatial and high time resolutions is important to support scientific discovery. SOLARSTUDIO allows users to browse large data volumes as still images, and/or movies of multiple resolution image files. An archive system is incorporated also to save the requested images, so next time they are needed there is no need to download them again (useful if no Internet connection is available). Users can display, process, zoom, build super resolution images and construct anaglyphs (from un-calibrated STEREO pairs) automatically, without strict network bandwidth penalties.

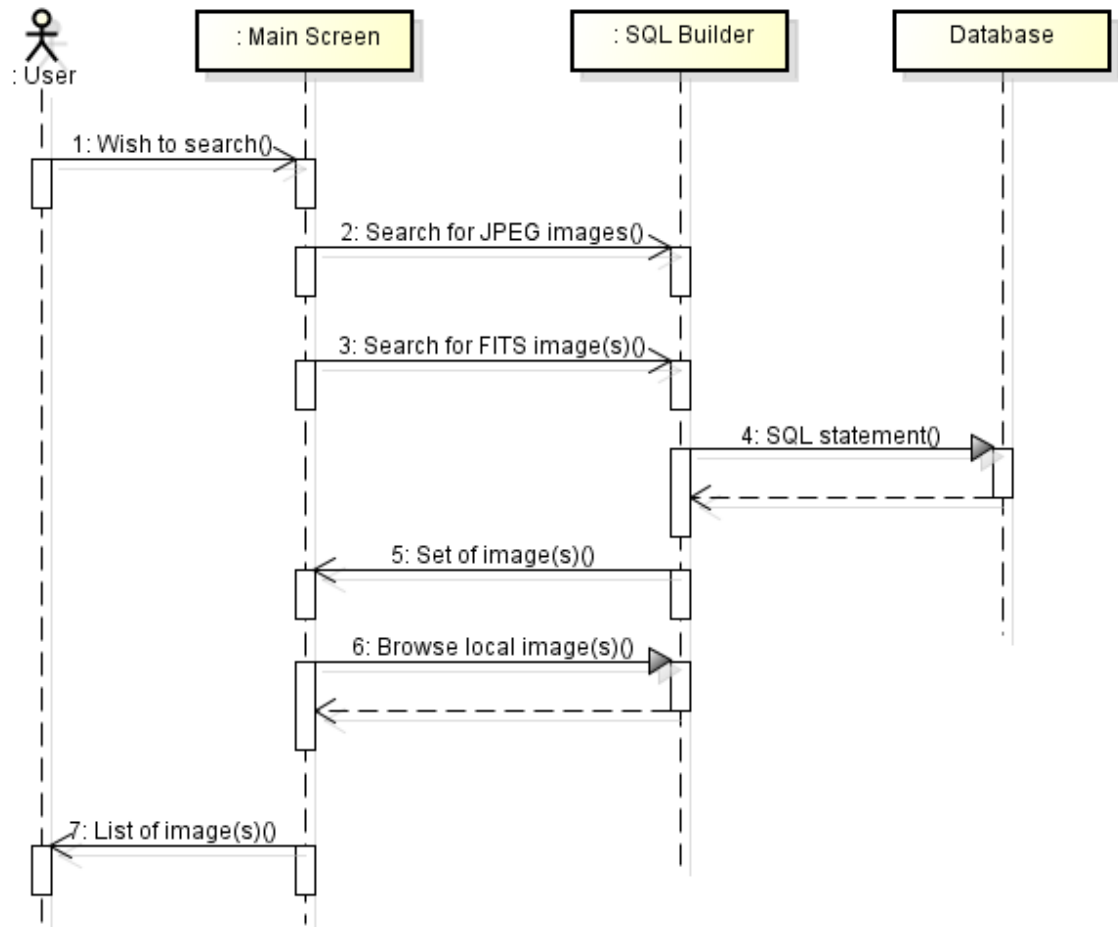


Figure 6.2 Sequence diagram to represent the process of browsing the remote and local image(s).

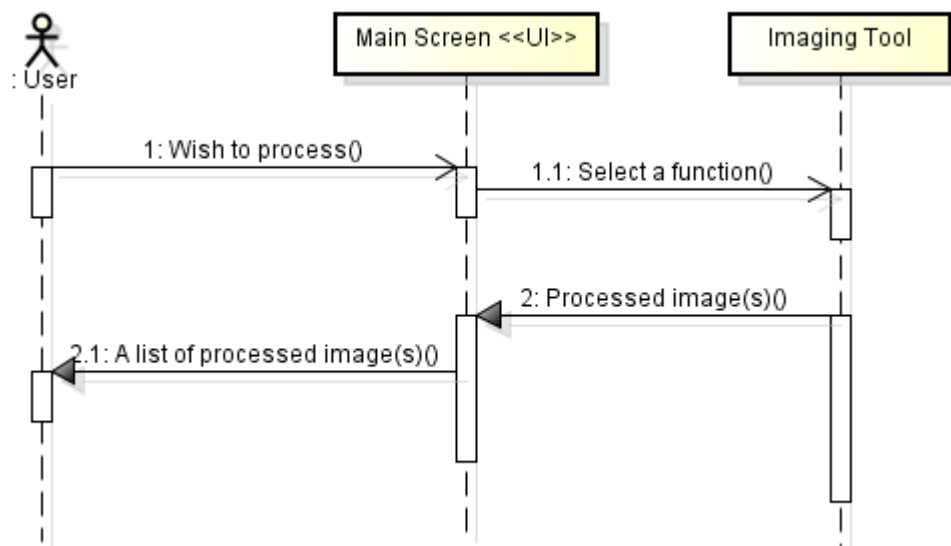
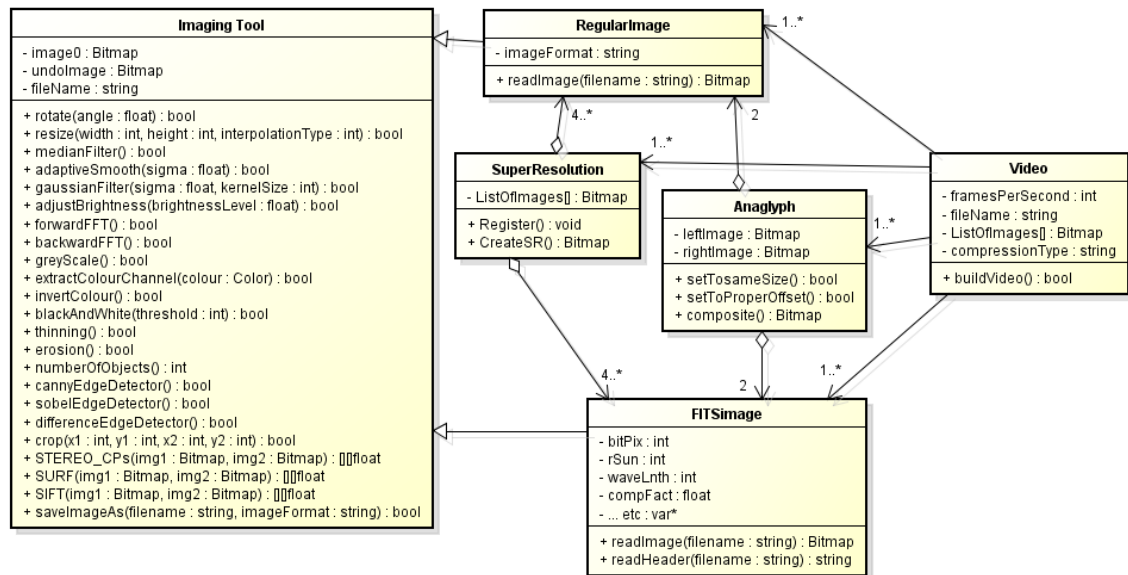


Figure 6.3 Sequence diagram to represent the process of applying an image tool.

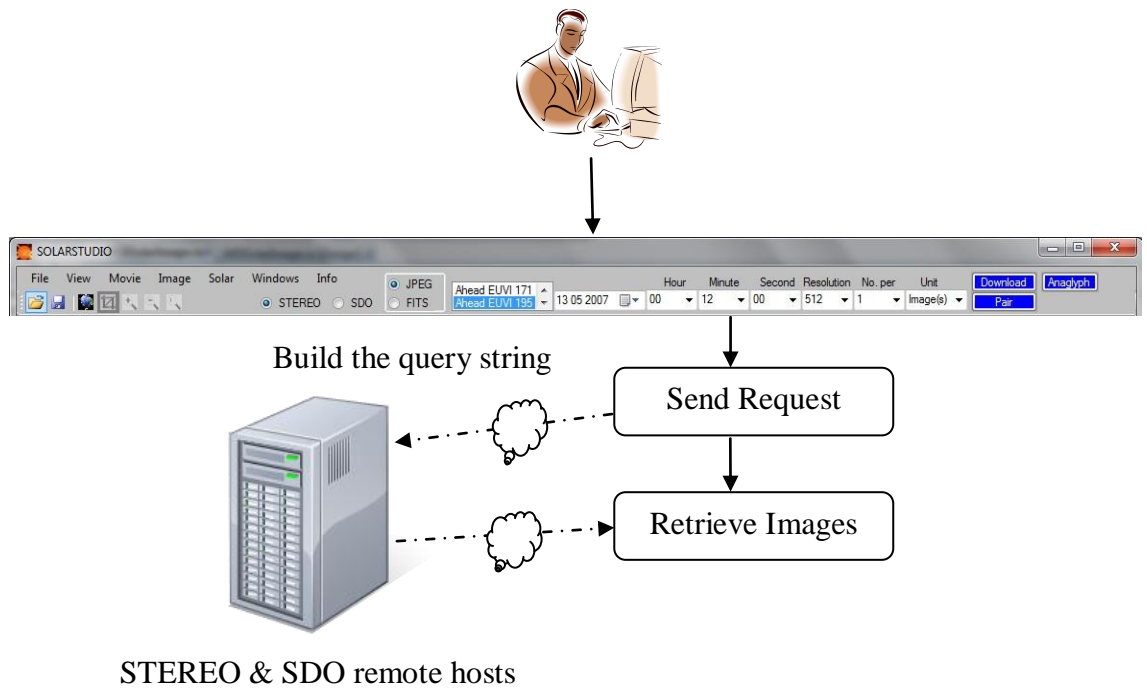


**Figure 6.4** Class diagram to represent all classes in the SOLARSTUDIO associated with their relations between them.

## 6.4 Remote Image Access with Web-Request Class

Web-Request is an abstract base class for the .NET Framework's request/response model for accessing data from the Internet. It makes a request to a Uniform Resource Identifier (URI) (see [90]). SOLARSTUDIO uses this class to request data from the official STEREO and SDO websites. For example, a request for images from STEREO or SDO is performed by sending a request to the URIs of [2] and [91], respectively.

The URI is a string that is built during run time from a query string. The query string represents the resource on the Internet that is created from the parameters requested from users as shown in Figure 6.5. The file names of images for both STEREO and SDO missions are saved into a relational database. Two relational tables are created to save the file names for each mission as shown in Table 6-1. An index key is created also for each table in order to speed up the query process. The URI structures for STEREO and SDO are shown in Table 6-2 and Table 6-3 respectively.



**Figure 6.5** The process of accessing remote images in SOLARSTUDIO platform.

**Table 6-1** Relational data definition created to save the data for both STEREO and SDO using information from the file names of images.

Field name	Data type	Description
Image Name	Text	Primary Key
Observation Time	Date/Time	Indexed key(yes for duplicate)

**Table 6-2** The URI structure for STEREO images.

Field	Description	Example
Host	Remote host address	<a href="http://stereo.gsfc.nasa.gov/browse">http://stereo.gsfc.nasa.gov/browse</a>
Year	The year is in YYYY format	2007
Month	The month is in MM format	05
Day	The day is in DD format	01
Spacecraft	Spacecraft name	Ahead
Instrument	Instrument type	Euvi
Telescope	Telescope type	171
Resolution	Resolution in pixels	128
ImageName	JPEG image file name in YYYYMMDD_HHMMSS_string_Telescope.jpg	20070501_235900_n4euA_171.jpg
URI	The URI composed from merging all above fields	<a href="http://stereo.gsfc.nasa.gov/browse//2007/05/01/ahead/euvi/171/128/20070501_235900_n4euA_171.jpg">http://stereo.gsfc.nasa.gov/browse//2007/05/01/ahead/euvi/171/128/20070501_235900_n4euA_171.jpg</a>

**Table 6-3** The URI structure for SDO images.

Field	Description	Example
Host	Remote host address.	<a href="http://sdo.gsfc.nasa.gov/assets/img/browse">http://sdo.gsfc.nasa.gov/assets/img/browse</a>

Year	The year is in YYYY format.	2010
Month	The month is in MM format.	06
Day	The day is in DD format.	01
ImageName	JPEG image file name in YYYYMMDD_HHMMSS_Resolution_Telescope.jpg format.	20100601_000136_512_0171.jpg
URI	The URI composed from merging all above fields	<a href="http://sdo.gsfc.nasa.gov/assets/img/browse/2010/06/01/20100601_000136_512_0171.jpg">http://sdo.gsfc.nasa.gov/assets/img/browse/2010/06/01/20100601_000136_512_0171.jpg</a>

## 6.5 SOLARSTUDIO Components

A user friendly interface has been created to provide image browsing capabilities. It offers access to local or remote images, creates animations for whole image(s) or regions of interest (sub-image(s)) and makes available several image processing methods including the extraction of colours, Gaussian, smoothing and median filters, thresholding, conversion to gray scale, resizing (Bicubic, Bilinear, Nearest Neighbour), cropping, sharpening, edge detection (Laplacian, Sobel and Difference), brightness adjustment, rotation, Fourier Transform (FFT) (backward and forward), thinning and erosion. All these image processing methods can be applied on the large image data sets related to STEREO and SDO. For example, the users could interactively browse a number N of images, seconds, minutes, hours, days or months after a predefined date/time, e.g. if N=100 and the user selects the value parameter images, then the download terminates after downloading 100 images, but by selecting the value parameter seconds, then it terminates after 100 seconds of the predefined date/time, and so on.

SOLARSTUDIO makes the local and remote image sets easily accessible via a .NET framework client application. Hence, all image processing methods are performed on the local machine (client side). A user selects a set of images for visualisation and processing and the system checks to see whether each image in the set already exists in the local machine. The user usually specifies the satellite (STEREO or SDO),

---

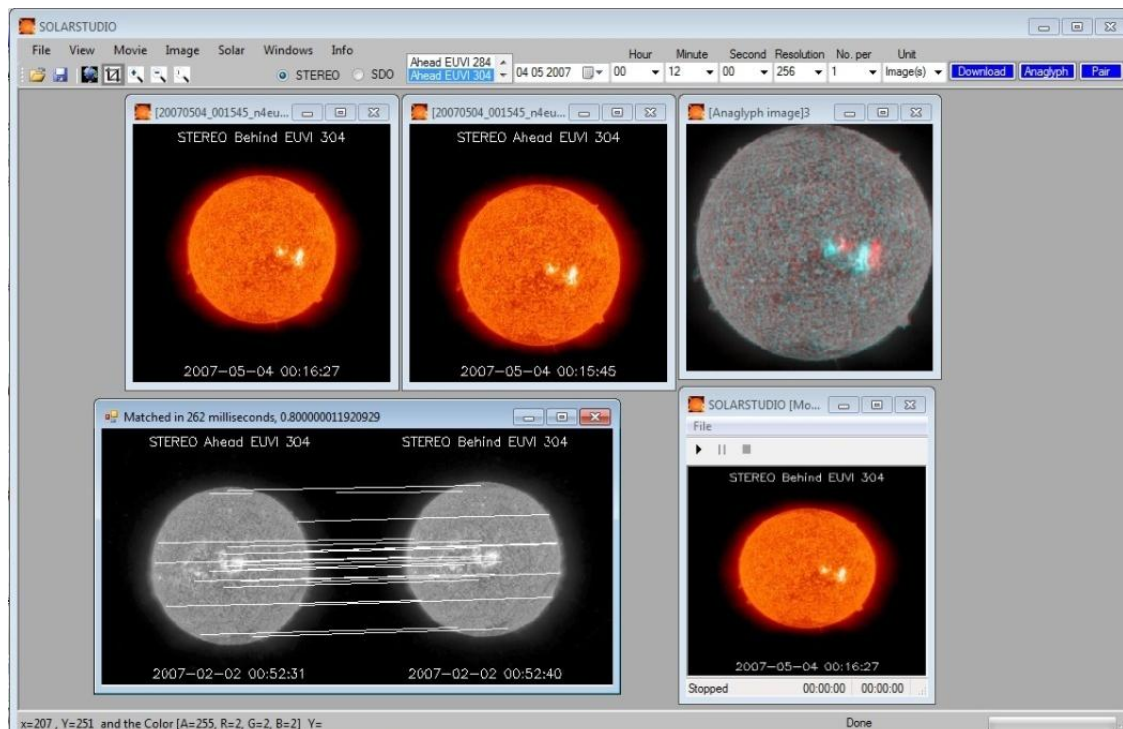
instrument and image dates. If the images do not exist locally, then a download will be performed based on the URI returned by the SQL query. This process is useful; it enhances the system efficiency by avoiding repeating processes on the same data set and the system is able to work on previously accessed data even if no Internet connection is available.

As shown in Figure 6.6, SOLARSTUDIO enables local and remote access for solar images. For instance, a pair of images taken from STEREO's Ahead and Behind spacecraft on 13-May-2007 at 00:13:00 is downloaded remotely and displayed on the local machine. The feature detection and matching method called STEREO-CPs (described in Chapter 3) is applied to this pair of images. The resulting CPs can be used to create an anaglyph image. Also multiple anaglyph images can be used to create a 3D video file.

The architecture of the SOLARSTUDIO client-server application is shown in Figure 6.7. SOLARSTUDIO is organized to request images from two servers if no images exist in the local archive (visited images) repository. The extracted images can be processed locally using any of the general image processing operations mentioned previously. Other image processing methods specifically designed for images from STEREO and SDO can also be applied including: adjusting the solar disks in a pair of STEREO images to the same size, segmenting active regions, tracking object(s) through sequences of images, forming composite images from multiple EU images, extracting the solar limb from images, creating an anaglyph image from pairs of STEREO images and creating a super-resolution image from a sequence of lower resolution images. It is worth mentioning that many of the basic image processing features are available in "SolarSoft" under IDL. However, SOLARSTUDIO is a standalone application and has no licensing requirements, unlike IDL applications. Moreover, SOLARSTUDIO offers



advanced and novel features such as super-resolution, feature detection and matching, 3D anaglyphs and videos creation, etc.

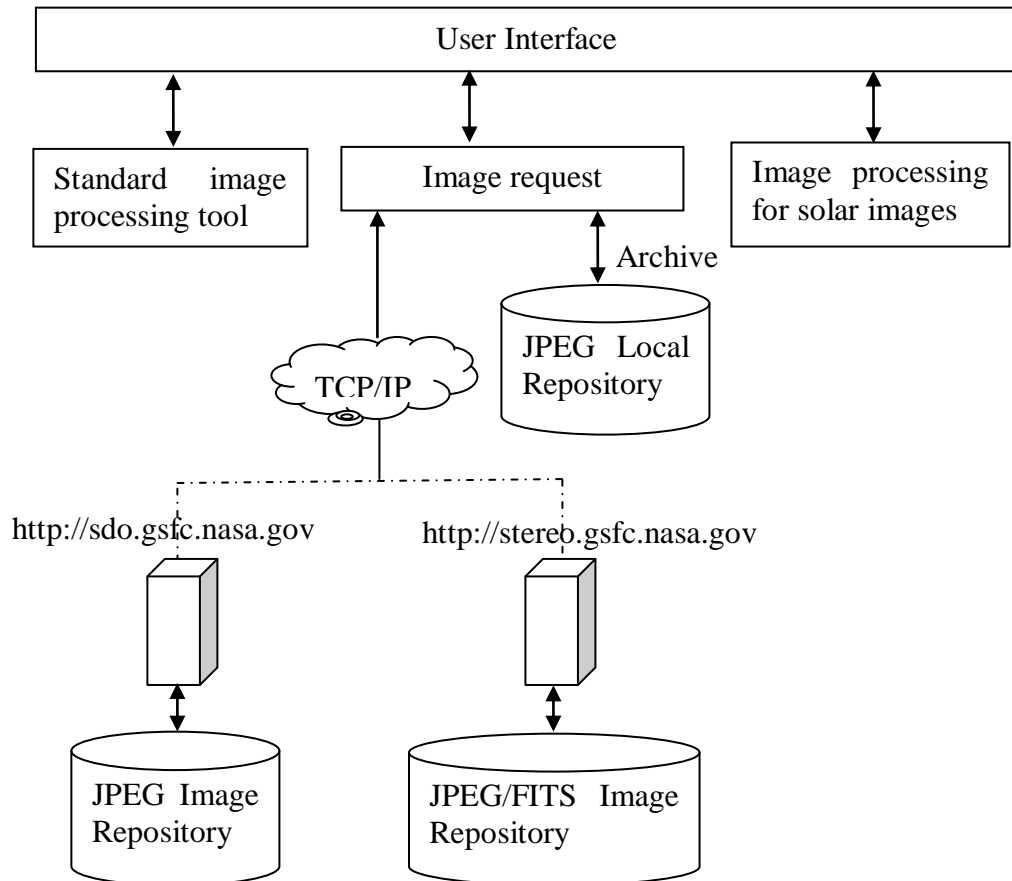


**Figure 6.6 Screenshot of the SOLARSTUDIO application. The above part of the application window is the database search interface. In this example a pair of images of EUVI 304 is used for feature detection and matching, and to create anaglyph and video files.**

## 6.6 SOLARSTUDIO Features

SOLARSTUDIO is designed to allow solar physicists to quickly browse through large volumes of images in JPEG format from both STEREO and SDO missions and provide individual image, video and, in suitable circumstances, 3D views. Having identified a temporal period of interest the relevant uncompressed STEREO FITS images can be downloaded by the user, but this is a slow process because of the large file sizes and also because the relevant images may take a few days to become available on the source servers. SOLARSTUDIO also provides several standard and advanced image processing functions and others specifically focused on solar applications which can be

applied to images saved in JPEG, FITS and several other formats. Resulting images can be saved in BMP, PNG, TIFF, or JPEG formats. The tools currently provided in the SOLARSTUDIO are described in subsections 6.6.1 and 6.6.2.

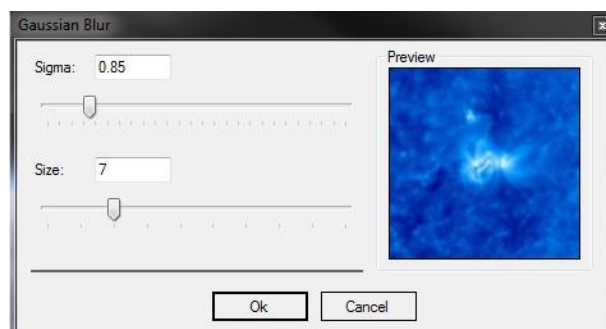


**Figure 6.7 The SOLARSTUDIO components: database interface, STEREO and SDO repositories, the standard image processing operations and specialised image processing operations for solar images.**

### **6.6.1 Standard Image Processing Tools**

Several image processing tools to process and analyse images are integrated in SOLARSTUDIO and the parameters required by the tools are assigned through user friendly interfaces; e.g. using slide bars and/or list boxes, etc. and show the effect on a preview image before applying it on the original image as shown in Figure 6.8. The image processing features and tools included in the SOLARSTUDIO application are:

- Resize and rotate performed using either nearest neighbour, bilinear or bicubic interpolation
- Animation creates a movie loop from displayed images which can be played in SOLARSTUDIO and exported as an AVI file
- Crop can be performed for an unlimited number of frames to extract regions specified by a window defined in the first frame
- Colour operations such as: gray scale, invert, channel extraction and brightness adjustment
- Binarization to produce a binary image based on a user-defined threshold value
- Mathematical morphology operations in 8-bits mode including erosion, objects labelling, dilation and thinning
- Convolution filters including Gaussian smoothing and edge sharpening
- Feature detectors including Harris and Fast corner detectors
- Feature detectors and matching such as Harris with correlation, SIFT and SURF
- Edge detectors including Canny, Sobel and difference methods
- Median and adaptive smoothing filters
- Fourier forward and backward transformations

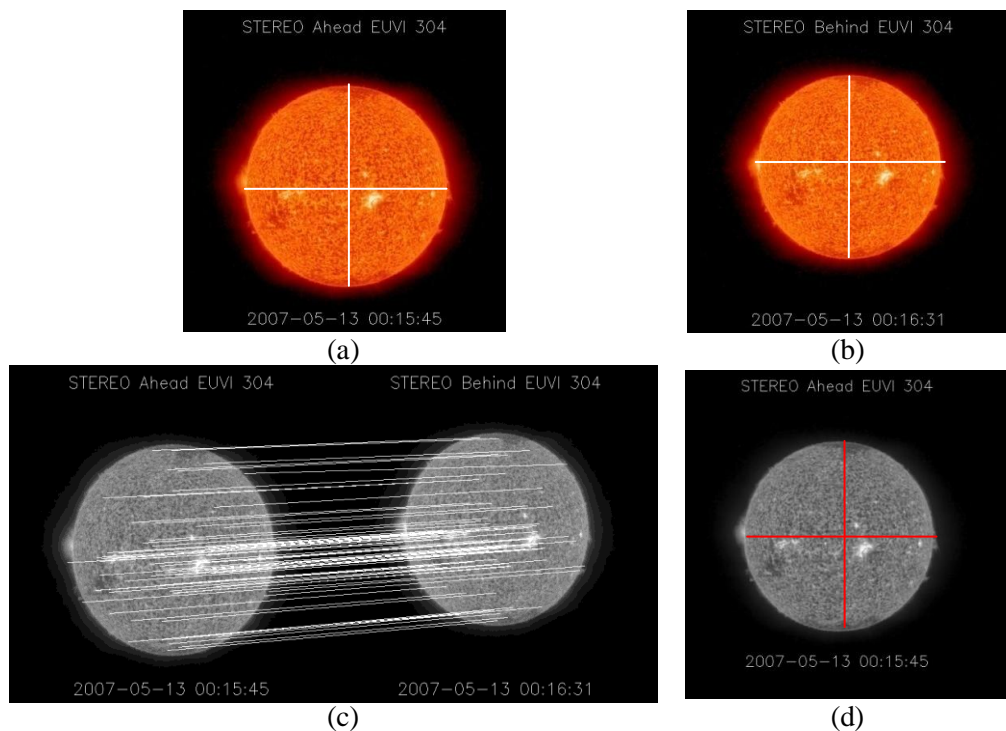


**Figure 6.8 A sample of SOLARSTUDIO's GUI offering a preview of the effect of a Gaussian filter before applying it to the image.**

## 6.6.2 Solar Image Processing Tools

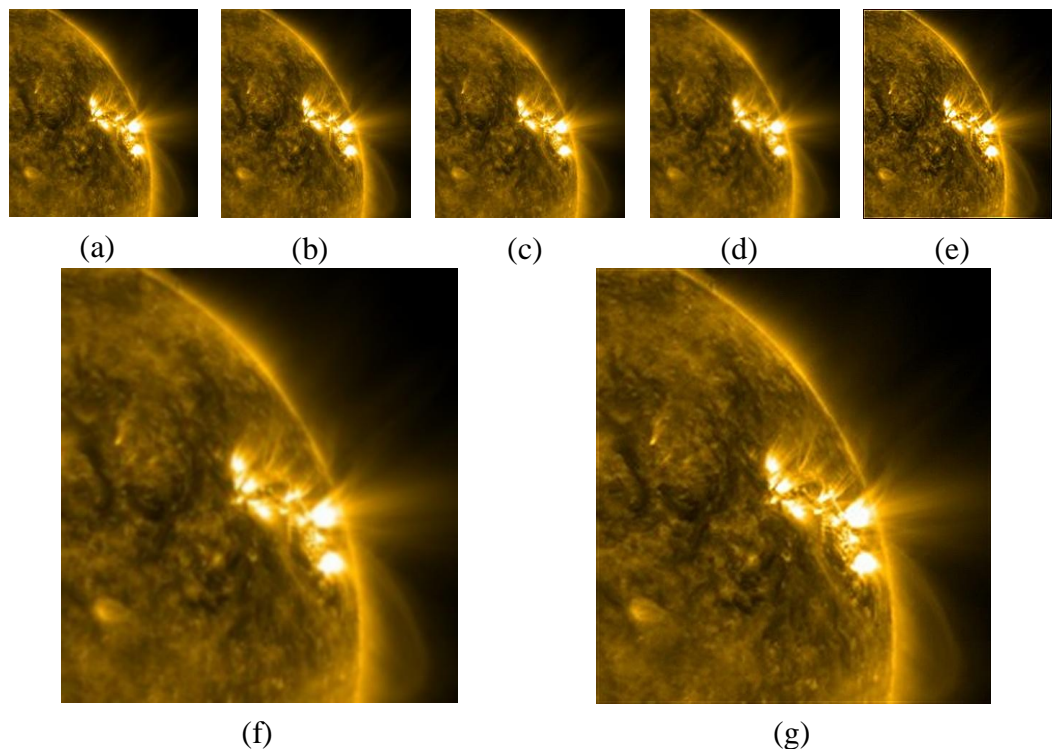
The SOLARSTUDIO functions that are specially designed for the processing of solar images are:

- A method (called STEREO-CPs) based on the SIFT and SURF methods but optimised to detect and match features between a pair of solar images, see Figure 6.9c for an example of corresponding points.
- Rescale the solar disks in different images to the same size using corresponding points.
- Translate the centres of the solar disks in a pair of images to the same locations as shown in Figure 6.9.



**Figure 6.9 Resizing solar disk using CPs obtained using the STEREO\_CP method. The images of size 512×512 pixels are taken from STEREO spacecrafts on 13/05/2007. The vertical and horizontal lines indicate the heights and widths of the solar disks. (a) Ahead EUVI 304 Å, solar disk of size 317×317 pixels (b) Behind EUVI, solar disk of size 290×290 pixels (c) Feature detection and matching generated from STEREO-CPs (d) Ahead EUVI 304 Å, solar disk resized to 290×290 pixels.**

- Super resolution [96] generates a higher resolution image from a minimum set of 4 lower resolution images captured with a cadence high enough to minimise dynamic changes of the sun between the images. A cadence of 2.5 minutes per image has been found to generally give good results. However, in some cases, where no significant changes take place at the Sun, longer cadences can be used shown in Figure 6.10.
- Anaglyphs can be generated from uncalibrated pairs of images using the corresponding points from the STEREO-CPs method, and can be generated from pairs that have been associated with predefined scale factors. The user can choose between two outputs: still image(s) or video files. This can be applied to the full solar disk or to an area of interest, as shown in Figure 6.11.

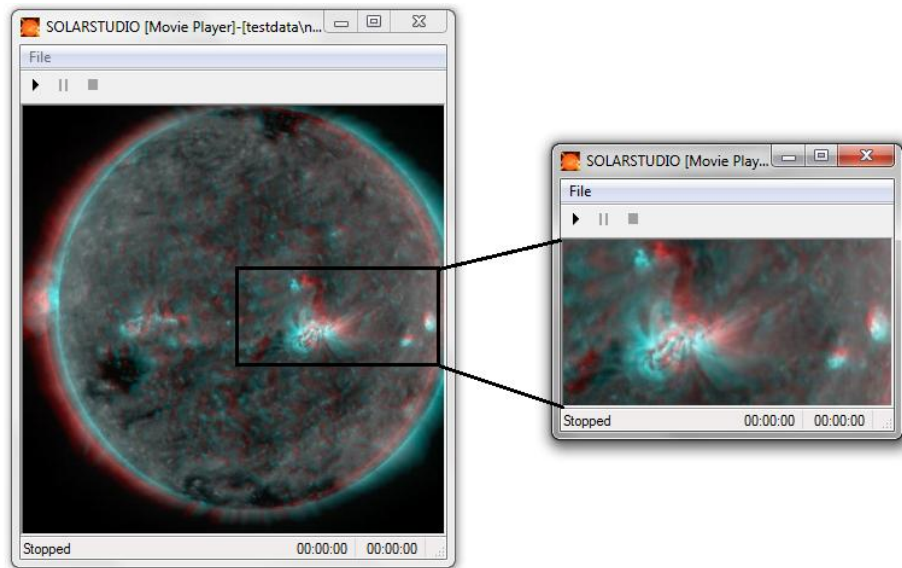


**Figure 6.10** An example applying the SR method, which is integrated in SOLARSTUDIO.

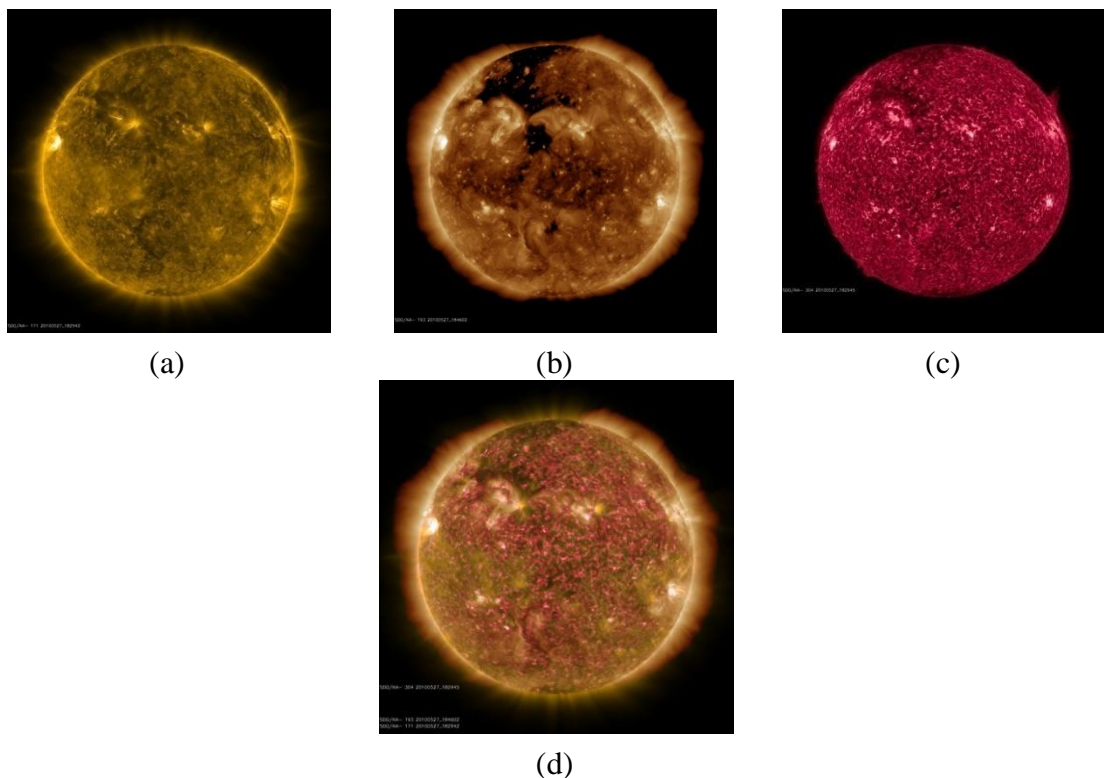
The SDO images shown in (a), (b), (c) and (d), were captured with a cadence rate of 8.25 minutes per image on 20 July, 2010 (the reference image taken at 00:26:48) to produce the

SR image (e) shown at the same size. Image (f) is that of (a) magnified 3 times using

Bicubic interpolation and image (g) is the SR image (e) displayed full size.



**Figure 6.11 SOLARSTUDIO generated 3D video (from whole images or from user defined sub-images) from STEREO pairs of images taken on 13/05/2007 between 12:41:15 UT and 13:06:15 UT.**



**Figure 6.12 Merging colour channels from a sequence of AIA images. This is useful to accentuate features and simultaneously compare between multiple wavelengths. The images were taken by the SDO spacecraft on 27/05/2010. (a) AIA 171 Å (b) AIA 193 Å (c) AIA 304 Å (d) Combined image.**

- 
- Track object(s) through a sequence of images.
  - Segment active regions in EUVI images.
  - Merging unlimited number of EUVI or AIA images building 24 bit colours in the combined image file as shown in Figure 6.12.
  - Movie creation for Active regions from a sequence of images.

### ***6.6.3 Near Real-Time Based System***

To search for the latest STEREO and SDO images can be a time consuming task, often worsened by slow internet access. SOLARSTUDIO is designed to enable the user to view the latest STEREO/SECCHI EUVI and SDO images without having to be concerned with the formats and locations of images. The local database updates automatically following a user request. The system keeps a track of the current date/time and sends automatic requests to download recent images.

It is believed this service is useful, because it provides an up to-date stream of images. SOLARSTUDIO can provide the infrastructure for other systems such as those concerned with space weather predictions which can make use of EUVI and AIA images. The anaglyph features of SOLARSTUDIO could be useful for producing 3D images and videos when the spacecrafts are on other side of the sun from the earth, around the time when the two STEREO spacecrafts meet again in 2015. However, there will be a period of a few months (estimated on the planning page <http://stereo-ssc.nascom.nasa.gov/plans.shtml>) when the STEREO spacecrafts will be completely out of contact. Radio noise from the Sun is a limiting factor on how close to the sun it is possible to communicate with the spacecraft.

## **6.7 Comparison with previous works**

The comparison conducted in Table 6-4 involves ASAP, SWB, JHelioviewer,

---

STEREO-GSFC (Goddard Space Flight Centre), SDO-GSFC and SOLARSTUDIO is based on three criteria: the missions covered (SOHO, STEREO and/or SDO); the information required to perform the image processing (e.g. calibrated or un-calibrated data); and the functionalities that are offered by each application. The comparisons reveal that SOLARSTUDIO is the only tool working with both STEREO and SDO missions, providing standard image processing tools, and offering more highly focused functions on uncalibrated solar images such as AR detection, super resolution and anaglyphs.

## **6.8 Conclusion**

To the best of the author's knowledge, SOLARSTUDIO is the first software that: firstly, locates STEREO and SDO repositories from a single interface. Secondly, offers image processing tools specifically designed for solar images such as: active region segmentation in multiple EUs through single or streams of images, solar event tracking (e.g. Active region), merging of several AIA beacon images to accentuate features and simultaneously compare multiple wavelengths, super-resolution from sets of consecutive frames available at high cadence rates, feature detection and matching between pairs of un-calibrated images, and creating single or streams of Anaglyph images from pairs of images taken from STEREO Ahead and Behind spacecraft.

SOLARSTUDIO offers a research platform for solar scientists who are interested in studying the solar atmosphere at different scales, times and wavelengths. It will be very useful also for researchers working on un-calibrated solar images. SOLARSTUDIO is a license-free and a standalone application that provides novel and advanced image processing features for the community.

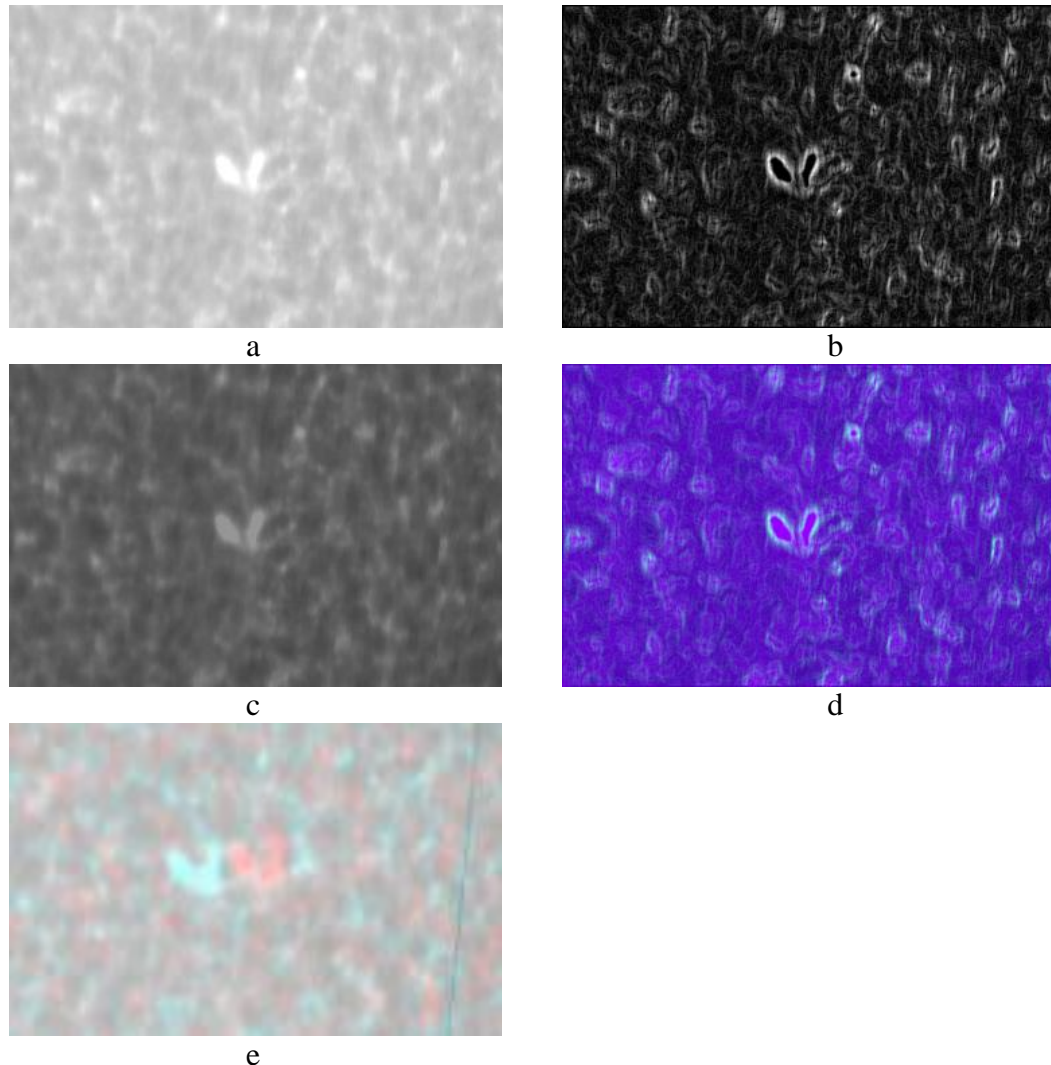


**Table 6-4 A comparison of Solar imaging tools based on missions covered, information needed and the functions offered.**

No	Software	Missions covered	Information needed	Functions
1.	ASAP [88]	SOHO	Sunspot group catalogue, Solar flare catalogues, SOHO/MDI Continuum and Magnetogram images	AR detection Sun spot detection McIntosh classification CME prediction
2.	SWB [22]	SOHO STEREO	Sunspot group catalogue, NOAA Active Regions, CACTus CME, SOHO/MDI Continuum and Magnetogram images, SOHO EIT images, STEREO-A and STEREO-B views with respect to the view of SOHO	Client browsing Information overlaying CME detection
3.	CACTus [22]	SOHO	LASCO images	CME detection
4.	JHeliowiewer [21]	SOHO	Sunspot group catalogue, NOAA Active Regions, LASCO catalogue, SOHO EIT images, CACTus CME	Client browsing, Movie creation streaming between two dates/times, Applying frame-by-frame basic image processing, Overlaying unlimited number of images or movies under adjustable transparency levels, and Locating solar events data.
5.	STEREO GSFC [3]	STEREO	SECCHI instruments: an extreme ultraviolet imager, two white-light coronagraphs and a heliospheric imager	Internet server browsing, Movie creation streaming for a day or between two dates/times.
6.	SDO GSFC [113]	SDO	Atmospheric Imaging Assembly (AIA) and Helioseismic and Magnetic Imager (HMI) images	Internet server browsing, Movie creation streaming for a day or between two dates/times.
7.	SOLARSTUDIO	STEREO SDO	STEREO- SECCHI EUVI, AIA images, HMI images	AR detection, Client browsing, Movie creation streaming between two dates/times, Applying frame-by-frame image processing, Merging various AIA images, Segment ARs within movie, Feature detection and matching, Tracking solar events, Anaglyphs, Super resolution, Adjusting the size of solar disk for a pair of STEREO A and B images to the same scale and offset

The future work will mainly aim to add further methods focused on solar images within the SOLARSTUDIO application such as: using the calibration information within FITS images to generate 3D images (obj or vrmf files) and view them locally,

accessing solar events catalogues and providing association methods [114]. SOLARSTUDIO will be extended in the near future to handle ground-based observations, an example applying SOLARSTUDIO to one of these images is shown in Figure 6.13, where an anaglyph image is created for CA II K3 images.



**Figure 6.13 CA II K3 sub-images for 20/07/2007, taken from BASS200. (a) Original sub-image. (b) Sobel edge detection applied on (a). (c) Brightness adjustment applied on (a). (d) Merging sub-images of (a), (b), and (c). (e) Anaglyph image constructed from pair of sub-images taken with about 3 hours separation time.**

# CHAPTER SEVEN

## 7 CONCLUSIONS AND SUGGESTIONS FOR FURTHER WORK

### 7.1 Overview

Image enhancement and anaglyph reconstruction of a scene from uncalibrated images taken from different viewpoints are topics of wide interest. One dissection of work in this area is by whether the images are from calibrated cameras or not. In the former, without any knowledge of the scene, recalibration must be done if the camera setup changes. The second case, which allows scenes to be reconstructed with no reliance on camera calibration, is more widely applicable. Such success can be applied to serve SR and anaglyphs applications. This thesis presents new algorithms for efficient browsing and the enhanced 2D/3D viewing of solar images provided by STEREO and SDO satellites. This chapter is organised as follows. Section 7.2 provides general conclusion with a more detailed breakdown in Section 7.3. Section 7.4 pinpoints major contributions to the field. The main data and software resources that were used in the work are described in Section 7.5. The potential integration with other techniques and other possible future work are suggested in Section 7.6. The implementations of the presented methods are provided in the enclosed CD-ROM (See Appendix A).

## 7.2 Overall Conclusions

In this research study, the focus is to further knowledge in the extraction of CPs from pairs of uncalibrated images, particularly solar images captured from STEREO and SDO spacecrafts. Four areas of research are investigated: automatic methods for finding accurate correspondences in pairs of solar images; creating SR image from a set of LR images providing details not available in any individual original image; creating 3D scenes (anaglyphs) from pairs of calibrated or uncalibrated solar images; creating a computer platform to integrate the presented methods in this thesis and serve multiple imaging tools for solar images and for other scenes. Moreover, the author presented a contribution to enhance the 3D views using SR method, which it is the first attempt of such anaglyph enhancement.

The research work behind this thesis has resulted in the improvement of the state of the art in SR and 3D visualization by introducing automatic sets of CPs from uncalibrated images. The data set of interest in this work consists of the huge volume of data taken from the STEREO and SDO spacecrafts. Applying SR, anaglyph and the easy access to these huge data volume at both high spatial and high time resolution within a single platform is important to support scientific discovery. The characteristics of these images in terms of size of up to  $2048 \times 2048$  and  $4096 \times 4096$  pixels for STEREO and SDO images respectively, uncalibrated bases with angular shifts increase the difficulties of the work. On the other hand, the majority of the existing SR methods in the literature were designed to work with set of images with small shifts and/or rotation between images, and the existing anaglyph methods were designed based on manual techniques such as: CPs selection, rescaling and/or fitting.

Working with solar images without calibration has three main advantages. Firstly, it avoids transferring any calibration error into subsequent processes such as tracking

objects. Secondly, it can use the immediately available JPEG files (provided at several resolutions with lossy compression) rather than the high resolution FITS files (provided uncompressed at full resolution and with calibration information), which require a few days to become available, which allows the efficient use of near real-time images to be created for applications where the jpegs provide useful information. Finally, it allows methods introduced in this thesis to be flexible to run on scenes other than the Sun.

### **7.3 Detailed conclusions**

Concluding remarks on this research are listed as follows:

- Chapter 2 presents a review of: STEREO and SDO data; methods for finding corresponding points; generating SR and anaglyphs; several exiting applications are designed to browse and process solar images. A number of methods are identified as bases for development for working with large solar images in the subsequent chapters. It is found that there is a continuous increase in satellite data volumes creating the need for efficient computer systems for the automated processing of these data. Also it is found that there is a lack of existing systems to provide data access and comparison for more than one mission. Furthermore, a lack of imaging systems to provide the user with advanced imaging capabilities in the fields of SR and 3D processing integrated within a single computer platform available in the public domain for the benefit of the scientific community.
- An automated method for generating sets of CPs from an uncalibrated pair of solar images of sufficient quality and number to be useful in further applications has been achieved and is presented in Chapter 3. This method (called STEREO-CPs) provides the flexibility for the SR and anaglyph approaches presented in this thesis to run on uncalibrated images of scenes other than the Sun. The work is demonstrated using uncalibrated JPEG images to provide efficient algorithms that are capable of use in

near real-time based systems which cannot access large-size solar data in time. Scientific data takes about 3 days before becoming available on the archive. The potential of this technology is huge because it can be used, for example, in the generation of SR images (to reduce the artefacts of the compressed near real-time images), anaglyphs and feature tracking.

Based on the experiments on the tested solar images, initial trials of two relatively simple methods, the Harris detector and the KLT algorithms, with STEREO images at several separation angle values provided poor results, whereas the SIFT and SURF methods gave promising results. Also it was found that the SURF method outperformed the SIFT method in speed, was usually better in terms of quality of matches and wide distribution of matches over the tested solar images but the output was associated with some mismatches. Thus the SURF method is preferred to generate the initial set of CPs. Then SIFT is used to confirm the correct matches for each pair points in the initial set generated after applying the SURF method. The resulting mismatches are minimised again by discarding the extreme deviation coordinates around the median of the resulting CPs.

Compared to standard methods including SIFT, SURF and RANSAC, in more than 100 experiments, it was found that the STEREO-CPs method is more discriminating, leading to significant improvements in the quality set of the CPs in pairs of STEREO images. It is concluded that the STEREO-CPs method works well with STEREO Ahead and Behind images with separation angles up to  $35^\circ$ . This is adequate with data from the early part of the STEREO mission between March and July 2007 and when the STEREO spacecrafts next have low separation angles which are convenient for the creation of anaglyphs. The STEREO-CPs method is also used in Chapter 4 to estimate the integer shifts between a set of images in the registration stage of the presented SR approach.

The limitations of the presented STEREO-CPs method are associated with the limitations of the SURF algorithm (used to generate initial CPs) which is sensitive to noise, varying illumination and contrast. Also it is always slower than SURF (because SIFT is used after SURF) and sometimes slower than SIFT in case of large number of CPs. These problems could be tackled by using machine learning to optimise the threshold values with reliance on the input images.

- An SR approach for solar images describing its main three stages: image registration, interpolation and filtration, is presented in chapter 4. The unsatisfactory results from several existing SR tools such as IBP, Robust SR, QE, and POCS on the tested images along with a desire to introduce and integrate an SR tool within a computer platform for solar images motivated this work to introduce a new SR approach. Registration of un-calibrated images is performed based on developing an automated method for ARs (or local maxima) detection using correlation. It was found that correlation is simple and suitable to match images with small shifts as assumed in this work but it is also sensitive to changes in scales and rotations. Hence, the STEREO-CPs method is used to overcome these limitations providing the ability to run the proposed SR method on scenes other than the Sun. Interpolation is applied to compensate unknown pixels and to resize the output image using a Bicubic technique with threshold parameter, and smoothing is done using a Gaussian filter with adjustable parameters.

Several practical tests have been performed to evaluate the performance of the proposed SR method using subjective (human judgement) and objective (PSNR and SSIM) assessments. The comparisons involved several competitive SR methods including IBP, Robust, QE, and POCS and the non SR based the Bicubic interpolation method. It is concluded that the proposed SR method works better on the tested images than the methods in both subjective and objective assessments

using images captured at high cadence rates. It is worth to mention that Bicubic interpolation method in general is used to resize images and not for the enhancement.

A limitation of the proposed SR method is that enhancement wouldn't be possible if any failure occurred from STEREO-CPs method to estimate the accurate displacement between the associated images. A number of images of a scene (captured at high cadence rate are recommended) are needed by all the SR techniques tested. Both these factors can cause image downgrading rather than enhancement.

- Automated 3D viewing methods using uncalibrated and/or calibrated pairs of images are presented in Chapter 5. The work presented is focused on uncalibrated images and efficiently creates anaglyphs for the Sun at low separation angles, and in addition, is able to work in near real-time using CPs resulting from the STEREO-CPs method. This will be useful to view the back side of the Sun in 3D when the near real-time beacon images become available from the two spacecraft except the period of few months in 2015 when the spacecrafts are out of communication. The near real-time images are compressed, so they are suffered from artefacts caused by the compression process. Thus, an attempt to enhance the 3D perception by combining a pair of images enhanced using SR rather than the original LR pair of images is introduced. Also STEREO-CPs method offers the flexibility to run the presented methods of anaglyph creation on scenes other than the Sun.

The performance of the presented rescaling method is compared with the process of rescaling using calibration information included in FITS file headers. The results show that the proposed rescaling method over the tested period gives very similar results to those obtained using calibration data with differences around 0.49%. Other advantages of this method are that it is simple and automatic so saves the user time



and effort. The main limitation of this method also is based on the performance of the STEREO-CPs method, e.g. the QF value which should be less than 1 must be considered before rectifying the images, otherwise the output should be distorted as explained earlier in Chapter 3.

- In Chapter 6, the work presented aims to build a unique computer platform for locating STEREO and SDO repositories from a single interface by streaming between two dates/times. Integration of the implementation methods presented in this thesis within this platform will be useful to support scientific discovery. Examples of other integrated methods are: active region segmentation in multiple EUs through single or streams of images, solar event tracking (e.g. active region), merging of several AIA images to accentuate features and simultaneously compare multiple wavelengths, etc. Hence, SOLARSTUDIO is introduced to provide a research infrastructure for solar scientists who are interested in studying the solar atmosphere at different scales, times and wavelengths. It will be very useful also for researchers who are interested in working without calibration information on images. SOLARSTUDIO will be available online as a standalone application including installation instructions and a user manual. Working with uncalibrated images means SOLARSTUDIO can be applied on images of other scenes in the future, such as medical diagnosis, high quality video conferencing, space and planetary surveillance, etc. Up to date images are obtained automatically following a user request.

The limitations of the SOLARSTUDIO can be summarised as follows: firstly, it does not yet deal with the event catalogues provided by the solar missions. Secondly, it cannot view or process the 3D mesh files such as: OBJ or VRML files. Finally, SOLARSTUDIO will fail, except for the visited images which are found in the archive system, to browse the remote data provided by STEREO or SDO

missions if the web services of their official websites are stopped suddenly.

## 7.4 Original Contributions

The main original contributions presented in this thesis are summarised as follows:

- A flexible technique for the automatic generation of a set of CPs from an uncalibrated pair of solar images is introduced. CPs are needed to match sequences of image to investigate time and spatial variations. They can also be used to automate the image registration process needed to construct super resolution images and to build 3D anaglyphs for the input image sequence. The comparisons reveal that CPs from STEREO-CPs are more distinguishable and more accurate than CPs from SURF, SIFT and RANSAC.
- A new SR technique, which consists of three main stages: image registration, interpolation and filtering, is developed. This novel technique is applied to STEREO and SDO images successfully at high cadence rate to view the Sun with a higher image resolution than is available in the original individual images of the Sun. The comparisons involved several competitive SR methods. It is concluded that the proposed SR method works better on the tested images than the alternative methods in both subjective and objective assessments using images captured at high cadence rates.
- Algorithms to create anaglyphs from uncalibrated or calibrated pairs of STEREO images are presented. For the first time, the uncalibrated JPEG images provided by STEREO mission can be utilised to enable the efficient automatic anaglyph creations. Also for the first time to enhance the view of anaglyph images by constructing from pairs of SR images rather than the available low quality images.
- A novel computer platform called SOLARSTUDIO is designed to provide

efficient access to STEREO and SDO images at both high spatial and high time resolution to support scientific discovery. SOLARSTUDIO is the first software that: firstly, locates STEREO and SDO repositories from a single interface. Secondly, offers image processing tools specifically designed for solar images such as: active region segmentation in multiple EUs through single or streams of images, solar event tracking (e.g. Active region), and merging of several EUVI images to accentuate features and simultaneously compare multiple wavelengths. SOLARSTUDIO also includes all methods presented in this thesis such as: STEREO-CPs, the proposed SR, and the anaglyphs creation methods. Furthermore, SOLARSTUDIO is a platform that can be extended to accommodate different imaging operations. It could be the future of solar imaging.

## 7.5 Research resources

In undertaking this research, a wide range of experience was gained in order to make full use of the following resources:

- The main sources of solar data were the STEREO-GSFC, SDO-GSFC in the US and the UK Solar System Data Centre (UKSSDC). Two programming languages (e.g. C#.NET and MATLAB) were used to implement the presented algorithms and to integrate them under one computer platform.
- Several computer tools were developed to process the solar data (FITS and JPEG) and provide data in appropriate format for the use of the C++ application implemented by Al-khadour et al.[85] . The data format is based on generating proprietary Two Camera Corresponding points (TCC) files, which include information regarding pair of images such as: the file names of images, number of CPs, CPs, and resolutions in pixels.

- The implementations of previous work were written in several computer languages. IBP, Robust SR, POCS and, SIFT were written in MATLAB, The KLT algorithm and the direct rectification algorithm for uncalibrated images called DRUI were written in C++ and SURF was written in C#.NET.

The work presented in this thesis can be developed further and some suggestions for future work are listed in the next section.

## **7.6 Suggestions for further work**

### ***7.6.1 Integration with other techniques***

One of the strengths of this work lies in its potential that SOLARSTUDIO is a platform that can be extended to accommodate different imaging operations. It could be the future of solar imaging. Thus, integration with other technologies that are developed within the space weather research group at the University of Bradford, for examples integration of SOLARSTUDIO with ASAP, would be useful to provide advanced space weather applications and data processing services.

### ***7.6.2 Improvements and research extensions***

Some of the challenges that still need to be overcome, with suggested solutions and some ideas for further research are included as follows:

- STEREO-CPs can be improved by optimizing the threshold values of SIFT and SURF by using machine learning on reliance of the input images. This should generate better quality CPs with fewer mismatched pairs of points.
- Processing the calibrated images to generate 3D graphics files (OBJ or VRML) and view them locally. Also accessing solar events catalogues and providing association methods [16].

- The proposed SR and anaglyph methods can be applied on other data sets such as: medical images for medical diagnosis, high quality video conference, Blu-ray movies, space and planets surveillance, etc.
- Investigate alternatives to the Bicubic interpolation method, which could offer fewer visible artefacts caused by image upsizing, such as: cubic B-spline [115], quadratic interpolation [116], or advanced interpolation using a fuzzy-inference system as described in [117].

# References

- [1] L. Feng, T. Wiegmann, B. Inhester, S. Solanki, W. Q. Gan, and P. Ruan, "Magnetic Stereoscopia of Coronal loops in NOAA 8891," *Solar Physics*, vol. 241, pp. 235-249, 2007.
- [2] "<http://stereo-ssc.nascom.nasa.gov/cgi-bin/images>", Last access Nov-2010.
- [3] "<http://stereo.gsfc.nasa.gov/gallery/item.php?id=stereoimages&iid=53>", Last access May-2009.
- [4] N. Team, "The Sun and Heliosphere In Three Dimensions: Report of the NASA Science Definition Team for the STEREO Mission," p. 80 pages, 1997.
- [5] S. Ma, L. Zhang, X. Zhang, and W. Gao, "Block Adaptive Super Resolution Video Coding," *Advances in Multimedia Information Processing-PCM*, pp. 1048-1057, 2009.
- [6] K. V. Suresh, G. M. Kumar, and A. N. Rajagopalan, "Superresolution of License Plates in Real Traffic Videos," *Intelligent Transportation Systems, IEEE Transactions on*, vol. 8, pp. 321-331, 2007.
- [7] H. Bay, T. Tuytelaars, and L. Van Gool, "Surf: Speeded up robust features," *Lecture notes in computer science*, vol. 3951, p. 404, 2006.
- [8] D. Capel, *Image mosaicing and super-resolution*: Springer-Verlag New York Inc, 2004.
- [9] GSFC-NASA, "<http://stereo.gsfc.nasa.gov/artifacts/artifacts.shtml>," Last access October 2010.
- [10] "[http://stereo.gsfc.nasa.gov/artifacts/artifacts\\_cosmic\\_rays.shtml](http://stereo.gsfc.nasa.gov/artifacts/artifacts_cosmic_rays.shtml)", Last access Oct 2010.
- [11] "<http://stereo.gsfc.nasa.gov/artifacts/artifacts.shtml>," Last access October 2010.
- [12] A. J. Woods and S. S. L. Tan, "Characterising sources of ghosting in time-sequential stereoscopic video displays," *Stereoscopic Displays and Applications XIII, published in Stereoscopic Displays and Virtual Reality Systems IX, Proceedings of SPIE*, vol. 4660, pp. 21-23, 2002.
- [13] W. Sanders and D. F. McAllister, "Producing anaglyphs from synthetic images," 2003, pp. 348-358.

- 
- [14] Cognitech-Inc, "Video Investigator Software available on [http://www.investigationsystem.com/?gclid=CPnM0qL4wacCFQoZ4Qodbhns\\_Q](http://www.investigationsystem.com/?gclid=CPnM0qL4wacCFQoZ4Qodbhns_Q)", Last access May-2010.
- [15] "<http://www.salientstills.com>," Last access Feb-2009.
- [16] P. J. Styles, "The production of anaglyphs from SPOT-HRV panchromatic data for geomorphological mapping," 1988.
- [17] M. W. Powell, J. S. Norris, M. A. Vona Iii, P. G. Backes, and J. V. Wick, "Scientific Visualization for the Mars Exploration Rovers," 2005, pp. 4290-4296.
- [18] J. E. Heuser, "Membrane traffic in anaglyph stereo," *Traffic*, vol. 1, pp. 35-37, 2000.
- [19] S. E. B. Sorensen, P. S. Hansen, and N. L. Sorensen, "Method for recording and viewing stereoscopic images in color using multichrome filters," ed: Google Patents, 2004.
- [20] Channel-4, "<http://www.channel4.com/programmes/3d-week/articles/3d-week>," glasses that will work for Channel 4's 3D week are the Amber and Blue ColourCode 3D glasses, 2009.
- [21] D. Müller, G. Dimitoglou, B. Caplins, J. P. G. Ortiz, B. Wamsler, K. Hughitt, A. Alexanderian, J. Ireland, D. Amadigwe, and B. Fleck, "JHelioviewer– Visualizing large sets of solar images using JPEG 2000," ed: Copublished by the IEEE CS and the AIP, pp. 38-47, 2009.
- [22] D. Berghmans, F. Clette, P. Cugnon, C. Foullon, J. F. Hochedez, R. A. M. Van der Linden, E. Verwichte, L. Wauters, and A. Zhukov, "THE SOLAR INFLUENCES DATA ANALYSIS CENTER (SIDC)," Copyright © 2004, 2005, 2006, 2007.
- [23] "<http://widgets.yahoo.com/widgets/solar-viewer>," Last access on Oct 2010.
- [24] "[http://stereo-ssc.nascom.nasa.gov/publications/STEREO\\_SRP08\\_Web.pdf](http://stereo-ssc.nascom.nasa.gov/publications/STEREO_SRP08_Web.pdf)," p. 39, Feb 2008.
- [25] T. S. W. P. C. (SWPC), "<http://www.swpc.noaa.gov/stereo>," Last access May -2009.
- [26] O. NASA, "[http://www.nasa.gov/mission\\_pages/stereo/spacecraft/](http://www.nasa.gov/mission_pages/stereo/spacecraft/)," Last access Nov-2009.
- [27] J.-P. W. Markus J. Aschwanden, Nariaki V. Nitta, James R. Lemen, and Anne Sandman Lockheed Martin Advanced Technology Center, Solar & Astrophysics Laboratory, Org. ADBS, Bldg.252, 3251 Hanover St., Palo Alto, CA 94304, USA; e-mail: [aschwanden@lmsal.com](mailto:aschwanden@lmsal.com), "First 3D Reconstructions of Coronal Loops with the STEREO A+B Spacecraft: III. Instant Stereoscopic Tomography of Active Regions " p. 31, 2008.
- [28] J. S. N. J.W. Cook, and R.A. Howard, "The STEREO Mission: A Three-Dimensional View of the Sun and Heliosphere, Space Science Division," 2007.

- 
- [29] J. Lewis, R. Argyle, P. Bunclark, D. Evans, and E. Gonzales-Solares, "Accessing eSDO Solar Image Processing and Visualization through AstroGrid," ed, 2008.
- [30] O. NASA, "[http://stereo-ssc.nascom.nasa.gov/where/make\\_where\\_gif.php](http://stereo-ssc.nascom.nasa.gov/where/make_where_gif.php)", Last access on March 2009.
- [31] S. D. T. NASA, "The Sun and Heliosphere In Three Dimensions, Report of the NASA Science Definition Team for the STEREO Mission," 1997.
- [32] J. Galloway, "STEREO Mission Design, NASA/ Goddard Space Flight Center," A report submitted in 1998.
- [33] M. J. N. Aschwanden, Nariaki V.; Wuelser, Jean-Pierre; Lemen, James R, "First 3D Reconstructions of Coronal Loops with the STEREO A+B Spacecraft. II. Electron Density and Temperature Measurements," *The Astrophysical Journal, Volume 680, Issue 2, pp. 1477-1495*, 2008.
- [34] N. R. L. E. O. H. C. F. S. RESEARCH, "Data Management Plan for the Sun Earth Connection Coronal and Heliospheric Investigation (SECCHI)," 2004.
- [35] GSFC-NASA, "[http://stereo.gsfc.nasa.gov/artifacts/artifacts\\_beacon.shtml](http://stereo.gsfc.nasa.gov/artifacts/artifacts_beacon.shtml)," last access October 2010.
- [36] B. Zitova and J. Flusser, "Image registration methods: a survey," *Image and vision computing*, vol. 21, pp. 977-1000, 2003.
- [37] T. Tuytelaars and L. Van Gool, "Wide baseline stereo matching based on local, affinity invariant regions," pp. 412–425, 2000.
- [38] S. Jianbo and C. Tomasi, "Good features to track," pp. 593-600, 1994.
- [39] B. D. Lucas and T. Kanade, "An iterative image registration technique with an application to stereo vision," p. 3, 1981.
- [40] D. G. Lowe, "Distinctive image features from scale-invariant keypoints," *International journal of computer vision*, vol. 60, pp. 91-110, 2004.
- [41] S. N. Sinha, J. M. Frahm, M. Pollefeys, and Y. Genc, "GPU-based video feature tracking and matching," 2006.
- [42] Y. Ke and R. Sukthankar, "PCA-SIFT: A more distinctive representation for local image descriptors," *cvpr*, vol. 2, pp.506-513, 2004 IEEE Computer Society Conference on Computer Vision and Pattern Recognition (CVPR'04) - Volume 2, 2004.
- [43] H. Sun, C. Wang, and N. El-Sheimy, "Joint detection and tracking of independently moving objects in stereo sequences using scale-invariant feature transform features and particle filter," *Optical Engineering*, vol. 49, pp. 037006-10, 2010.
- [44] H. Zhou, Y. Yuan, and C. Shi, "Object tracking using SIFT features and mean shift," *Computer Vision and Image Understanding*, vol. 113, pp. 345-352, 2009.
- [45] G. Roth, "Automatic correspondences for photogrammetric model building,"



- International Archives of the Photogrammetry, Remote Sensing and Spatial Information Sciences*, vol. 35, pp. 713-718, 2004.
- [46] K. Mikolajczyk and C. Schmid, "A performance evaluation of local descriptors," ed: Published by the IEEE Computer Society, pp. 1615-1630, 2005.
- [47] C. Rieth, "SURF-ing a Model of Spatiotemporal Saliency," A report submitted by department of psychology, University of California, San Diego, 2006.
- [48] C. Valgren and A. Lilienthal, "SIFT, SURF and seasons: Long-term outdoor localization using local features," ed: Citeseer, pp. 253–258, 2007.
- [49] X. Huang, Y. Sun, D. Metaxas, F. Sauer, and C. Xu, "Hybrid image registration based on configural matching of scale-invariant salient region features," 2004.
- [50] T. Kadir and M. Brady, "Saliency, scale and image description," *International Journal of Computer Vision*, vol. 45, pp. 83-105, 2001.
- [51] K. Mikolajczyk and C. Schmid, "Scale & affine invariant interest point detectors," *International Journal of Computer Vision*, vol. 60, pp. 63-86, 2004.
- [52] M. Pollefeys, R. Koch, M. Vergauwen, and L. Van Gool, "Automated reconstruction of 3D scenes from sequences of images," *ISPRS Journal Of Photogrammetry And Remote Sensing*, vol. 55, pp. 251-267, 2000.
- [53] B. Boufama and R. Mohr, "Epipole and fundamental matrix estimation using the virtual parallax property," ed: Citeseer, pp. 1030–1036, 1995.
- [54] B. S. Boufama and R. Mohr, "A stable and accurate algorithm for computing epipolar geometry," *International journal of pattern recognition and artificial intelligence*, vol. 12, pp. 817-840, 1998.
- [55] U. o. Oxford, "active region." A Dictionary of Astronomy 1997. originally published by Oxford University, retrieved on May 20, 2009 from Encyclopedia.com:" <http://www.encyclopedia.com/doc/1O80-activeregion.html>," 1997.
- [56] N. S. W. P. C. SWPC, "http://www.swpc.noaa.gov/stereo/STEREO\_SWB\_Support.html#ScienceCenter," 2007.
- [57] A. Benkhalil, V. Zharkova, S. Ipson, and S. Zharkov, "Automatic identification of active regions (plages) in the full-disk solar images using local thresholding and region growing techniques," pp. 74-78, 2003.
- [58] Z. Mouradian, "Synoptic Data Findings, Synoptic Solar Physics ASP Conferences Series, (140):181-204," 1998.
- [59] S. Zharkov, V. Zharkova, S. Ipson, and A. Benkhalil, "Technique for automated recognition of sunspots on full-disk solar images," *EURASIP Journal on Applied Signal Processing*, vol. 2005, pp. 2573-2584, 2005.

- 
- [60] J. Aboudarham, I. Scholl, N. Fuller, M. Fouesneau, M. Galametz, F. Gonon, A. Maire, and Y. Leroy, "Automatic detection and tracking of filaments for a solar feature database," pp. 243-248, 2008.
- [61] S. Zharkov, V. Zharkova, S. Ipson, and A. Benkhalil, "Automated Recognition of Sunspots on the SOHO/MDI White Light Solar Images," *LECTURE NOTES IN COMPUTER SCIENCE*, pp. 446-452, 2004.
- [62] A. Zomet, A. Rav-Acha, and S. Peleg, "Robust super-resolution," in *Computer Vision and Pattern Recognition, 2001. CVPR 2001. Proceedings of the 2001 IEEE Computer Society Conference on*, pp. I-645-I-650 vol.1, 2001.
- [63] N. K. Bose, H. C. Kim, and H. M. Valenzuela, "Recursive implementation of total least squares algorithm for image reconstruction from noisy, undersampled multiframe," 1993.
- [64] P. Sung Cheol, P. Min Kyu, and K. Moon Gi, "Super-resolution image reconstruction: a technical overview," *Signal Processing Magazine, IEEE*, vol. 20, pp. 21-36, 2003.
- [65] D. M. Rust and A. Kumar, "Helicity charging and eruption of magnetic flux from the sun," 1994.
- [66] J. Clark, M. Palmer, and P. Lawrence, "A transformation method for the reconstruction of functions from nonuniformly spaced samples," *Acoustics, Speech, and Signal Processing*, vol. 33, pp. 1151-1165, 1985.
- [67] R. Y. Tsai and T. S. Huang, "Multiframe image restoration and registration," *Advances in Computer Vision and Image Processing*, vol. 1, pp. 317-339, 1984.
- [68] M. C. Hong, M. G. Kang, and A. K. Katsaggelos, "Iterative weighted regularized algorithm for improving the resolution of video sequences," pp. 474-477, 1997.
- [69] A. Nasonov, A. S. Krylov, and A. Lukin, "Post-processing by Total Variation Quasi-solution Method for Image Interpolation," 2006.
- [70] A. M. Tekalp, M. K. Ozkan, and M. I. Sezan, "High-resolution image reconstruction from lower-resolution image sequences and space-varying image restoration," in *Acoustics, Speech, and Signal Processing, 1992. ICASSP-92., 1992 IEEE International Conference on*, pp. 169-172 vol.3, 1992.
- [71] M. Elad and A. Feuer, "Super-resolution reconstruction of image sequences," vol. 21, ed, pp. 817-834, 1999.
- [72] P. E. Eren, M. I. Sezan, and A. M. Tekalp, "Robust, object-based high-resolution image reconstruction from low-resolution video," vol. 6, pp. 1446-1451, 1997.
- [73] S. B. a. T. Kanade, " "Super resolution optical flow," Tech. Rep. CMU-RI-TR-99-36, Robotics Institute, Carnegie Mellon University, Pittsburgh, PA," October 1999.

- 
- [74] W. Zhao and H. S. Sawhney, "Is Super-Resolution with Optical Flow Feasible?," pp. 599-613, 2002.
- [75] S. Baker and T. Kanade, "Limits on Super-Resolution and How to Break Them," *IEEE TRANSACTIONS ON PATTERN ANALYSIS AND MACHINE INTELLIGENCE*, pp. 1167-1183, 2002.
- [76] M. Irani and S. Peleg, "Improving resolution by image registration," *CVGIP: Graphical Models and Image Processing*, vol. 53, pp. 231-239, 1991.
- [77] P. Vandewalle, S. Susstrunk, and M. Vetterli, "A Frequency Domain Approach to Registration of Aliased Images with Application to Super-Resolution," *EURASIP JOURNAL ON APPLIED SIGNAL PROCESSING*, vol. 10, 2006.
- [78] B. Marcel, M. Briot, and R. Murrieta, "Calcul de translation et rotation par la transformation de Fourier," *TS. Traitement du signal*, vol. 14, pp. 135-149, 1997.
- [79] D. Keren, S. Peleg, and R. Brada, "Image sequence enhancement using sub-pixel displacements," pp. 742-746 ed, 1988.
- [80] L. Rudin, F. Guichard, and P. Yu, "Video super-resolution via contrast-invariant motion segmentation and frame fusion (with applications to forensic video evidence)," ed, 1999.
- [81] E. Dubois, "A projection method to generate anaglyph stereo images," 2001.
- [82] "[http://www.stereoeye.jp/software/index\\_e.html](http://www.stereoeye.jp/software/index_e.html)," Ver 1.08, Last access Jun-2010.
- [83] Z. Zhang and D. F. McAllister, "A Uniform Metric for Anaglyph Calculation," pp. 366-377, 2006.
- [84] I. Ideses and L. Yaroslavsky, "Three methods that improve the visual quality of colour anaglyphs," *JOURNAL OF OPTICS A PURE AND APPLIED OPTICS*, vol. 7, p. 755, 2005.
- [85] I. S. Alkhadour W., Haigh J. and Zraqou J., "Creating Colour Anaglyph With Less Ghosting From Stereo Pair Images. International Conference in Information Technology, Amman, Jordan. 8 pages," 2009.
- [86] ISO/IEC, "ISO/IEC 15444-1/2: Information Technology, JPEG 2000 Image Coding System, Core Coding System and Extensions, ISO," 2000.
- [87] D. Taubmana and R. Prandolinib, "Architecture, philosophy and performance of JPIP: Internet protocol standard for JPEG2000," vol. 100, p. 0ed: Citeseer, 2003.
- [88] T. Colak and R. Qahwaji, "Automated Solar Activity Prediction: A hybrid computer platform using machine learning and solar imaging for automated prediction of solar flares," American Geophysical Union, ed: 2009.
- [89] T. Colak, R. Qahwaji, S. Ipson, and H. Ugail, "Representation of Solar Features in 3D for Creating Visual Solar Catalogues, Advances in Space Research," ed: Elsevier, 2010.

- 
- [90] "<http://msdn.microsoft.com/en-us/library/system.net.webrequest.aspx>," Last Access Oct 2010.
- [91] "<http://sdo.gsfc.nasa.gov/assets/img/browse>," Last access Aug-2010.
- [92] "<http://stereo-ssc.nascom.nasa.gov/software.shtml>," last access 16-Nov-2010.
- [93] D. Lowe, "Implementation of standard SIFT Version 4, <http://www.cs.ubc.ca/~lowe/keypoints/>," Last access 2005.
- [94] Emgu-CV, "OpenCV SURF Example rewritten in C#, [http://www.emgu.com/wiki/index.php/Download\\_And\\_Installation](http://www.emgu.com/wiki/index.php/Download_And_Installation)," Last access Sept-2010.
- [95] Kanade-Lucas-Tomas, "KLT: An Implementation of the Kanade-Lucas-Tomasi Feature Tracker. <http://www.ces.clemson.edu/~stb/klt/>, Last access April 2010," 1991.
- [96] A. W. Zraqou J., Qahwaji R., Ipson S., Ugail H, "Enhanced 3D Perception using Super-Resolution and Saturation Control Techniques for Solar Images," *Ubiquitous Computing And Communication Journal*, vol. 4 (4): 1-23, 2009.
- [97] A. Al-Zahrani, S. S. Ipson, and J. G. B. Haigh, "Applications of a direct algorithm for the rectification of uncalibrated images," *Information Sciences*, vol. 160, pp. 53-71, 2004.
- [98] T. Saito and T. Komatsu, "Super-resolution total-variation decoding of JPEG-compressed image data," p. 65020G, 2007.
- [99] R. Keys, "Cubic convolution interpolation for digital image processing," *IEEE Transactions on Acoustics Speech and Signal Processing*, vol. 29, pp. 1153-1160, 1981.
- [100] X. Li and M. Orchard, "New edge-directed interpolation," *Image Processing, IEEE Transactions on*, vol. 10, pp. 1521-1527, 2002.
- [101] D. Glasner, S. Bagon, and M. Irani, "Super-resolution from a single image," pp. 349-356, 2010.
- [102] A. S. K. Alexey Lukin, Andrey Nasonov, "Image Interpolation by Super-Resolution" Graphicon conference proceedings, , pp.239-242, Novosibirsk Akademgorodok, Russia, 2006.
- [103] M. Elad and A. Feuer, "Restoration of a single superresolution image from several blurred, noisy, and undersampled measured images," *Image Processing, IEEE Transactions on*, vol. 6, pp. 1646-1658, 1997.
- [104] Z. W. a. A. C. Bovik, "Mean squared error: love it or leave it? - A new look at signal fidelity measures," *IEEE Signal Processing Magazine*, vol. 26, Jan. 2009.
- [105] A. C. Laboratory, "<http://lcavwww.epfl.ch/software/superresolution>," Last access 07 Nov, 2010.
- [106] Q. LABS, "[http://download.cnet.com/QE-SuperResolution/3000-2169\\_4-10392416.html](http://download.cnet.com/QE-SuperResolution/3000-2169_4-10392416.html)," Last access Oct-2009.

- 
- [107] NASA, "[http://stereo-ssc.nascom.nasa.gov/publications/STEREO\\_SRP08\\_Web.pdf](http://stereo-ssc.nascom.nasa.gov/publications/STEREO_SRP08_Web.pdf)," p. 39, Feb 2008.
- [108] N. Ayache and C. Hansen, "Rectification of images for binocular and trinocular stereovision," pp. 11–16, 1988.
- [109] R. I. Hartley, "A linear method for reconstruction from lines and points," p. 882, 1995.
- [110] I. S. Alkhadour W., Zraqou J., Qahwaji R., Haigh J., "Creating a Color Anaglyph from a Pseudo-Stereo Pair of Images," *Accepted in the International Conference on Information Technology (ICIT'2009), at Al-Zaytoonah University, Paper ID= 578*, 2009.
- [111] K. Al-Shalfan, "Investigation of 3-D reconstruction from Uncalibrated Images, in Electronic and Telecommunications. University of Bradford, England, UK," 2001.
- [112] "<http://stereo.gsfc.nasa.gov/gallery/item.php?id=3dimages&iid=50>," Last access on Oct-2010.
- [113] "<http://sdo.gsfc.nasa.gov>," Last access Oct-2010.
- [114] R. Qahwaji, T. Colak, M. Al-Omari, and S. Ipson, "Automated Prediction of CMEs Using Machine Learning of CME–Flare Associations," *Solar Image Analysis and Visualization*, pp. 261-273, 2009.
- [115] M. Unser, A. Aldroubi, and M. Eden, "Fast B-spline transforms for continuous image representation and interpolation," *Pattern Analysis and Machine Intelligence, IEEE Transactions on*, vol. 13, pp. 277-285, 2002.
- [116] N. Dodgson, "Quadratic interpolation for image resampling," *Image Processing, IEEE Transactions on*, vol. 6, pp. 1322-1326, 2002.
- [117] H. Ting and H. Hang, "Edge Preserving Interpolation of Digital Images Using Fuzzy Inference\* 1," *Journal of Visual Communication and Image Representation*, vol. 8, pp. 338-355, 1997.

## APPENDIX A. RESULTS OF THE STEREO-CPs METHOD

Results of 102 experiments carried out on pairs of STEREO images with separation angles between  $0.624^\circ$  and  $39.088^\circ$ . For conciseness, the type of Extreme Ultra Violet and the size (Width×Height) of the images are abbreviated by EUVI×Size. ThrX and ThrY denote Threshold-X and Threshold-Y respectively which represent the x-axis and y-axis thresholds generated by STEREO-CPs.

No.	STEREO A & B pairs of images			SURF			RANSAC			STEREO-CPs			Thresholds	
	EUVI×Size	Date/Time	Angle(°)	CPs	QF	LQb	CPs	QF	LQb	CPs	QF	LQb	ThrX	ThrY
1	195x1k	15-03-07 18:51:40	1.926	88	0.34	1.41	88	0.34	1.41	76	0.30	1.58	0.0146	0.0093
2	195x1k	15-03-07 23:35:40	1.938	95	0.32	1.83	95	0.32	1.83	86	0.31	1.76	0.0356	0.0082
3	304x1k	15-04-07 00:11:45	4.293	628	4.55	201.2	621	2.84	17.93	578	0.33	5.280	0.0014	0.0014
4	195x1k	15-03-07 22:15:40	1.935	72	1.74	9.81	71	0.46	3.10	64	0.35	1.82	0.0115	0.0104
5	195x1k	15-03-07 21:35:40	1.933	62	0.27	1.66	62	0.27	1.66	56	0.28	0.95	0.0192	0.0117
6	304x1k	20-03-07 07:31:41	2.198	748	5.09	31.74	745	2.24	12.91	672	0.36	3.00	0.0013	0.0003
7	304x1k	20-03-07 16:41:41	2.223	664	3.32	158.3	658	0.68	125.5	593	0.36	4.72	0.0014	0.0003
8	304x1k	20-06-07 00:16:15	13.932	294	11.51	198.5	287	0.36	2.38	167	0.36	2.51	0.0022	0.0016
9	304x1k	20-03-07 05:01:41	2.192	750	3.03	89.71	744	0.41	5.15	713	0.37	4.33	0.0013	0.0007
10	304x1k	20-03-07 08:21:41	2.201	694	2.32	156.3	690	0.49	4.58	629	0.37	4.06	0.0014	0.0003
11	304x1k	20-03-07 10:51:41	2.207	780	2.65	230.3	774	0.59	4.33	764	0.37	2.07	0.0049	0.0006
12	304x1k	20-03-07 15:51:41	2.220	638	5.23	231.4	631	0.38	3.72	583	0.37	3.68	0.0015	0.0003

13	304x1k	20-03-07 00:51:41	2.181	695	2.19	132.9	691	0.65	7.57	634	0.38	4.59	0.0014	0.0003
14	304x1k	20-03-07 12:31:41	2.211	731	2.56	204.7	724	1.55	9.59	681	0.38	2.12	0.0026	0.0003
15	195x1k	15-03-07 18:06:40	1.925	98	0.45	1.54	98	0.45	1.54	84	0.39	1.63	0.0105	0.0077
16	304x1k	20-03-07 05:51:41	2.194	721	3.88	106.8	716	1.83	12.45	656	0.39	2.55	0.0013	0.0003
17	195x1k	10-05-07 01:31:20	7.274	62	7.34	40.85	61	0.48	2.71	47	0.40	2.13	0.0149	0.0063
18	195x1k	15-03-07 20:55:40	1.932	76	0.38	2.01	76	0.38	2.01	69	0.40	2.03	0.0158	0.0102
19	304x1k	20-03-07 00:01:41	2.179	713	1.18	50.84	710	0.39	9.35	644	0.40	9.37	0.0013	0.0003
20	304x1k	20-03-07 02:31:41	2.185	730	3.18	148.3	722	0.38	3.15	678	0.40	3.31	0.0028	0.0003
21	304x1k	20-06-07 01:36:15	13.942	273	7.62	102.1	268	1.08	5.46	254	0.40	2.73	0.0019	0.0015
22	171x2k	01-02-07 02:05:51	0.624	582	1.68	193.8	579	1.01	7.20	433	0.42	4.02	0.0032	0.0006
23	304x1k	20-03-07 06:41:41	2.197	737	2.22	226.3	732	1.96	11.55	719	0.42	3.17	0.0032	0.0003
24	304x1k	20-03-07 11:41:41	2.209	710	2.65	96.64	704	1.68	34.86	689	0.42	4.21	0.0040	0.0006
25	171x2k	01-02-07 02:25:51	0.624	576	1.26	8.30	576	1.26	8.30	488	0.43	4.28	0.0032	0.0011
26	195x1k	15-03-07 22:55:40	1.936	75	0.39	1.69	75	0.39	1.69	67	0.43	1.84	0.0158	0.0110
27	304x1k	20-03-07 10:01:41	2.205	687	3.34	214.0	680	0.69	7.72	655	0.43	6.21	0.0043	0.0003
28	304x1k	20-03-07 14:11:41	2.216	773	3.97	259.5	764	1.34	10.98	747	0.43	3.78	0.0013	0.0010
29	304x1k	20-06-07 23:56:15	14.114	348	9.22	192.6	331	3.56	22.94	317	0.44	2.33	0.0018	0.0024
30	171x2k	01-02-07 02:15:51	0.624	581	0.98	5.52	579	0.44	7.23	449	0.45	5.17	0.0034	0.0006
31	304x2k	01-06-07 23:56:15	10.765	1698	12.19	801.3	1661	1.67	21.50	1502	0.47	4.110	0.0004	0.0002
32	304x1k	20-03-07 09:11:41	2.203	786	9.99	389.6	773	0.97	8.59	716	0.47	5.03	0.0091	0.0002
33	195x1k	10-05-07 01:21:20	7.273	68	0.58	3.79	68	0.58	3.79	53	0.48	3.26	0.0115	0.0050

34	195x2k	01-04-07 23:32:00	3.111	128	0.52	2.89	128	0.52	2.89	73	0.49	2.68	0.0276	0.0138
35	304x1k	20-06-07 03:16:15	13.955	334	9.50	272.7	322	0.77	14.34	301	0.49	2.00	0.0020	0.0012
36	304x1k	20-03-07 15:01:41	2.218	670	5.39	184.0	663	2.07	30.85	648	0.50	23.25	0.0035	0.0006
37	304x1k	20-03-07 04:11:41	2.189	735	3.68	425.4	724	3.89	49.09	709	0.54	4.27	0.0046	0.0007
38	304x1k	20-03-07 13:21:41	2.214	737	9.80	161.6	728	1.99	21.70	712	0.59	6.70	0.0051	0.0007
39	195x1k	10-05-07 02:01:20	7.277	68	4.64	22.34	68	4.64	22.34	55	0.61	4.26	0.0146	0.0047
40	284x1k	09-05-07 00:41:55	7.133	124	4.41	68.98	122	0.87	3.86	114	0.61	3.510	0.0180	0.0102
41	195x2k	01-04-07 23:22:00	3.110	91	0.78	3.62	91	0.78	3.62	58	0.62	2.95	0.0301	0.0147
42	195x1k	15-03-07 19:35:40	1.928	43	0.37	1.64	43	0.37	1.64	37	0.63	2.23	0.0297	0.0183
43	195x1k	10-05-07 01:11:20	7.272	70	0.48	3.64	70	0.48	3.64	60	0.65	3.56	0.0131	0.0060
44	195x1k	10-05-07 01:51:20	7.276	69	0.62	4.48	69	0.62	4.48	62	0.65	4.43	0.0132	0.0057
45	171x1k	09-05-07 04:40:45	7.155	116	8.45	37.04	115	1.19	9.25	95	0.66	4.67	0.0084	0.0033
46	284x1k	09-05-07 06:41:55	7.166	162	5.66	51.31	158	0.79	7.51	145	0.69	3.640	0.0155	0.0072
47	171x1k	09-05-07 18:40:45	7.235	153	9.91	51.91	150	0.69	5.57	126	0.71	4.97	0.0071	0.0027
48	284x1k	20-06-07 16:46:30	14.059	106	9.80	163.7	102	2.94	12.44	81	0.74	4.65	0.0092	0.0171
49	304x1k	20-03-07 03:21:41	2.187	693	2.62	20.18	690	0.67	4.57	647	0.75	4.46	0.0013	0.0003
50	284x1k	20-06-07 08:26:30	13.995	79	11.19	140.4	75	1.45	12.68	68	0.76	2.45	0.0191	0.0216
51	195x1k	10-05-07 01:41:20	7.275	61	6.77	40.28	59	0.70	4.49	52	0.78	5.07	0.0149	0.0057
52	171x2k	01-02-07 01:35:51	0.624	476	1.17	8.60	475	0.78	9.37	431	0.78	9.45	0.0005	0.0059
53	195x1k	15-03-07 20:15:40	1.930	94	1.97	12.40	94	1.97	12.40	79	0.80	3.47	0.0123	0.0078
54	195x1k	10-05-07 02:11:20	7.277	77	0.82	5.15	77	0.82	5.15	61	0.82	4.02	0.0125	0.0044



55	284x1k	20-06-07 18:26:30	14.072	84	8.78	80.75	83	1.74	8.92	63	0.86	5.02	0.0097	0.0134
56	171x1k	09-05-07 06:40:45	7.166	133	8.80	39.00	132	1.09	6.79	108	0.88	5.44	0.0075	0.0030
57	195x1k	10-05-07 01:01:20	7.271	75	0.77	4.75	75	0.77	4.75	61	0.93	4.52	0.0112	0.0045
58	171x1k	09-05-07 00:40:45	7.132	141	3.22	23.70	139	0.75	4.55	125	0.94	4.88	0.0076	0.0042
59	304x1k	25-05-07 23:56:15	9.629	462	10.73	323.2	451	0.72	17.54	441	0.98	18.40	0.0024	0.0080
60	171x2k	25-04-07 22:41:30	5.480	276	3.70	168.2	274	3.33	18.49	221	0.98	19.52	0.0044	0.0033
61	171x1k	25-04-07 22:41:30	5.480	184	4.93	66.31	181	2.90	27.45	161	0.99	14.68	0.0051	0.0017
62	284x1k	20-06-07 13:26:30	14.033	85	9.09	86.12	82	1.80	8.43	68	1.01	8.35	0.0094	0.0184
63	304x1k	20-03-07 01:41:41	2.183	746	6.71	183.8	739	1.93	16.96	723	1.04	7.87	0.0039	0.0007
64	284x1k	20-06-07 15:06:30	14.046	63	1.15	4.93	62	1.22	5.25	53	1.16	4.55	0.0134	0.0199
65	304x1k	15-04-07 23:51:45	4.392	703	4.40	261.1	695	0.59	7.38	651	1.19	45.10	0.0014	0.0012
66	171x1k	09-05-07 22:40:45	7.257	131	5.92	26.49	129	0.91	7.43	106	1.20	5.48	0.0092	0.0031
67	284x1k	20-06-07 23:26:30	14.110	96	22.72	203.5	91	4.21	25.14	76	1.20	7.00	0.0210	0.0141
68	284x1k	20-06-07 11:46:30	14.021	70	14.10	113.8	65	2.58	16.82	52	1.23	8.29	0.0165	0.0204
69	304x1k	25-05-07 00:06:15	9.473	499	3.61	75.34	495	0.96	5.59	463	1.29	6.140	0.0044	0.0011
70	171x1k	19-05-07 00:06:30	8.554	133	3.85	60.62	130	1.18	5.92	110	1.35	5.91	0.0973	0.0060
71	171x1k	09-05-07 08:40:45	7.178	120	0.83	7.28	120	0.83	7.28	100	1.38	6.50	0.0085	0.0030
72	171x1k	15-06-07 00:06:00	13.020	108	5.73	26.67	95	2.21	14.52	91	1.43	8.560	0.0089	0.0042
73	304x1k	20-06-07 04:56:15	13.968	333	12.65	354.3	317	1.38	14.71	294	1.59	13.55	0.0016	0.0011
74	171x1k	09-05-07 14:40:45	7.212	156	8.07	77.17	153	1.27	7.09	128	1.75	20.36	0.0060	0.0024
75	171x2k	01-07-07 00:08:30	16.006	138	16.17	329.7	132	8.84	37.30	100	4.37	19.37	0.0036	0.0045

76	171x1k	15-06-07 00:08:30	13.020	117	22.33	132.8	111	1.82	11.45	90	2.92	16.76	0.0080	0.0038
77	195x2k	01-09-07 23:45:30	28.588	15	34.21	195.0	15	34.21	195.0	10	1.88	5.18	0.0146	0.1156
78	171x1k	05-07-07 00:06:00	16.780	85	7.55	81.69	82	1.11	8.82	66	2.52	9.23	0.0084	0.0084
79	171x1k	09-05-07 16:40:45	7.223	151	8.63	44.87	149	2.58	14.40	119	2.08	13.69	0.0075	0.0028
80	171x1k	09-05-07 20:40:45	7.246	126	7.68	45.14	123	7.95	35.64	107	2.12	20.23	0.0097	0.0037
81	171x1k	15-06-07 00:11:00	13.021	108	4.10	53.17	102	1.75	10.23	85	2.22	18.04	0.0083	0.0038
82	171x1k	09-05-07 02:40:45	7.144	130	2.72	55.05	127	1.92	10.16	103	2.24	10.69	0.0084	0.0031
83	171x2k	01-07-07 00:11:00	16.006	148	24.57	447.6	137	5.98	38.43	89	1.66	7.53	0.0055	0.0058
84	284x1k	09-05-07 02:41:55	7.144	141	8.80	87.66	138	1.03	20.06	128	2.33	14.32	0.0167	0.0091
85	284x1k	20-06-07 01:46:30	13.944	100	11.91	76.05	97	2.01	14.29	79	2.35	9.85	0.0100	0.0258
86	171x2k	01-07-07 00:06:00	16.006	135	17.89	169.0	129	12.80	112.3	65	2.39	9.27	0.0085	0.0065
87	284x1k	20-06-07 05:06:30	13.969	79	20.23	205.7	73	1.27	7.08	66	2.42	14.94	0.0128	0.0175
88	304x1k	20-06-07 06:36:15	13.981	328	9.63	142.8	316	3.13	19.34	304	2.55	13.97	0.0024	0.0013
89	195x2k	01-09-07 23:25:30	28.586	30	32.39	138.6	25	5.95	37.32	10	3.44	11.09	0.0129	0.1196
90	171x1k	09-05-07 12:40:45	7.200	117	2.71	41.41	115	2.64	30.52	107	3.51	18.16	0.0100	0.0046
91	171x1k	05-09-07 00:06:00	29.169	41	21.13	147.9	38	3.03	11.84	20	2.94	11.29	0.0170	0.0168
92	284x1k	09-05-07 04:41:55	7.155	172	6.44	111.3	166	2.98	20.88	157	4.77	30.06	0.0117	0.0071
93	171x1k	09-05-07 10:40:45	7.189	148	15.61	226.9	143	6.98	32.34	118	4.81	26.52	0.0070	0.0027
94	284x1k	20-06-07 03:26:30	13.956	101	4.92	51.49	96	3.86	16.02	81	4.84	20.80	0.0093	0.0154
95	284x1k	20-06-07 21:46:30	14.098	71	6.06	60.00	67	3.85	19.29	59	5.04	27.94	0.0124	0.0216
96	284x1k	20-06-07 06:46:30	13.982	87	9.04	53.31	86	1.82	9.31	69	5.32	20.79	0.0088	0.0198

---

97	284x1k	20-06-07 10:06:30	14.008	109	9.45	107.5	99	3.78	23.87	87	5.4	31.38	0.0107	0.0212
98	284x1k	20-06-07 20:06:30	14.085	55	12.10	111.0	51	7.07	34.32	45	6.55	37.81	0.0151	0.0189
99	171x2k	01-07-07 00:13:30	16.006	117	17.52	233.6	11	3.14	15.01	80	3.19	8.47	0.0068	0.0076
100	195x2k	01-09-07 23:15:30	28.584	23	305.8	1256	18	21.38	198.1	6	null	null	0.0816	0.0992
101	171x1k	05-10-07 00:06:00	34.560	25	75.32	219.1	16	8.32	30.63	5	null	null	0.1575	0.0753
102	171x1k	05-11-07 00:06:00	39.088	25	80.20	190.5	15	57.35	147.0	4	null	null	0.1725	0.1186

## APPENDIX B. CONTENTS OF ENCLOSED CD-ROM

The CD-ROM attached to this thesis contains useful resources related to the addressed research work. The following is an index of the attached CD-ROM:

Folder	Contents
<b>Source Code</b>	This folder includes the source code for all methods presented in the thesis and integrated under one MDI form.
<b>STEREO</b>	This folder contains images provided by STEREO-Ahead and STEREO-Behind. The structure of the subfolders is organized to show the provided spacecraft and the resolution. For instance, STEREO\Ahead\2048.
<b>SDO</b>	This folder contains the images provided by SDO. The included subfolders also are organized to show the type of telescope and the resolution, e.g. SDO\0094\512.
<b>FITS</b>	This folder includes some of FITS files extracted from UKSSDC. Some of them were used as ground truth data.
<b>SOLARSTUDIO</b>	Includes the setup package for the SOLARSTUDIO application.